

Synthesis and Evaluation of a Metabolically Stabilized Analog and  
Conjugates of Pironetin

A Dissertation

SUBMITTED TO THE FACULTY OF  
UNIVERSITY OF MINNESOTA

BY

Sara Kathleen Coulup

IN PARTIAL FULFILLMENT OF THE REQUIREMENTS  
FOR THE DEGREE OF  
DOCTOR OF PHILOSOPHY

Dr. Gunda I. Georg

August 2019

©2019

Sara K. Coulup

All Rights Reserved

## Acknowledgements

It is with the utmost sincerity and gratitude that I acknowledge my advisor, Dr. Gunda Georg. Thank you for your support and mentorship, and for allowing me the freedom to take advantage of opportunities to develop myself as a scientist, writer, leader, and individual.

Thank you to Dr. Henry Wong for your advice on the folate conjugate work; Dr. David Huang for your work on pironetin; Dr. Peter Villalta and Xun Ming for your expertise with Orbitrap method development; Dr. Natalia Tretyakova for discussions about metabolism and mass spectrometry; Dr. Carrie Haskell-Luevano for your encouragement and mentorship; Dr. Tom Hoyer for teaching the most interesting and useful class I've ever taken and inspiring me to be a better presenter; Dr.'s Mike Walters and Peter Dosa for their career advice, guidance, and mentorship; Dr.'s Narsi Cheryala and Kristen Stolz for their depth of chemistry knowledge and for always having an encouraging word or two when most needed; and Dr. Soma Maitra for her friendship and synthesis expertise. I am extremely appreciative to the NIH for funding my graduate training with a T32 and then an F31.

For a few months, I was fortunate to learn new techniques in protein expression, purification, and crystallography in Marburg, Germany in Dr. Wibke Diederich's working group. I am extremely thankful to Wibke for not only allowing me to work in her group, but also for patiently taking care of all of the logistics. Thank you to Dr. Gerhard Klebe for graciously providing lab space and equipment. This experience would not have been the same without the James (Willie) Scanlan, Jud Badran, and Dr. Hans-Dieter Gerber, and I will always be incredibly grateful for the comradery and welcome I felt while in Marburg, particularly from Lukas Dempwolff, Iris Nee, Lukas Heyder, and Steffi Dörr.

Thank you to Dr. C. Leigh Allen for your expertise in finalizing manuscripts, perfecting figures, and editing. I am indebted to Caitlin Boley for everything you do for the department and the graduate students, for editing, and for your friendship.

I would not have embarked on this road if it weren't for Dr. Hang Yin (University of Colorado at Boulder) for giving me a chance in his lab, or Dr.'s Sherry Chavez and Jonel Saludes for encouraging me to apply for grants, opportunities to present, and internships. Thank you for teaching me the bench and analytical skills necessary to succeed in graduate school.

To Mike and Kathy Coulup, thank you for supporting me, and for encouraging me to be persistent and thorough.

Thank you, Ozgun Kilic and Denise Casemore, for the best ice breaker and for always picking up where we left off. To Erick Carlson, I can not give a heartier "cheers" or a more genuine thank you. It's been an honor grinding through this madness with you. Thank you for all the scientific discussion and advice, but mostly, thank you for an irreplaceable friendship.

And finally, I can not express how grateful I am to my partner, Peter Ycas. Your insight and approach to life are refreshing, thoughtful, and balancing. Thank you for cheerfully

supporting all of my endeavors, providing insightful critiques and discussions, and for helping me find my strength and confidence when I need it most. Thank you for making these years the best yet.

“But those aren’t always the best tales to hear, though they may be the best tales to get  
landed in.”

John Ronald Reuel Tolkien

## Abstract

Molecules that bind to tubulin and disrupt tubulin dynamics are known as microtubule targeting agents. Treatment with a microtubule targeting agent leads to cell cycle arrest followed by apoptosis. Tubulin inhibitors have been highly effective in the clinical treatment of a variety of tumors and are being investigated for treatment of several other diseases. Currently, all FDA approved microtubule inhibitors bind to  $\beta$ -tubulin. Given the overall success of tubulin-binding agents in anticancer chemotherapy,  $\alpha$ -tubulin is an attractive and unexplored target. Herein, we will discuss the natural product pironetin, the only compound known to bind  $\alpha$ -tubulin.

Despite the potent in vitro activity against ovarian cancer cell lines both sensitive and resistant to current chemotherapeutics, pironetin was only marginally effective at high doses in mice and resulted in severe weight loss, indicating poor pharmacokinetic/pharmacodynamic (PK/PD) properties and significant off target toxicities. The research presented in this dissertation seeks to improve the therapeutic properties of pironetin by addressing the PK/PD and off target binding concerns. In Chapter 2, we determined that pironetin has a short half-life in liver microsomes and identified pironetin's major site of metabolism in human liver microsomes to be the unconjugated olefin utilizing tandem mass spectrometry. We then confirmed the identity of the major metabolite as epoxyironetin through semi-synthesis and identified a very minor metabolite, demethylpironetin, with similar potency as pironetin.

With the knowledge that the unconjugated olefin is the major site of metabolism, we sought to block this site through total synthesis. We thus completed the total synthesis of 4-fluorophenyldemethylpironetin (19 linear steps, 31 total steps) with the goal of improving the metabolic stability while maintaining potency (Chapter 3). This represents the first total synthesis of demethylpironetin analogs. Finally, in Chapter 4 we describe our efforts to establish a proof-of-concept method for the targeted delivery of pironetin to ovarian cancer cells by targeting the folate receptor. Our results suggest that pironetin conjugates do not enter the cell in a folate receptor mediated manner, therefore necessitating exploration of additional means of targeting for pironetin delivery.

## Table of Contents

List of Figures	vii
List of Schemes	ix
List of Tables	x
List of Compounds	xi
List of Abbreviations	xiii

### Chapter 1: Introduction

1.1 General Background	1
1.2 Current Chemotherapeutics: Microtubule Targeting Agents	2
1.3 $\alpha$ -Tubulin Binding Agents	6
1.3.1 Pironetin	6
1.4 Pironetin's Biological Activity	8
1.4 Total Syntheses of Pironetin	12
1.5 Development of Pironetin's Structure-Activity Relationship	17
1.5.1 Early Studies – Isolated and Semi-Synthetic Analogs	17
1.5.2 Simplified Pironetin Analogs	19
1.5.3 Fully Elucidated Analogs Through Total Synthesis	20
1.5.4 Lessons from Structural Biology	22
1.6 Future Directions and Questions of Interest	22

### Chapter 2: Identification of Pironetin's Metabolic Liabilities

2.1 Introduction	25
2.2 Preliminary In Vitro PK Evaluation	26
2.3 Identification of Metabolic Soft Spots in HLM	27
2.4 Semisynthesis of Epoxypironetin and Demethylpironetin	30
2.5 Biological Evaluation	32
2.6 Discussion and Conclusion	33

### Chapter 3: Total Synthesis and Evaluation of a Metabolically Stabilized Pironetin Analog

3.1 Introduction	35
3.2 Synthesis of 4-Fluorophenyldemethylpironetin (3.2)	36
3.2.1 Route Design	36
3.2.2 Retrosynthesis and Synthesis of Auxiliaries	38
3.2.3 Synthesis of Alcohol Intermediate 3.18	39

3.2.4 Deoxygenation and Debenzylation Optimization	41
3.2.5 Completion of the Synthesis	46
3.3 Discussion and Future Directions	47
<b>Chapter 4: Synthesis and Evaluation of Pironetin-Folate Conjugates</b>	
4.1 Introduction	50
4.2 Design and Synthesis of the First Generation Pironetin-Folate Conjugate and a Camptothecin-Conjugate Positive Control	56
4.3 Characterization of Pironetin Release	59
4.4 Selection and Characterization of Cell Lines for Folate Conjugate Evaluation	61
4.5 Confirmation of Camptothecin Conjugate Activity and Internalization	62
4.6 First Generation Pironetin Conjugate Activity	63
4.7 Second Generation Pironetin Conjugate Synthesis and Activity	67
4.8 Discussion	68
<b>Chapter 5: Experimental Data</b>	
5.1 General Chemistry Procedures	72
5.2 Chapter 2 Metabolite Identification	73
5.2.1 Pironetin Extraction	73
5.2.2 Synthesis of Epoxypironetin and Demethylpironetin.	73
5.2.3 Metabolite Identification in Human Liver Microsomes	75
5.2.4 Cell Viability Assay	78
5.3 Chapter 3 Total Synthesis of 4-Fluorophenyldemethylpironetin	80
5.4 Chapter 4 Synthesis and Evaluation of Pironetin Conjugates	100
5.4.1 Synthesis of Conjugates	100
5.4.2 Characterization of Pironetin Release	104
5.4.3 Cell Adaptation to FF Conditions	105
5.4.4 Cell Viability Assay	105
5.4.5 Internalization Assay	106
5.5 References	108

## List of Figures

<b>Figure 1.1.</b> Overview of microtubules and MTAs.	3
<b>Figure 1.2.</b> Pironetin ( <b>1.1</b> ) covalently binds to $\alpha$ -tubulin by an induced-fit mechanism.	8
<b>Figure 1.3.</b> Summary of published pironetin total syntheses sorted into type of strategy	12
<b>Figure 1.4.</b> Chiron approach to the lactone fragment <b>1.29</b> by Sarabia and coworkers.	17
<b>Figure 1.5.</b> Early SAR exploration of pironetin	18
<b>Figure 1.6.</b> Simplified pironetin analogs.	19
<b>Figure 1.7.</b> Pironetin analogs exploring C2, C4, and C5 through total synthesis and C13 through semisynthesis.	21
<b>Figure 1.8.</b> Insight into pironetin's SAR (PDB: 5FNV).	23
<b>Figure 2.1.</b> Structure and binding mode of pironetin.	25
<b>Figure 2.2.</b> SMARTCyp predicted sites of pironetin metabolism.	27
<b>Figure 2.3.</b> Pironetin has two major metabolites ( <b>M2</b> and <b>M4</b> ) and three minor metabolites ( <b>M1/M3</b> and <b>M5</b> ).	29
<b>Figure 2.4.</b> LC traces of human liver microsome reaction	31
<b>Figure 3.1.</b> Cytotoxicity and metabolism evaluation of phenylpironetin ( <b>3.1</b> )	35
<b>Figure 3.2.</b> Structure of target molecule 4-fluorophenyldemethylpironetin.	36
<b>Figure 4.1.</b> Structure of the most advanced folate conjugate, Vintafolide.	52
<b>Figure 4.2.</b> Mechanism of cellular internalization and cleavage of a folate conjugate.	54
<b>Figure 4.3.</b> General structure of a folate conjugate.	55
<b>Figure 4.4.</b> First generation pironetin conjugate <b>4.2</b> is made of folic acid (blue), a peptide spacer (red), the self-immolative disulfide linker (green), and pironetin (black).	57
<b>Figure 4.5.</b> Conversion of conjugate to peptide is rapid, but pironetin is not UV active.	60
<b>Figure 4.6.</b> Pironetin is released from the conjugate upon incubation with DTT as confirmed by LC-MS.	60
<b>Figure 4.7.</b> Pironetin, when treated with 10x excess DTT, forms a very minor new peak after an overnight incubation.	61
<b>Figure 4.8.</b> Camptothecin conjugate <b>4.7</b> shows folate receptor mediated activity.	63
<b>Figure 4.9.</b> Evaluation of pironetin conjugate <b>4.2</b> in FF adapted cells.	64

<b>Figure 4.10.</b> Confirmation that addition of 50 $\mu$ M FA does not alter the activity of pironetin (n=1).	65
<b>Figure 4.11.</b> Internalization of pironetin conjugate <b>4.2</b> .	66
<b>Figure 4.12.</b> Evaluation of the second-generation conjugate ( <b>4.9</b> ).	68

## List of Schemes

<b>Scheme 2.1.</b> Synthesis of epoxyironetin ( <b>M4</b> ) and demethylpironetin ( <b>M5</b> )	30
<b>Scheme 3.1.</b> Retrosynthesis of Dias's total synthesis using Evans' oxazolidinone auxiliaries starting from 1,3-propane diol	37
<b>Scheme 3.2.</b> Crimmins' total synthesis utilized thiazolidinonethione auxiliaries	38
<b>Scheme 3.3.</b> Retrosynthesis of 4-fluorophenyldemethylpironetin	39
<b>Scheme 3.4.</b> Synthesis of thiazolidinone thione chiral auxiliaries	39
<b>Scheme 3.5.</b> First half of the synthesis of 4-fluorophenyldemethylpironetin	40
<b>Scheme 3.6.</b> Key conversion in the phenylpironetin synthesis	41
<b>Scheme 3.7.</b> Initial attempt at deoxygenation and debenylation	41
<b>Scheme 3.8.</b> Test scheme with phenyldemethylpironetin derivative	42
<b>Scheme 3.9.</b> Barton McCombie deoxygenation	43
<b>Scheme 3.10.</b> Final optimization of deoxygenation and debenylation chemistry	45
<b>Scheme 3.11.</b> Synthesis of the ketal for confirmation of the anti-diol	45
<b>Scheme 3.12.</b> Completion of 4-fluorophenyldemethylpironetin	46
<b>Scheme 3.13.</b> Preparation of phosphonate <b>3.36</b>	47
<b>Scheme 4.1.</b> Synthesis of the folate peptide and activated pironetin	57
<b>Scheme 4.2.</b> Convergent synthesis of pironetin conjugate <b>4.2</b>	58
<b>Scheme 4.3.</b> Synthesis of positive control camptothecin conjugate <b>4.7</b>	59
<b>Scheme 4.4.</b> Synthesis of the second-generation pironetin conjugate <b>4.8</b>	67

## List of Tables

<b>Table 1.1.</b> Compilation of pironetin's cellular cytotoxicity	9
<b>Table 1.2.</b> Effect of pironetin on the generation of cytotoxic T cells in EL4 bearing mice	10
<b>Table 1.3.</b> Antitumor activity of pironetin in P388 bearing mice	11
<b>Table 2.1.</b> In vitro PK properties of pironetin	26
<b>Table 2.2.</b> Inhibition of P450 isoforms by pironetin	27
<b>Table 2.3.</b> In vitro cytotoxicity evaluation of pironetin, epoxy pironetin, and demethylpironetin	32
<b>Table 3.1.</b> Optimization of benzyl ether deprotection	44

## List of Compounds

(5 <i>R</i> ,6 <i>R</i> )-5-Ethyl-6-((2 <i>R</i> ,3 <i>S</i> ,4 <i>R</i> ,5 <i>S</i> )-2-hydroxy-4-methoxy-3,5-dimethyl-6-(3-methyloxiran-2-yl)hexyl)-5,6-dihydro-2 <i>H</i> -pyran-2-one (epoxypironetin, <b>M4</b> ).	73
(5 <i>R</i> ,6 <i>R</i> )-6-((2 <i>R</i> ,3 <i>S</i> ,4 <i>R</i> ,5 <i>S</i> , <i>E</i> )-2,4-Dihydroxy-3,5-dimethylnon-7-en-1-yl)-5-ethyl-5,6-dihydro-2 <i>H</i> -pyran-2-one (demethylpironetin, <b>M5</b> ).	74
3-(Benzyloxy)propan-1-ol ( <b>3.12</b> ).	80
3-(Benzyloxy)propanal ( <b>3.13</b> ).	80
(2 <i>S</i> ,3 <i>R</i> )-1-(( <i>S</i> )-4-Benzyl-2-thioxothiazolidin-3-yl)-5-(benzyloxy)-3-hydroxy-2-methylpentan-1-one ( <b>3.14</b> ).	81
(2 <i>S</i> ,3 <i>R</i> )-1-(( <i>S</i> )-4-Benzyl-2-thioxothiazolidin-3-yl)-5-(benzyloxy)-3-(( <i>tert</i> -butyldimethylsilyl)oxy)-2-methylpentan-1-one ( <b>3.15</b> ).	82
(2 <i>S</i> ,3 <i>R</i> )-5-(Benzyloxy)-3-(( <i>tert</i> -butyldimethylsilyl)oxy)-2-methylpentanal ( <b>3.8</b> ).	83
(2 <i>R</i> ,3 <i>S</i> ,4 <i>R</i> ,5 <i>R</i> )-1-(( <i>R</i> )-4-Benzyl-2-thioxothiazolidin-3-yl)-7-(benzyloxy)-5-(( <i>tert</i> -butyldimethylsilyl)oxy)-3-hydroxy-2,4-dimethylheptan-1-one ( <b>3.16</b> ).	84
(2 <i>R</i> ,3 <i>S</i> ,4 <i>S</i> ,5 <i>R</i> )-1-(( <i>R</i> )-4-Benzyl-2-thioxothiazolidin-3-yl)-7-(benzyloxy)-3,5-bis(( <i>tert</i> -butyldimethylsilyl)oxy)-2,4-dimethylheptan-1-one ( <b>3.17</b> ).	85
(2 <i>R</i> ,3 <i>S</i> ,4 <i>S</i> ,5 <i>R</i> )-7-(Benzyloxy)-3,5-bis(( <i>tert</i> -butyldimethylsilyl)oxy)-2,4-dimethylheptanal ( <b>3.7</b> ).	86
(2 <i>S</i> ,3 <i>R</i> ,4 <i>S</i> ,5 <i>R</i> )-7-(Benzyloxy)-3,5-bis(( <i>tert</i> -butyldimethylsilyl)oxy)-1-(4-fluorophenyl)-2,4-dimethylheptan-1-ol ( <b>3.18</b> ).	87
(2 <i>S</i> ,3 <i>R</i> ,4 <i>S</i> ,5 <i>R</i> )-7-(Benzyloxy)-3,5-bis(( <i>tert</i> -butyldimethylsilyl)oxy)-1-(4-fluorophenyl)-2,4-dimethylheptyl 2,2,2-trifluoroacetate ( <b>3.18a</b> ).	88
<i>O</i> -((2 <i>S</i> ,3 <i>R</i> ,4 <i>S</i> ,5 <i>R</i> )-7-(Benzyloxy)-3,5-bis(( <i>tert</i> -butyldimethylsilyl)oxy)-1-(4-fluorophenyl)-2,4-dimethylheptyl) 1 <i>H</i> -imidazole-1-carbothioate ( <b>3.24</b> ).	89
(5 <i>R</i> ,6 <i>S</i> ,7 <i>R</i> )-5-(2-(Benzyloxy)ethyl)-7-(( <i>S</i> )-1-(4-fluorophenyl)propan-2-yl)-2,2,3,3,6,9,9,10,10-nonamethyl-4,8-dioxo-3,9-disilaundecane ( <b>3.25</b> ).	89
(2 <i>S</i> ,3 <i>R</i> ,4 <i>S</i> ,5 <i>R</i> )-7-(Benzyloxy)-1-(4-fluorophenyl)-2,4-dimethylheptane-3,5-diol ( <b>3.28</b> ).	90
(4 <i>R</i> ,5 <i>S</i> ,6 <i>R</i> )-4-(2-(Benzyloxy)ethyl)-6-(( <i>S</i> )-1-(4-fluorophenyl)propan-2-yl)-2,2,5-trimethyl-1,3-dioxane ( <b>3.29</b> ).	91
(3 <i>R</i> ,4 <i>S</i> ,5 <i>R</i> ,6 <i>S</i> )-3,5-bis(( <i>tert</i> -Butyldimethylsilyl)oxy)-7-(4-fluorophenyl)-4,6-dimethylheptan-1-ol ( <b>3.26</b> ).	92
(3 <i>R</i> ,4 <i>S</i> ,5 <i>R</i> ,6 <i>S</i> )-3,5-bis(( <i>tert</i> -Butyldimethylsilyl)oxy)-7-(4-fluorophenyl)-4,6-dimethylheptanal ( <b>3.27</b> ).	93

(2 <i>S</i> ,3 <i>R</i> ,5 <i>R</i> ,6 <i>S</i> ,7 <i>R</i> ,8 <i>S</i> )-1-(( <i>S</i> )-4-Benzyl-2-thioxothiazolidin-3-yl)-5,7-bis((tert-butyl)dimethylsilyloxy)-2-ethyl-9-(4-fluorophenyl)-3-hydroxy-6,8-dimethylnonan-1-one ( <b>3.30</b> ).	93
(2 <i>S</i> ,3 <i>R</i> ,5 <i>R</i> ,6 <i>S</i> ,7 <i>R</i> ,8 <i>S</i> )-1-(( <i>S</i> )-4-Benzyl-2-thioxothiazolidin-3-yl)-3,5,7-tris((tert-butyl)dimethylsilyloxy)-2-ethyl-9-(4-fluorophenyl)-6,8-dimethylnonan-1-one ( <b>3.31</b> ).	95
(2 <i>S</i> ,3 <i>R</i> ,5 <i>R</i> ,6 <i>S</i> ,7 <i>R</i> ,8 <i>S</i> )-3,5,7-tris((tert-Butyl)dimethylsilyloxy)-2-ethyl-9-(4-fluorophenyl)-6,8-dimethylnonan-1-one ( <b>3.32</b> ).	96
Ethyl di- <i>o</i> -Tolyl Phosphite ( <b>3.35</b> ).	96
Ethyl 2-(bis( <i>o</i> -Tolyl)oxy)phosphorylacetate ( <b>3.36</b> ).	97
Ethyl (4 <i>R</i> ,5 <i>R</i> ,7 <i>R</i> ,8 <i>S</i> ,9 <i>R</i> ,10 <i>S</i> , <i>Z</i> )-5,7,9-tris((tert-Butyl)dimethylsilyloxy)-4-ethyl-11-(4-fluorophenyl)-8,10-dimethylundec-2-enoate ( <b>3.33</b> ).	97
(5 <i>R</i> ,6 <i>R</i> )-5-Ethyl-6-((2 <i>R</i> ,3 <i>S</i> ,4 <i>R</i> ,5 <i>S</i> )-6-(4-fluorophenyl)-2,4-dihydroxy-3,5-dimethylhexyl)-5,6-dihydro-2 <i>H</i> -pyran-2-one (4-fluorophenyldemethylpironetin, <b>3.2</b> )	98
N2-(4-(((2-Amino-4-oxo-3,4-dihydropteridin-6-yl)methyl)amino)benzoyl)-N5-((( <i>S</i> )-3-carboxy-1-((( <i>S</i> )-1-((( <i>S</i> )-3-carboxy-1-((( <i>S</i> )-3-carboxy-1-((( <i>S</i> )-1-carboxy-2-mercaptoethyl)amino)-1-oxopropan-2-yl)amino)-1-oxopropan-2-yl)amino)-5-guanidino-1-oxopentan-2-yl)amino)-1-oxopropan-2-yl)amino)- <i>L</i> -glutamine ( <b>4.3</b> ).	100
2-(Pyridin-2-yl)disulfaneyl)ethan-1-ol ( <b>4.4</b> ).	101
(2 <i>R</i> ,3 <i>S</i> ,4 <i>R</i> ,5 <i>S</i> , <i>E</i> )-1-((2 <i>R</i> ,3 <i>R</i> )-3-Ethyl-6-oxo-3,6-dihydro-2 <i>H</i> -pyran-2-yl)-4-methoxy-3,5-dimethylnon-7-en-2-yl (2-(pyridin-2-yl)disulfaneyl)ethyl) Carbonate ( <b>4.5</b> ).	101
First Generation Pironetin Conjugate ( <b>4.2</b> ).	102
(2 <i>S</i> ,5 <i>S</i> ,23 <i>S</i> )-23-(4-(((2-Amino-4-oxo-3,4-dihydropteridin-6-yl)methyl)amino)benzamido)-5-(carboxymethyl)-2-(mercaptomethyl)-6,20-dioxo-9,12,15,18-tetraoxa-3,4,19-triazatetracosanedioic Acid ( <b>4.8</b> ).	103
Second Generation Pironetin Conjugate ( <b>4.9</b> ).	103
Camptothecin Conjugate <b>4.7</b> .	104

## List of Abbreviations

ACN	acetonitrile
ADC	antibody drug conjugate
AIBN	Azobisisobutyronitrile
APCI	atmospheric pressure chemical ionization
Bcl-2	B-cell lymphoma 2
BCL-XL	B-cell lymphoma extra large
CP	cisplatin
DAVLBH	deacetylvinblastine hydrazide
DCM	dichloromethane
DIBAL-H	diisobutylaluminum hydride
DIPEA	diisopropylethylamine
DMAP	dimethylaminopyridine
DMF	dimethylformamide
DMSO	dimethylsulfoxide
DTT	dithiothreitol
EDT	1,2-ethanedithiol
EH	epoxide hydrolase
ELISA	enzyme-linked immunosorbent assay
EtOAc	ethylacetate
EtOH	ethanol
FA	folic acid
FBS	fetal bovine serum
FDA	food and drug administration
FF	folate free
Fmoc	Fluorenylmethyloxycarbonyl
FR	folate receptor
GDP	guanosine diphosphate
GI <sub>50</sub>	50% growth inhibitory concentration
GPI	glycosylphosphatidylinositol
GSH	glutathione
GTP	guanosine triphosphate
HLM	human liver microsomes
HoBt	hydroxybenzotriazole
HPLC	high performance liquid chromatography
HRMS	high resolution mass spectrometry
IC <sub>50</sub>	50% inhibitory concentration

IP	intraperitoneal
ITDD	Institute for Therapeutics Discovery and Development
LC-MS	liquid chromatography-mass spectrometry
LC-MS/MS	liquid chromatography tandem mass spectrometry
mAb	monoclonal antibody
MALDI	matrix-assisted laser desorption/ionization
MALDI/TOF-MS	matrix-assisted laser desorption/ionization time-of-flight mass spectrometry
mCPBA	meta-chloroperoxybenzoic acid
MDA	microtubule destabilizing agent
MDR	multi-drug resistant
MeOH	methanol
MSA	microtubule stabilizing agent
MTA	microtubule targeting agent
MTT	3-(4,5-dimethylthiazol-2-yl)-2,5-diphenyltetrazolium bromide
NADPH	nicotinamide adenine dinucleotide phosphate
NIH	national institutes of health
NMP	N-Methyl-2-pyrrolidone
NMR	nuclear magnetic resonance
OR	optical rotation
PBS	phosphate buffered saline
Pd/C	palladium on carbon
PEG	polyethyleneglycol
P-gp	P-glycoprotein
PK/PD	pharmacokinetics/pharmacodynamics
Plk1	polo-like kinase 1
PMSF	phenylmethylsulfonyl fluoride
Pte	pteroic acid
PTSA	p-toluene sulfonic acid
PTX	paclitaxel
PyBOP	benzotriazol-1-yl-oxytripyrrolidinophosphonium hexafluorophosphate
QSAR	quantitative structure-activity relationship
RPMI	Roswell Park Memorial Institute (Media)
rt	room temperature
SAR	structure-activity relationship
siRNA	small interfering ribonucleic acid
TBAI	tertbutylammonium iodide
TBS	tertbutyldimethylsilane

TBSOTf	tertbutyldimethylsilyl trifluoromethanesulfonate
TEA	triethylamine
TFA	trifluoroacetic acid
TFAA	trifluoroacetic anhydride
THF	tetrahydrofuran
TIPS	triisopropylsilane
TLC	thin layer chromatography
UV	ultraviolet

# Chapter 1: Introduction

This chapter was adapted from: Coulup, S.K. & Georg, G.I. *Bioorg. Med. Chem. Lett.*, **2019**, 29, 1865-1873.

## 1.1 General Background

Cancer is the second leading cause of death in the United States and includes at least 100 distinct types characterized by abnormal cell growth caused by the combination of mutations that alter cell signaling and survival.<sup>1</sup> Tumorigenesis, or the conversion of normal, healthy cells into their malignant derivatives, is now understood to be a multistep process, however, many dimensions of cancer, and what separates a benign tumor from a malignant tumor, are still far from understood.<sup>2,3</sup> The progression of tumorigenesis occurs due to several acquired capabilities that confer a growth advantage, similar to Darwinian evolution.<sup>4</sup> While the vast amount of research and resources put towards developing cancer therapeutics and earlier detection methods has provided a great number of successes, many cancer types are still largely untreatable. In addition, many cancer patients relapse following chemotherapy, malignancies metastasize, and many develop resistance to current therapeutics.

Over the past 50 years, the progress made in the treatment and diagnosis of tumors has been astounding, however many cancers are still not diagnosed until late stages of the disease. Ovarian cancer is one such variety. A total of 25,000 cases of ovarian cancer are expected to be diagnosed this year and more than half of the women diagnosed will die within five years. This is predominantly because the majority of patients presenting with

ovarian cancer (60%) are diagnosed in the late stages in which the cancer has already metastasized.<sup>5</sup> In addition to improved diagnostics for earlier detection of ovarian cancer, there is a critical need to develop therapeutics with novel mechanisms of action that can be used to treat women whose ovarian cancer has become resistant to current therapeutics.

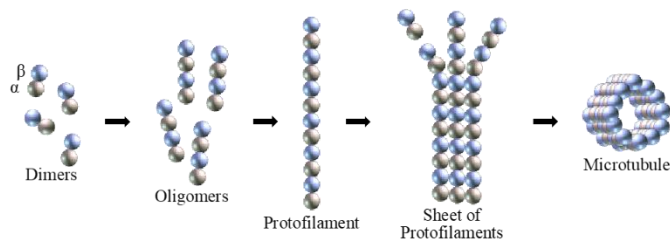
## **1.2 Current Chemotherapeutics: Microtubule Targeting Agents**

The current treatment options for patients presenting with ovarian cancer are relatively few. If the tumor can be debulked, patients will first undergo cytoreduction to surgically remove as much tumor as possible and follow up with chemotherapy. The combination of the DNA crosslinking agent carboplatin and the microtubule targeting agent paclitaxel has been the first line of treatment for the past three decades. Despite the high initial response rate, most patients relapse and become resistant to currently available chemotherapeutics, highlighting the critical need for the discovery of new therapeutics, including microtubule targeting agents.<sup>6</sup>

Microtubules are polymers of  $\alpha$ - and  $\beta$ -tubulin protein heterodimers that associate longitudinally into protofilaments. Lateral assembly of protofilaments forms the microtubule, which can be further elongated or shortened by single  $\alpha$ - and  $\beta$ -tubulin heterodimers (Figure 1.1A).<sup>7</sup> The slow, sustained polymerization and rapid depolymerization, called dynamic instability, is fueled by GTP hydrolysis and occurs at both ends of the polymer. The constant alteration of the polymerization and depolymerization dynamics of individual and populations of microtubules gives microtubules a fundamental and essential role in many cellular processes including cell

division, cell structure, and intracellular transport.<sup>8</sup> Due to the importance of microtubules in cells, particularly in rapidly dividing cells, compounds that bind microtubules, called

**A.**



**B.**

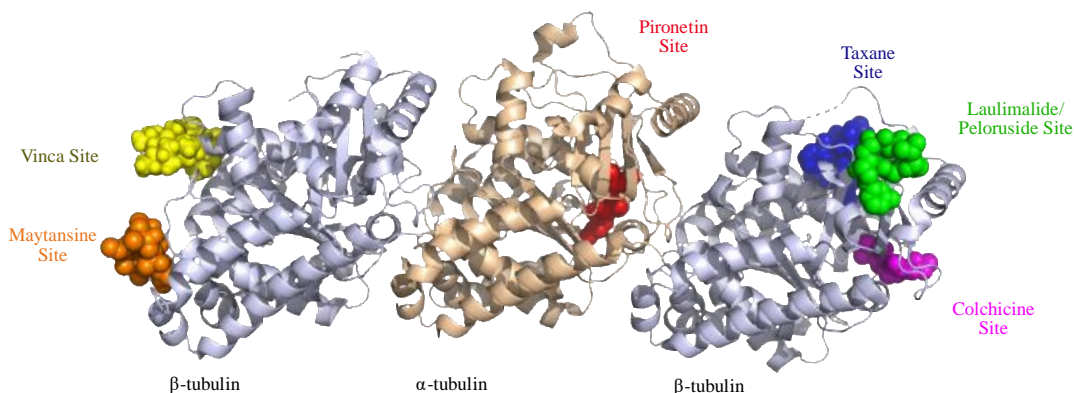


**Figure 1.1.** Overview of microtubules and MTAs. **A.** Microtubules are formed when dimers of  $\alpha$ - and  $\beta$ -tubulin polymerize, forming protofilaments, which cyclize into microtubules. **B.** Overlay of co-crystal structures showing the six known binding sites on  $\alpha$ - and  $\beta$ -tubulin.

microtubule targeting agents (MTAs), have long been one of the most important drug classes for cancer chemotherapy.<sup>8,9</sup> In addition, these molecules are also approved to treat fungal and bacterial infections<sup>10,11</sup> as well as non-neoplastic conditions such as gout<sup>12</sup> and nonfamilial Mediterranean fever.<sup>13</sup> MTAs are currently under investigation for the treatment of many neurological disorders.<sup>14</sup>

MTAs suppress and alter tubulin dynamics, therefore disrupting dependent cellular processes. Treatment with all MTAs results in cell cycle arrest during the late G2/M phase at the metaphase/anaphase transition due to inhibiting the separation of sister chromatids

to the poles, leading to apoptosis.<sup>15</sup> There are currently six known MTA binding sites identified on tubulin (Figure 1.1B). These efforts have been enabled by the recent advances in structural biology, including x-ray crystallography and cryo-electron microscopy, and have revealed the finer molecular mechanisms of microtubule targeting agents.<sup>16, 17</sup>

The taxane site, bound by paclitaxel, epothilone, and several other ligands, and the laulimalide/peloruside site, which are targeted by the named natural products, are known as microtubule stabilizing sites. Microtubule stabilizing agents (MSAs) are known to promote tubulin assembly or stabilize microtubules by either improving longitudinal contacts or by stabilizing lateral connections between protofilaments. MSAs that bind at the same site do not necessarily affect stabilization by the same mechanism.<sup>18-20</sup>

The other four sites bind ligands known as microtubule destabilizing agents (MDAs) and include the vinca, maytansine, colchicine, and pironetin sites. MDAs display diverse mechanisms of inhibiting proper microtubule formation, including inhibiting the curved-to-straight transformation of the tubulin heterodimer, inserting a wedge between assembled heterodimers, stabilizing assembly-incompetent polymers, or blocking longitudinal interactions.<sup>21-23</sup> Unfortunately, the use of terms such as “stabilizers” or “destabilizers” is simplistic. The effects of MTAs on microtubule polymer mass (stabilization/destabilization) as discussed above is a phenomenon observed at high concentrations. Thus, this would only be observed if a patient was maintained at a very high dose of MTA. At 10-100× lower concentration, MTAs significantly suppress spindle tubulin dynamics. The suppression of dynamics leads to apoptosis by blocking mitosis due

to improperly attached sister chromatids to the spindle microtubules during G2/M phase checkpoint.<sup>24</sup>

Both types of tubulin inhibitors have been highly effective in the treatment of a variety of tumors as individual and combination therapies, but all MTAs approved by the FDA bind to  $\beta$ -tubulin. Cancer cells in culture acquire resistance to these drugs through multiple mechanisms, including overexpression of multi-drug resistant genes, mutations in  $\beta$ -tubulin, changes in the tubulin isoform expression, delay of the G2/M transition, defects in mitotic checkpoints, and alterations in apoptotic pathways.<sup>8, 25</sup> In patients, the best documented source of resistance is overexpression of efflux pumps, such as P-glycoprotein (P-gp).<sup>26-28</sup> Additionally, a connection between tubulin isoform expression and resistance has been seen in some cancers.<sup>29</sup> It was recently shown that some covalent MTAs can counteract and partially overcome drug resistance that is mediated by  $\beta$ III-tubulin overexpression in vitro.<sup>30</sup> In contrast, the initial results showing that  $\beta$ -tubulin mutations could confer taxol resistance in patients have not been corroborated and is still a subject of debate.<sup>31, 32</sup> Current anti-tubulin drugs display significant bone marrow toxicity, immunosuppression, and neuropathy.<sup>33, 34</sup> Thus, there is a critical need to develop novel and safer chemotherapeutics, including anti-tubulin therapeutics, that can escape the acquired resistance mechanisms and minimize off-target toxicity. Due to the success of  $\beta$ -tubulin targeting agents,  $\alpha$ -tubulin is an attractive alternative therapeutic target, particularly in cancers that overexpress P-gp and certain  $\alpha$ -tubulin isoforms.<sup>35</sup>

## 1.3 $\alpha$ -Tubulin Binding Agents

Each known family of MDAs (vinca alkaloids, maytansines, colchicines, and pironetin) interact in some way with  $\alpha$ -tubulin, however only the pironetin binding site is exclusively located within  $\alpha$ -tubulin. The other three binding pockets are located at the interface between the tubulin heterodimer and are formed primarily by residues on  $\beta$ -tubulin. The growing utility and ease of crystallography has shown that some molecules previously thought to bind  $\alpha$ -tubulin, namely the hemiasterlin-peptides, actually bind at the interface of  $\beta$ -tubulin. The discovery of this information by crystallography means that only the natural product pironetin is known to bind exclusively to  $\alpha$ -tubulin.

### 1.3.1 Pironetin

Pironetin (**1.1**, Figure 1.2A) is the only natural product crystallographically characterized to bind solely to  $\alpha$ -tubulin. Originally known as PA-48153C, this polyketide was isolated concurrently from the fermentation broth and cell paste of *Streptomyces prunicolor*<sup>36, 37</sup> and *Streptomyces* sp. NK10958<sup>38</sup> bacteria strains. Pironetin was initially identified to reduce plant height<sup>36</sup> and later identified as a covalent cell cycle regulator.<sup>39</sup> In order to identify the putative binding site, rat 3Y1 cells were treated with a biotinylated-pironetin derivative labeled as the O7 ester. Subsequent enrichment and pulldown of the biotinylated protein-pironetin adduct identified  $\alpha$ -tubulin as the protein target. Partial digestion of the adduct allowed for a targeted approach to replace lysines and cysteines with alanine, leading to the original hypothesis that pironetin undergoes a Michael addition with Lys352 of  $\alpha$ -tubulin.<sup>40</sup> However, two crystallographic studies definitively

demonstrate that pironetin binds to Cys316 of  $\alpha$ -tubulin by Michael addition (Figure 1.2B).<sup>41,42</sup> Due to the proximity of Lys352 to Cys316, it is possible that these residues are involved in proton transfer, enhancing pironetin binding.

These results identified a new ligand binding site on tubulin, the first to be exclusively within  $\alpha$ -tubulin. The binding pocket is not present in the apo structure, indicating that pironetin binds through an induced fit mechanism (Figure 1.2C). Pironetin binding opens a pocket that is formed by a significant shift in the T7 loop with some residues shifting more than 10 Å. In the apo structure, Val250 occupies the space in which the methoxy group later sits. When in complex, the T7 loop appears to be stabilized by a salt bridge as well as hydrogen bond interactions with both  $\alpha$ - and  $\beta$ -tubulin. This could promote microtubule disassembly since the interface between the  $\alpha$ - and  $\beta$ -tubulin subunits is disrupted, preventing longitudinal assembly.

In addition to the large shift of the T7 loop, the N-terminal end of helix H8, namely residues Phe255 and Glu254, re-orient due to the T7 shift. This could further explain the mechanism of pironetin's ability to destabilize microtubule assembly as Glu254 is a key catalytic residue. In the apo structure, Glu254 binds to a water molecule that then binds to a  $Mg^{2+}$  ion present in the neighboring  $\beta$ -tubulin, which in turn stabilizes GDP.<sup>43</sup> When in complex with pironetin, Glu254 does not interact with  $Mg^{2+}$  due to the shift. Glu254 is thought to significantly enhance the GTPase activity of  $\beta$ -tubulin and, as expected, pironetin-treated microtubules display a significant decrease in the GTPase activity.<sup>41</sup>

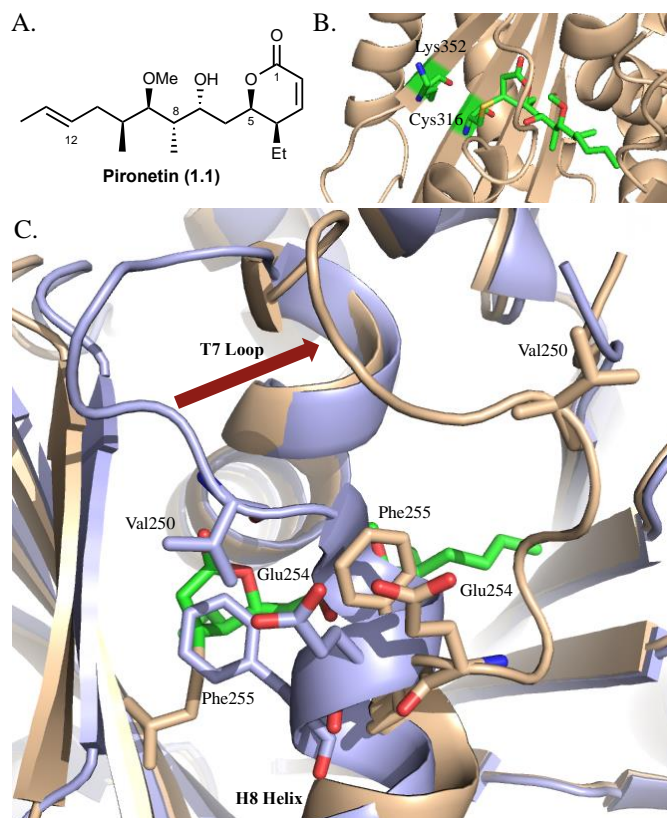


**Figure 1.2.** Pironetin (1.1) covalently binds to  $\alpha$ -tubulin by an induced-fit mechanism. **A.** Structure of the natural product pironetin. **B.** Co-crystal structure of pironetin covalently bound to Cys316 of  $\alpha$ -tubulin. Lys352 is also highlighted (PDB: 5FNV). **C.** The apo structure is in blue (PDB: 4I55), the pironetin co-crystal structure is in tan (PDB: 5FNV). The red arrow shows the movement of the T7 loop upon pironetin binding. Glu254, Phe255, and Val250 are highlighted.

#### 1.4 Pironetin's Biological Activity

Many groups have shown that pironetin displays potent *in vitro* activity against cell lines both sensitive and resistant to current first-line therapeutics (Table 1.1).<sup>39, 44-50</sup> Importantly, pironetin is cancer-cell specific as it was inactive against normal human lung fibroblasts (IMR-90), which displayed normal cell-cycle bias and no indications of apoptosis following treatment.<sup>46</sup> Furthermore, pironetin is not a P-gp substrate.<sup>48</sup> Additionally, in a zebrafish model of blood vessel formation, treatment with pironetin

resulted in anti-angiogenesis activity.<sup>46</sup> Pironetin has been shown to induce apoptosis through the intrinsic pathway through B-cell lymphoma 2 (Bcl-2) phosphorylation and caspase-3 activation.<sup>47</sup> Further, polo-like kinase 1 (Plk1) was found to phosphorylate and inactivate Bcl-XL following treatment with pironetin; however, siRNA knockdown of Plk1 did not suppress pironetin-induced apoptosis, suggesting multiple mechanisms.<sup>51</sup> Despite the initial characterization of the intrinsic caspase-dependent apoptosis pathway,<sup>47, 51</sup> nothing has yet been reported for pironetin-induced extrinsic apoptosis.

**Table 1.1.** Compilation of pironetin's cellular cytotoxicity

Cell Line	Tumor Type	Pironetin GI <sub>50</sub> (nM)	Reference
A2780	Ovarian	24.3 ± 0.9	39, 45, 49
A2780CP	CP resistant A2780	22.3 ± 0.3	49
A549	Lung	7.5 ± 0.9	46
DC-3F	MDR Chinese Hamster Lung	9.5 ± 1.2	46
EL4	Thymoma	~15	50
H69	Lung	17.5 ± 0.9	48
H69/Tax	PTX resistant H69	11.5 ± 0.4	48
H69/VDS	Vindesine resistant H69	20.3 ± 2.3	48
Hela	Cervical	~30	39
HL-60	Leukemia	~20	47
K-NRK	Murine sarcoma transformed rat kidney	~30	39
K562	Leukemia	17.3 ± 0.8	48
K562/ADM	MDR/P-gp overexpressing K562	16.0 ± 1.3	48
MCF-7	Breast	5.0 ± 0.2	46
MDA-MB231	Breast	4.6 ± 1.2	46
OVCAR5	Ovarian	14.4 ± 0.8	44, 45
P388	Mouse Leukemia	~100	47
T98G	Glioma	7.5 ± 1.2	46
VCRd5L	MDR Chinese Hamster Lung	31.0 ± 5.0	46

Abbreviations: GI<sub>50</sub>, 50% growth inhibitory concentration; PTX, paclitaxel; CP, cisplatin; MDR, multi-drug resistant; P-gp, P-glycoprotein.

Despite pironetin's potent in vitro activity, only two in vivo studies have been reported in literature.<sup>39, 50</sup> Towards demonstrating pironetin's immunosuppressant activity, mice bearing EL4 thymoma cells were treated with intraperitoneal (IP) pironetin injection (Table 1.2). After 16 days, the mice were sacrificed and the spleen was harvested to create effector cells, which were utilized to understand pironetin's effect on the generation of cytotoxic T cells. Pironetin significantly suppressed the generation of cytotoxic T cells as compared to vehicle treatment at a 5 mg/kg dose, indicating that pironetin has potent immunosuppressant activity.<sup>50</sup> While no positive control was reported in vivo, cyclosporine was run in the preliminary in vitro assay and showed a 4- and 800-fold loss in IC<sub>50</sub> as compared to pironetin against concanavalin A-stimulated T cell and lipopolysaccharide-stimulated B cell proliferation, respectively.

**Table 1.2.** Effect of pironetin on the generation of cytotoxic T cells in EL4 bearing mice<sup>50</sup>

<b>Compound</b>	<b>Dose</b>	<b>% Specific Lysis (Effector/Target Cells=50)</b>
Control	0 mg/kg	18.6 ± 4.1
Pironetin	5 mg/kg	7.4 ± 2.2

In the second in vivo study, pironetin was monitored for its antitumor activity (Table 1.3). Pironetin was injected IP daily for five days (day 1 through day 5) into mice bearing P388 murine leukemia cells. Mortality was monitored and the mice were weighed on days 1 and 10. At relatively high doses as compared with other microtubule targeting agents, pironetin led to a very modest improvement in mean survival time, however this was accompanied by significant weight loss.<sup>39</sup> Together, these in vivo studies demonstrate that

pironetin was only moderately effective in reduction of P388 tumor burden, caused significant weight loss, and was highly immunosuppressant.

**Table 1.3.** Antitumor activity of pironetin in P388 bearing mice<sup>39</sup>

<b>Compound</b>	<b>Dose</b>	<b>Body Weight Change (g)</b>	<b>Mean Survival Time (days)</b>
Control	0 mg/kg	5.3	11.2 ± 0.8
Pironetin	0.78 mg/kg	3.7	11.2 ± 0.6
	1.56 mg/kg	0.5	11.7 ± 0.6
	3.13 mg/kg	-0.1	13.3 ± 1.2
	6.25 mg/kg	-2.6	14.3 ± 0.6

The minimal antitumor activity could be explained by pironetin's decreased cytotoxicity against P388 cultured cells as compared to other tumor cell lines and by the observation that >500 nM pironetin was required to induce apoptosis in cultured P388 cells.<sup>47</sup> It is probable that the optimal tumor type to demonstrate pironetin's activity was not used. Alternatively, pironetin could display poor pharmacokinetic/pharmacodynamic (PK/PD) properties or off-target binding, limiting the amount of cytotoxic agent that reaches the site of the tumor. While an extensive amount of work has been published highlighting these synthetic efforts, no pironetin analogs have yet been evaluated in vivo for cytotoxicity.

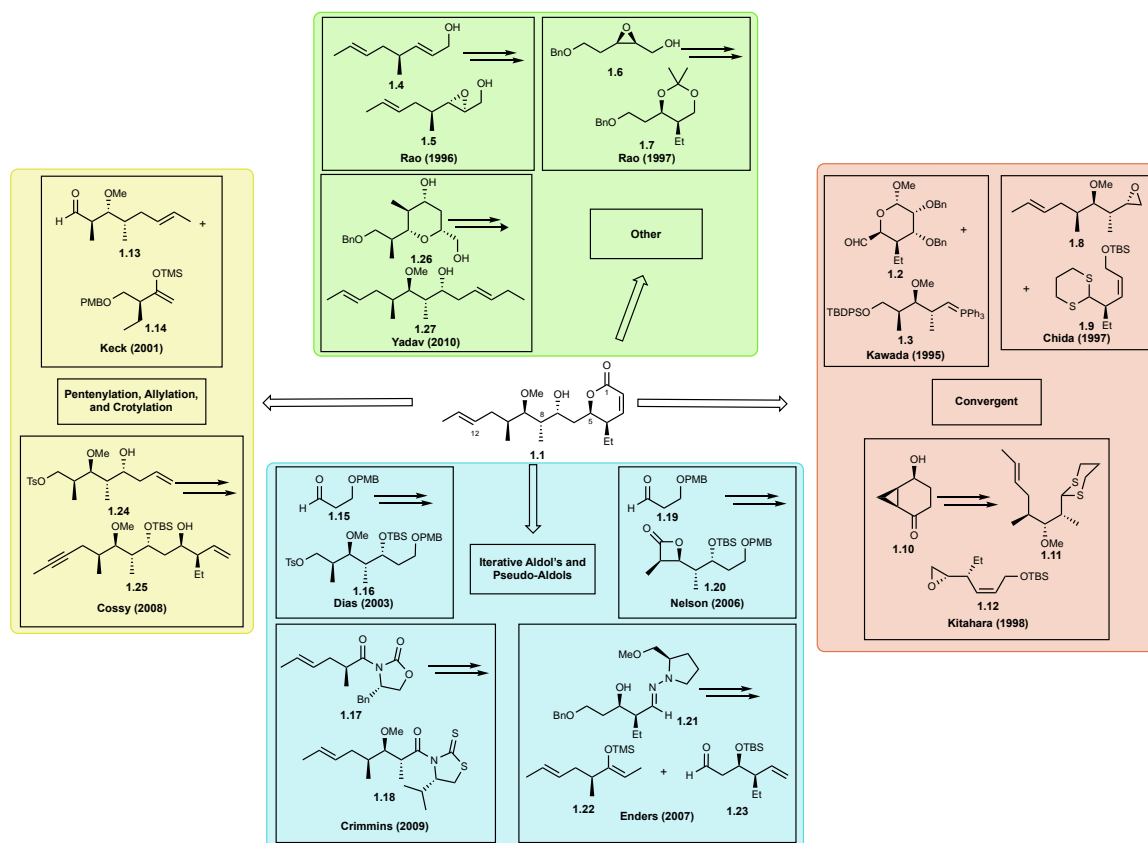


**Figure 1.3.** Summary of published pironetin total syntheses sorted into type of strategy: convergent, iterative aldols and pseudo-aldols, pentenylation, allylation, and crotylation, and other.

## 1.4 Total Syntheses of Pironetin

At the time of submission of this dissertation, 12 distinctive total syntheses of pironetin have been published, highlighting the synthetic and biological intrigue of this natural product. These syntheses have enabled the study of pironetin and its analogs and are summarized in Figure 1.3. They are divided into several classes: iterative aldol and pseudo-aldol condensations (blue), convergent syntheses (red), iterative pentenylation or crotylation (yellow), and other (green). While the authors have attempted to classify the syntheses in a simple manner, many of the syntheses do not conform to a single class and are placed where the most novel chemistry was developed.

The first total synthesis of pironetin was reported by Kawada and coworkers in 1995 and employed a convergent route starting from (*S*)-Roche ester and a substituted  $\alpha$ -D-glucopyranoside.<sup>52</sup> In 13 and 8 steps, respectively, the ester was converted to polypropionate fragment **1.3** and the pyranoside was converted to aldehyde **1.2**, which were then coupled under Wittig conditions. An additional 13 steps were required for installation of the unconjugated olefin and generation of the unsaturated lactone, a total of 34 steps. This total synthesis established the absolute configuration of the natural product.

In 1996, Rao and coworkers reported their first total synthesis of pironetin which relied upon iterative olefination, generating intermediate allylic alcohol **1.4**, followed by a highly diastereoselective Sharpless epoxidation to yield epoxide **1.5**. The linear synthesis was initiated from diethyl methylmalonate and required 35 total steps.<sup>53,54</sup> Improving upon their first synthesis, Rao and coworkers published a second linear total synthesis in 1997, the only non-convergent one to date which builds the molecule out from an established lactone core at an early stage. This synthesis began from propargylic alcohol and relied on a key Grignard addition to epoxide **1.6**, leading to **1.7**. The remaining *syn* stereochemistries were installed via an Evans aldol and a regiospecific reductive opening of a tertiary epoxide, yielding pironetin in 33 overall steps.<sup>55</sup>

In 1997, Chida and coworkers reported the convergent synthesis of pironetin from L-quebrachitol to set four consecutive chiral centers of the polyketide core **1.8** in 14 steps and L-malic acid to form alkene **1.9** in 9 steps. These intermediates were coupled and following functional group manipulation, pironetin was completed in 28 total steps.<sup>56</sup>

The final convergent synthesis of pironetin was reported in full by Kitahara and coworkers in 1998<sup>57</sup> and the route was utilized again in 1999 to generate demethylpironetin and other analogs, but these were not evaluated for biological activity.<sup>58</sup> Using chiral building block **1.10** (9 steps to synthesize), intermediate **1.11** was obtained in 13 steps, which was coupled with epoxide **1.12**. Compound **1.12** was synthesized from propargylic alcohol in 14 steps through addition of propargyl ether followed by hydrogenation, protecting group exchanges, and epoxidation. Coupling of **1.11** and **1.12** was followed by additional manipulation of the skeleton into pironetin, a total of 28 steps.

Keck's 2001 total synthesis applied three new methodologies developed by his group. Many other groups would continue to use these methods in pironetin total syntheses and analog development. Starting from (*S*)-Roche ester, aldehyde **1.13** was synthesized in 11 steps utilizing a diastereoselective crotylstannane addition<sup>59</sup> followed by conversion to the trans-olefin. Aldehyde **1.13** then underwent a Mukiyama aldol condensation with silyl enol ether **1.14** (generated in 5 steps), followed by the reduction of a  $\beta$ -hydroxy ketone to the *anti*-1,3-diol using samarium iodide,<sup>60</sup> and finished with a lactone annulation series,<sup>61</sup> a total of 17 steps.<sup>62</sup>

Following Keck's synthesis, a number of groups began on iterative aldol and pseudo-aldol condensations to generate the pironetin backbone. In 2003, Dias published the total synthesis highlighting iterative Evans' oxazolidinone mediated *syn*-aldol condensations to build out the backbone. This synthesis commenced from 1,3-propane diol and the condensations started with aldehyde **1.15** to grow out to intermediate **1.16**, which was converted into pironetin after additional steps.<sup>63</sup> Of note is the first use of a *Z* selective

olefination as the penultimate step.<sup>64</sup> Dias's synthesis of pironetin required 21 total steps, not including auxiliary synthesis.

One of the disadvantages of Evans' auxiliaries is the cleavage. In 2000 Crimmins disclosed the use of thiazolidinethione auxiliaries, which are easily cleavable directly to the aldehyde and other functional groups.<sup>65</sup> In 2009, Crimmins and coworkers reported the total synthesis of pironetin using this strategy starting from alkene **1.17** through intermediate **1.18** in 11 steps, including the penultimate *Z* olefination.<sup>64</sup> Synthesis of **1.17** requires four additional steps, for a total of 15 steps.<sup>66</sup>

In an effort to apply catalytic asymmetric aldols to pironetin's total synthesis, Nelson and coworkers developed acyl halide-aldehyde cyclocondensations (AACs) which generate enantioenriched  $\beta$ -lactones as propionate aldol units.<sup>67</sup> The total synthesis utilizing this approach was reported in 2006. Starting from 1,3-propane diol, aldehyde **1.19** was synthesized and underwent iterative AACs to generate intermediate **1.20**, followed by acylation, and lactonization to generate pironetin in 15 linear steps.<sup>68</sup>

The final iterative pseudo-aldol approach was published by Enders and coworkers in 2007 and employed the SAMP/RAMP hydrazone methodology that he developed throughout his career. Beginning from butanone, an asymmetric aldol with the SAMP hydrazone and subsequent trapping with 3-(benzyloxy)propanal generated hydrazone **1.21**, which was converted to aldehyde **1.23** in 5 steps. Silyl enol ether **1.22** was prepared from 3-pentanone in 5 steps. Mukiyama aldol condensation between **1.22** and **1.23** provided the  $\beta$ -hydroxyketone, which was converted to pironetin in a similar manner to Keck's total synthesis,<sup>62</sup> taking 17 total steps.<sup>69</sup>

In 2008, Cossy and coworkers published the total synthesis of pironetin by disclosing two methodologies developed in house. The synthesis began from (*S*)-Roche ester and underwent an enantio- and diastereoselective titanium mediated crotylation followed by an allylation with a similar complex to generate tosylate **1.24**. After tosyl displacement with propyne and methylation, the terminal olefin was oxidatively cleaved and subjected to a boron-mediated pentenylation, generating homoallylic alcohol **1.25**. The synthesis was completed through a one-pot hydrosilylation/ring-closing metathesis/protodesilylation, a total of 14 steps and the shortest synthesis of pironetin to date.<sup>70</sup>

The most recent total synthesis was reported in 2010 by Yadav's group and relied on iterative Prins cyclizations followed by reductive cleavage. Prins cyclization between an (*S*)-Roche ester-derived aldehyde and a diol generated tetrahydropyran **1.26**. Installation of the unconjugated olefin via functional group manipulation led to homoallylic alcohol **1.27**, which then underwent a second Prins cyclization. Pironetin was obtained following reductive opening, transformation to an acrylate, and ring-closing metathesis in 28 total steps.<sup>71</sup>

In addition to the total syntheses discussed above, a key fragment towards pironetin's synthesis has been synthesized (Figure 1.4), however the completed route has not been published.<sup>72</sup> Starting from a modified D-glucal (**1.28**), Ferrier rearrangement afforded the O-glycoside, which underwent protecting group exchange and Grignard addition to install pironetin's C4 ethyl substituent. Conversion to ketone intermediate **1.29** was achieved by a one carbon homologation using sodium cyanide followed by conversion to the aldehyde, a Grignard addition, and final oxidation. Synthesis of ketone **1.29** was completed in 11

steps. The Sarabia group envisioned completion of the total synthesis in a convergent manner through an aldol condensation with the remaining western fragment of pironetin followed by reveal of the lactone, however this has not yet been reported.

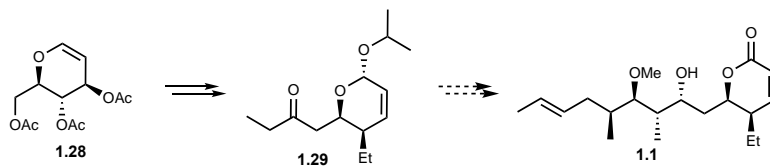


**Figure 1.4.** Chiron approach to the lactone fragment 1.29 by Sarabia and coworkers.

In all, many of the 12 total syntheses published highlight the utility of novel or new methodology. While this exceedingly short discussion does not do any of the chemistry justice, it becomes obvious that despite the small size of pironetin, this natural product is challenging to prepare and will hopefully continue to inspire chemists to invent new chemistry for its synthesis. Furthermore, the total syntheses discussed above have facilitated much of the discovery and development of fully elucidated pironetin analogs in order to explore the structure activity relationship (SAR).

## 1.5 Development of Pironetin's Structure-Activity Relationship

### 1.5.1 Early Studies – Isolated and Semi-Synthetic Analogs

Soon after pironetin's isolation from the *Streptomyces prunicolor*<sup>36, 37</sup> and *Streptomyces* sp. NK10958<sup>38</sup> bacteria strains, several additional derivatives were isolated from these same strains and semisynthesis led to a handful of others (Figure 1.5). Of note, demethylpironetin (**1.29**) and 2,3-dihydropironetin (**1.32**) were isolated from bacteria,<sup>73</sup> and epoxy-pironetin (**1.34**) was synthesized from pironetin.<sup>39</sup> These analogs were shown to be equipotent, 1000×, and 25× less potent than pironetin, respectively, in cell cycle arrest

assays, while tetrahydropironetin (**1.33**) lost 2000× activity.<sup>73</sup> A total synthesis of 3-hydroxy pironetin (**1.30**) and (+)-pironetin (**1.35**) revealed a 75× loss and a complete loss (10,000×) of activity, respectively.<sup>46</sup> Finally, total synthesis of epi-C7 pironetin (**1.31**) and C7 oxidation to generate ketone **1.28** led to 1000× and 100× loss of activity, respectively, as compared to pironetin.<sup>73</sup>

A number of O7 ethers, esters, carbonates, and carbamates have been synthesized from pironetin (Figure 1.4).<sup>50</sup> Each of these analogs lost activity as compared to pironetin. Notably, methyl ether **1.36** was 10× less potent; however installation and elongation of esters (series **1.37**) with alkyl chains showed that the activity could be mostly recovered in a few instances.<sup>73</sup> Conversion to carbonates (series **1.38**) or carbamate reduced activity by 30-80× over pironetin. The four O7 series of analogs were also evaluated for immunosuppressant activity. It was discovered that each of these analogs were potent in vitro immunosuppressants that inhibited the proliferative response of mouse spleen cells in

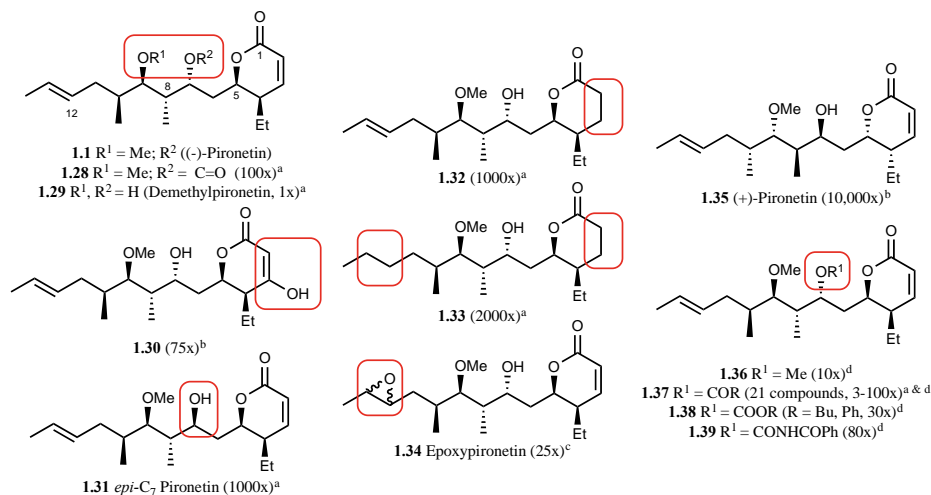


**Figure 1.5.** Early SAR exploration of pironetin (a. M phase arrest and microtubule disassembly;<sup>73</sup> b. MCF-7 cells;<sup>46</sup> c. M phase arrest;<sup>39</sup> d. EL4 cells<sup>50</sup>).

response to both T cell and B cell mitogens. The analog activities were comparable to pironetin's immunosuppressant activity (1-10× less active).<sup>50</sup>

### 1.5.2 Simplified Pironetin Analogs

Due to the complex syntheses required to generate pironetin analogs, several simplified pironetin series have been prepared and are summarized in Figure 1.6. Despite the simplified nature, these analogs still required at least eight steps to synthesize. The eight diastereomers making up Series I and the four of Series II were synthesized and both series of molecules showed a significant loss in cytotoxicity as compared to pironetin ( $\mu\text{M}$  vs nM) in the A2780 cell line.<sup>74</sup> The four pyrones in Series III and IV explored the necessity

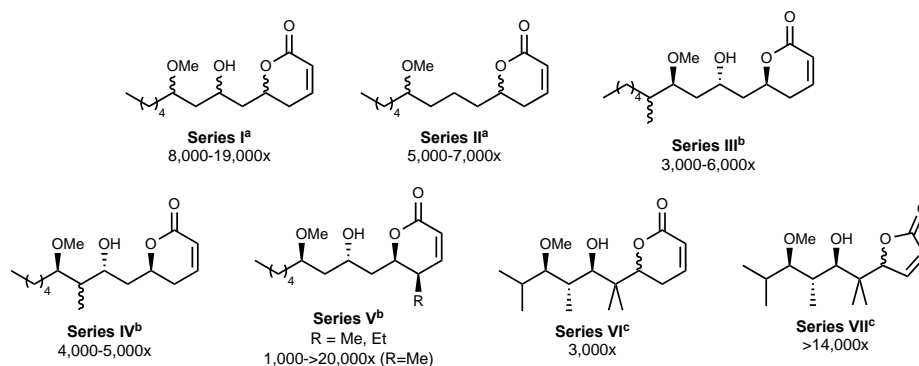


**Figure 1.6.** Simplified pironetin analogs. (a. A2780 cells;<sup>74</sup> b. A2780 cells;<sup>75</sup> c. MCF-7 cells<sup>76</sup>).

of the alkyl substituents along the polyketide backbone and again these analogs showed a significant loss of cytotoxicity in the A2780 cell line.<sup>75</sup> Finally, the last three series, V,<sup>75</sup> VI,<sup>76</sup> and VII,<sup>76</sup> evaluated the size of the lactone ring and substitution at the C4 position, demonstrating the importance of the  $\delta$ -lactone for cytotoxicity.

Taken together, these series demonstrate the importance of all alkyl pendants and the size of the lactone. Additionally, the presence of the C4 ethyl substituent in the *R*

configuration seems to significantly improve activity, as is evident when comparing series I and V, and an *anti*-relationship between the C5 and C7 substituents appears to be slightly preferred. The importance of the relative and absolute configuration between C5, C7, and C9 remains ambiguous as no clear preference was observed. Despite the loss in cytotoxicity as compared to pironetin, treatment with each series of compounds caused accumulation of cells in the G2/M phase and disrupted the microtubule network in a similar manner to pironetin, albeit at much higher concentrations than pironetin. This is important as it suggests that these simplified analogs interact with tubulin with the same general mechanism as pironetin.<sup>74</sup>

### 1.5.3 Fully Elucidated Analogs Through Total Synthesis

The lessons learned from the simplified pironetin SAR campaign showed that all alkyl pendants along the polyketide backbone seem necessary for high activity, highlighting the need for an extended study of fully elucidated pironetin analogs. Since pironetin covalently modifies  $\alpha$ -tubulin through the unsaturated lactone<sup>41, 42</sup> and an *in vivo* study reported significant weight loss,<sup>39</sup> the possibility of off-target effects through a covalent mechanism is likely, prompting an extensive SAR at the C2, C4, and C5 positions through total synthesis. These series are shown in Figure 1.7 and were evaluated for cytotoxicity against A2780, OVCAR5, or EL4 cell lines.

The C2 series was aimed at generating reversible covalent modification of  $\alpha$ -tubulin<sup>45</sup> to reduce off-target reactivity by incorporating electron-deficient groups.<sup>77, 78</sup> Analogs **1.40-1.43** demonstrated that alteration of the C2 site abolished activity, with only the  $\alpha$ -bromo analog **1.44**, retaining some activity. The C4/C5 series investigated the importance

of the lactone configuration<sup>44</sup> and determined that, unlike previous studies with simplified analogs by Marco and coworkers,<sup>74-76</sup> modification of the C5 configuration is not well tolerated, as is evident by the reduced activity of analogs **1.45** through **1.47**. The C4 analogs (**1.48-1.57**) probed the effects of epimerization, incorporation of larger and smaller substituents, and disubstitution. The results for this series suggested that a single substituent at C4 with the same configuration as the natural product is required. Some small alkyl C4 analogs were well tolerated, including cyclopropyl (**1.53**) and *n*-propyl (**1.51**), however bulkier groups, such as benzyl (**1.55**) and *iso*-propyl (**1.56**) resulted in substantial loss of activity.

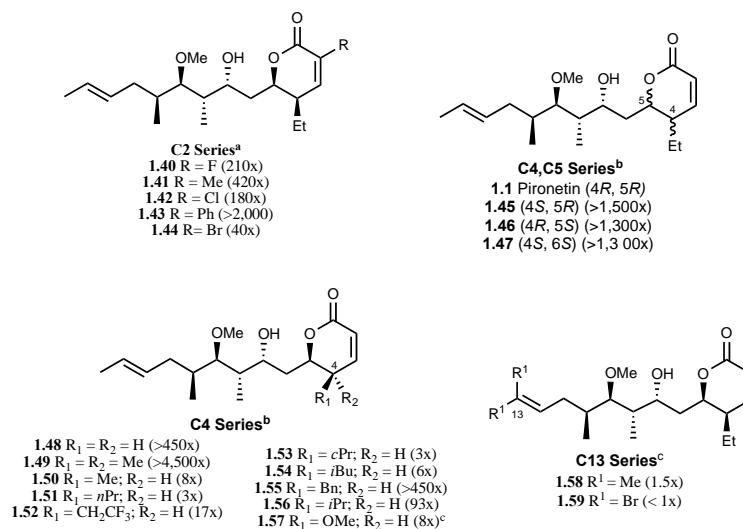


**Figure 1.7.** Pironetin analogs exploring C2, C4, and C5 through total synthesis and C13 through semisynthesis. (a. A2780 cells;<sup>45</sup> b. OVCAR5 cells,<sup>44</sup> c. EL4 cells<sup>50</sup>).

Finally, a small C13 series was generated in which the unconjugated olefin was converted to the 14,14-dimethyl (**1.58**) and the 14,14-dibromo (**1.59**) analogs. This was accomplished through ozonolysis of pironetin followed by olefination of the resulting aldehyde.<sup>50</sup> Both analogs were about equipotent to pironetin, suggesting that further

exploration of this olefin could be the key to improving the properties of this molecule towards future drug development.

#### **1.5.4 Lessons from Structural Biology**

Following the release of the co-crystal structures of pironetin with  $\alpha$ -tubulin, much of the reported SAR can be explained and rationalized (Figure 1.8). The C4 ethyl substituent binds in a narrow hydrophobic pocket and contacts Leu378. Inclusion of a smaller group, such as methyl, reduces this hydrophobic interaction, while inclusion of a bulkier group, such as isopropyl, cannot be accommodated in this small hydrophobic pocket. Further, altering the configuration at C4 or C5, or including two substituents at C4 would alter the ring conformation. The removal of the alkyl side chains along the polyketide backbone may alter the preferred conformation of the pironetin analogs. In addition, the lactone of pironetin is positioned near a  $\beta$ -sheet, at a distance of 4.7 Å, which indicates why the introduction of C2 substituents could not be tolerated. Finally, the most successful analogs have been the C13 series, which take advantage of a small pocket of available space flanked by hydrophobic residues and Cys4. Despite the extensive SAR around pironetin, no analogs have been co-crystallized with tubulin.

#### **1.6 Future Directions and Questions of Interest**

The development of new microtubule targeting agents remains of quintessential importance, particularly the discovery and development of agents with novel interactions with microtubules. Many questions remain, some of which were recently highlighted,<sup>16</sup> however many other ideas require attention, including studying how microtubule

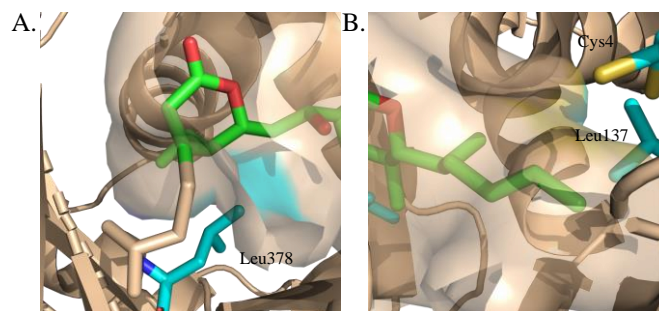


**Figure 1.8.** Insight into pironetin's SAR (PDB: 5FNV). **A.** Pironetin's lactone is placed against a  $\beta$ -sheet strand. The C4 ethyl substituent fills a hydrophobic pocket, favorably contacting Leu378. **B.** Pironetin's polyketide backbone ends in a partially open pocket framed by Cys4 and Leu137. The alkyl pendants do not appear to make direct interactions but could aid in pironetin's assembly into the proper conformation for binding.

targeting agents impact the interaction of microtubules and microtubule associated proteins. Understanding the disparity between  $\beta$ -tubulin and  $\alpha$ -tubulin targeting molecules is of interest and could be aided by developing methodology in which to better study and characterize MTA interactions with microtubules in cellular, biophysical, and biochemical assays. Particularly with the improvements in structural biology and screening technologies, discovery of natural product and non-natural product-like molecules that bind  $\alpha$ -tubulin should be possible.

In addition to discovering new  $\alpha$ -tubulin targeting scaffolds, further development of the pironetin SAR is key. Due to the difficulty in synthesizing analogs, there remains a significant gap in knowledge, and of utmost importance is the development of pironetin analogs that show improved PK/PD properties, generating at least tool compounds that would allow in vivo evaluation of an  $\alpha$ -tubulin targeting agent. Further, development of non-covalent or targeted  $\alpha$ -tubulin specific agents is critical as this would likely reduce off-target binding and increase the utility and safety profile significantly. Despite the reported

crystal structures, the complexity of pironetin's binding mode (covalent and induced fit) substantially complicate and limit computational methods which should be used to discover additional scaffolds or design analogs. Using protein-based methods, for example, docking, even using CovDock, is oversimplified and does not correlate with activity data.<sup>44</sup> Using ligand-based methods, such as QSAR or pharmacophore modeling, could provide more accurate predictions for driving the development of pironetin and other pironetin-site binding molecules.

Finally, the importance and utility of targeting  $\alpha$ -tubulin instead of (or in combination with)  $\beta$ -tubulin is entirely unknown territory. Pironetin's binding site is separate from all approved  $\beta$ -tubulin targeting molecules, explaining why pironetin is active in cells that have become resistant to  $\beta$ -tubulin targeting drugs. Interestingly, a pironetin-resistant cell line has not been disclosed. This indicates that pironetin or  $\alpha$ -tubulin binders could be useful probes to understand  $\beta$ -tubulin resistant cancers and show great utility against tumors that have become resistant to first line tubulin-binding chemotherapeutics.

## Chapter 2: Identification of Pironetin's Metabolic Liabilities

\*Adapted from Coulup, S.K. et al. J. Med. Chem. 2019, 62, 1684-1689.

### 2.1 Introduction

All microtubule inhibitors currently approved by the FDA bind to  $\beta$ -tubulin, and the development of an agent that binds instead to  $\alpha$ -tubulin has the potential to be active in cancers resistant to taxanes and other microtubule inhibitors which target  $\beta$ -tubulin. Given the overall success of  $\beta$ -tubulin-binding anticancer agents in cancer chemotherapy,  $\alpha$ -tubulin is an attractive target. In addition, it was recently shown that the gene encoding  $\alpha$ -tubulin isoform TUBA3C is overexpressed in ovarian cancers and is associated with increased resistance to first-line chemotherapeutics and shorter survival time.<sup>35</sup> Pironetin (**1.1**, Figure 2.1A) is the only natural product structurally characterized by x-ray crystallography to bind  $\alpha$ -tubulin. Pironetin covalently binds to Cys316 of  $\alpha$ -tubulin (Figure 2.1B).<sup>40, 41</sup>

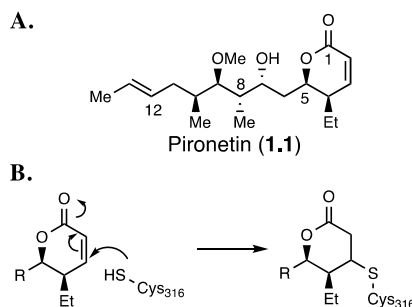


**Figure 2.1.** Structure and binding mode of pironetin. **A.** Pironetin (**1.1**) is an  $\alpha,\beta$ -unsaturated lactone which **(B.)** covalently binds with Cys316 of  $\alpha$ -tubulin in a 1,4-conjugate addition.

Due to pironetin's unique properties, several groups have recently reported the synthesis and in vitro evaluation of pironetin analogs, including structurally simplified

analogs.<sup>44, 45, 74, 75, 79</sup> While pironetin has promising in vitro activity, the causes of the poor in vivo activity need to be identified and addressed in order to arrive at a lead compound. To address these issues, we report the identification of pironetin's major metabolites in human liver microsomes (HLM) using mass spectrometry and semisynthesis.

## 2.2 Preliminary In Vitro PK Evaluation

In an effort to explain pironetin's poor in vivo efficacy, we first characterized the in vitro PK profile of pironetin (Table 2.1). Pironetin displays a short serum half-life in human, mouse, and rat preparations (performed by Dr. David Huang) and a short half-life in each species of liver microsomes. These data suggest that a key reason for the marginal in vivo activity could be rapid metabolism.

**Table 2.1.** In vitro PK properties of pironetin

	<b>Human</b>	<b>Mouse</b>	<b>Rat</b>
Serum Stability (%) <sup>b</sup>	50	35	56
Metabolic t <sub>1/2</sub> (min) <sup>a</sup>	7	<15 <sup>c</sup>	<15 <sup>c</sup>
% Protein Bound <sup>a</sup>	87	98	93

<sup>a</sup> Performed by Eurofins-CEREP

<sup>b</sup> % Remaining after 24 h

<sup>c</sup> Undetected after 15 min

In addition to serum and microsomal half-life, we submitted pironetin for P450 inhibition studies to evaluate the potential for drug-drug interactions against Cyp2C9, 2D6, and 3A4 and found pironetin slightly inhibits metabolism of midazolam and testosterone by Cyp3A4 but not at relevant concentrations based on pironetin's cytotoxicity in vitro (Table

2.2). Pironetin does not significantly inhibit metabolism of tolbutamide (by 2C9) or dextromethorphan (by 2D6) but has a small effect on the metabolism of midazolam or testosterone (both by 3A4).

**Table 2.2.** Inhibition of P450 isoforms by pironetin

	IC <sub>50</sub> (μM) <sup>a</sup>			
	2C9	2D6	3A4- Midazolam	3A4- Testosterone
Sulfaphenazole	0.54	-	-	-
Quinidine	-	0.11	-	-
Ketoconazole	-	-	0.018	0.30
Pironetin	>50	>50	28.99	37.79

<sup>a</sup> Performed by Pharmaron

### 2.3 Identification of Metabolic Soft Spots in HLM

Identification of metabolic soft spots can aid in lead design and also minimize potential safety concerns, such as the formation of reactive or toxic metabolites<sup>80, 81</sup> or drug-drug interactions.<sup>82</sup> Liquid chromatography-mass spectrometry (LC-MS) is a leading method for metabolite identification.<sup>83-86</sup>

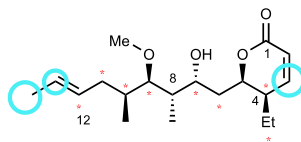


**Figure 2.2.** SMARTCyp predicted sites of pironetin metabolism. The top three predicted sites for the Cyp3A class are circled. Sites with a score of <70 are indicated with a star.

Pironetin's sites of metabolism were predicted using the SMARTCyp software prior to performing experiments.<sup>87</sup> SMARTCyp is a 2D method primarily used to predict P450-

mediated metabolites from the Cyp3A, 2D, and 2C classes. Sites are scored based on fragment matching reactivity, accessibility of the site of metabolism to the heme core of the cytochrome P450's, and solvent accessible surface area with the lowest score being the most likely site of metabolism. When pironetin was evaluated by SMARTCyp, nearly every carbon along the pironetin backbone held reasonably low scores (score of 70 or less, Figure 2.2 red stars), while the remaining sites, C5 and C10, had scores less than two above the cut off. The C8 methyl groups and C10 were scored between 10 and 12 above the cut off. The score cut off was determined based on known metabolites of current therapeutics. This prediction suggests that pironetin is labile to P450-mediated oxidation, further strengthening our hypothesis that pironetin's utility could be significantly limited by rapid metabolism.

To identify the sites of metabolism, pironetin was incubated with HLM and a NADPH regeneration system for up to an hour. The resulting samples were analyzed by LC-MS on a Thermo Orbitrap Velos using atmospheric pressure chemical ionization (APCI). LC-MS revealed that pironetin has two major metabolites, **M2** and **M4**, and at least three minor metabolites, **M1**, **M3**, and **M5** (Figure 2.3A). Analysis of the MS spectrum of pironetin (Figure 2.3B) and the major metabolite **M4** (Figure 2.3E) revealed a single oxidation site near the unconjugated olefin. The MS spectrum of **M2** (Figure 2.3D) suggests secondary oxidation of **M2** predicted to occur around the lower half of the lactone or along the backbone closest to the lactone. Metabolites **M1** and **M3** are predicted to be isomers of the pironetin ketone which has also been oxidized along the eastern most backbone (Figure 2.3C) and the minor metabolite **M5** is formed by a demethylation (Figure 2.3F). Based on

the importance of **M4**, we next sought to confirm the structure of this major metabolite through semisynthesis of epoxy-pironetin (**M4**). Further, as demethylpironetin (**M5**) has previously been isolated from pironetin-producing bacteria strains, we wished to confirm demethylpironetin as a minor metabolite.<sup>88</sup>

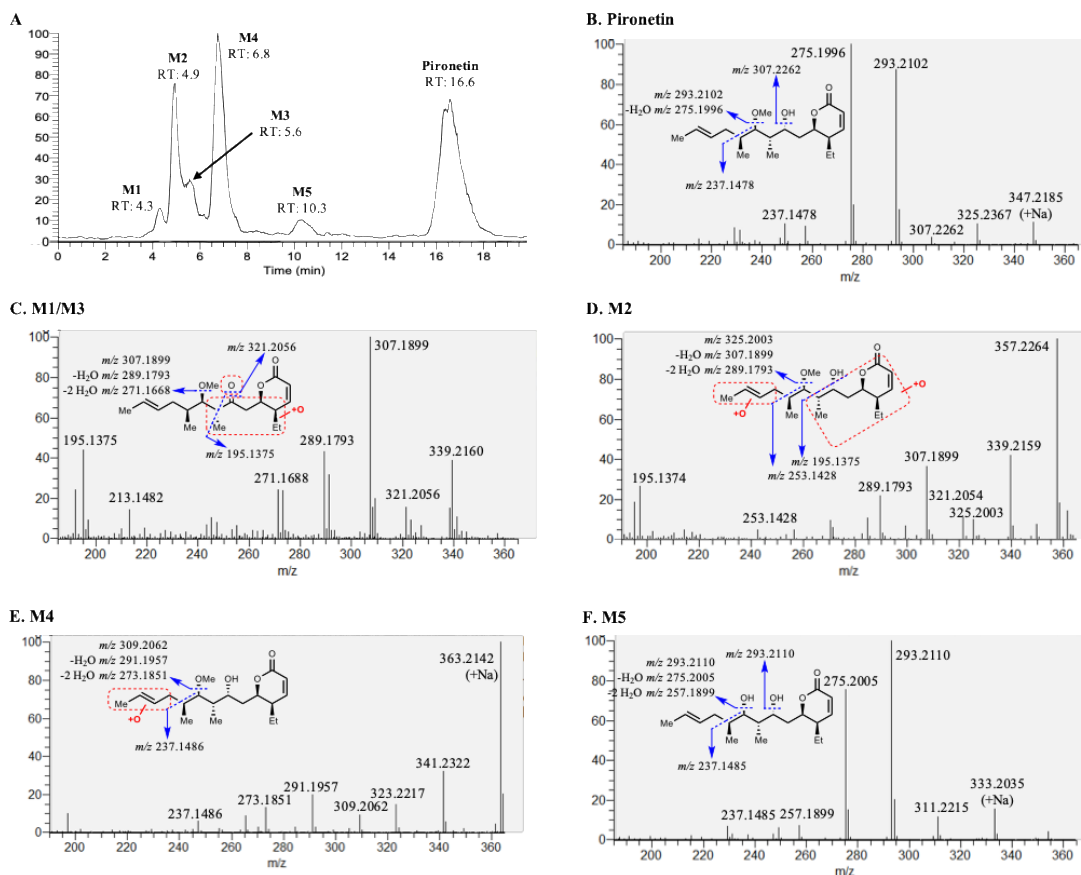
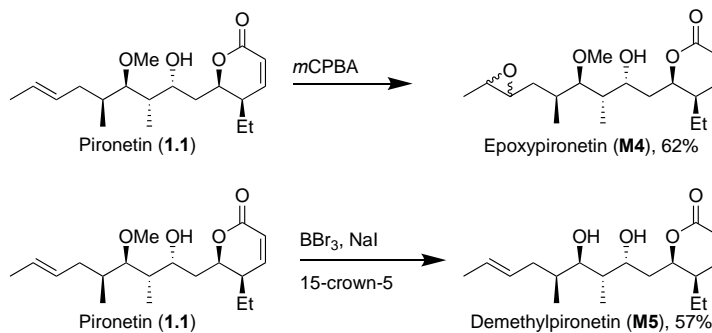


**Figure 2.3.** Pironetin has two major metabolites (**M2** and **M4**) and three minor metabolites (**M1/M3** and **M5**). A. LC trace of human liver microsome sample showing pironetin and its five metabolites formed after a 30 min incubation. MS traces of B. pironetin; C. **M1/M3**; D. **M2**; E. **M4**; and F. **M5** with fragmentation patterns and the predicted locations of metabolism highlighted.

## 2.4 Semisynthesis of Epoxypironetin and Demethylpironetin

Since the primary pironetin metabolite (**M4**) showed oxidation around the non-conjugated olefin, we hypothesized this could correspond to either epoxidation of the olefin or oxidation at one allylic position. An authentic sample of the predicted metabolite epoxypironetin was synthesized from pironetin as shown in Scheme 2.1. Pironetin was obtained from the fermentation broth of *Streptomyces prunicolor* as previously described,<sup>36,37</sup> and was then treated with *m*CPBA to afford epoxypironetin. Efforts towards allylic oxidation of the model substrate using selenium dioxide were unsuccessful, and due to the limited amount of pironetin available, Riley oxidation of pironetin was not attempted. In addition to epoxypironetin, demethylpironetin is a natural product which has also been isolated from pironetin producing *Streptomyces* strains.<sup>88</sup> Since **M5** from the metabolite

**Scheme 2.1.** Synthesis of epoxypironetin (**M4**) and demethylpironetin (**M5**)



identification studies suggested demethylation as a minor metabolic pathway, we hypothesized this metabolite could correspond to demethylpironetin. An authentic sample of demethylpironetin was synthesized from pironetin with BBr<sub>3</sub> as shown in Scheme 2.1.<sup>89</sup> To evaluate whether epoxypironetin or demethylpironetin were metabolites **M4** and **M5**, respectively, we obtained LC-MS traces of both potential metabolites and determined that

the retention time (Figure 2.4) and fragmentation pattern (Figure 2.5) of the major pironetin metabolite produced by HLM (**M4**) matched the epoxy pironetin trace. Demethylpironetin was present (**d**) but in trace amounts as compared to epoxy pironetin. Together, these data suggest that epoxy pironetin is a major metabolite in HLM while demethylation is not a significant metabolic liability. As epoxy pironetin matched the major metabolite, further efforts towards synthesizing pironetin allylic alcohols were not pursued.

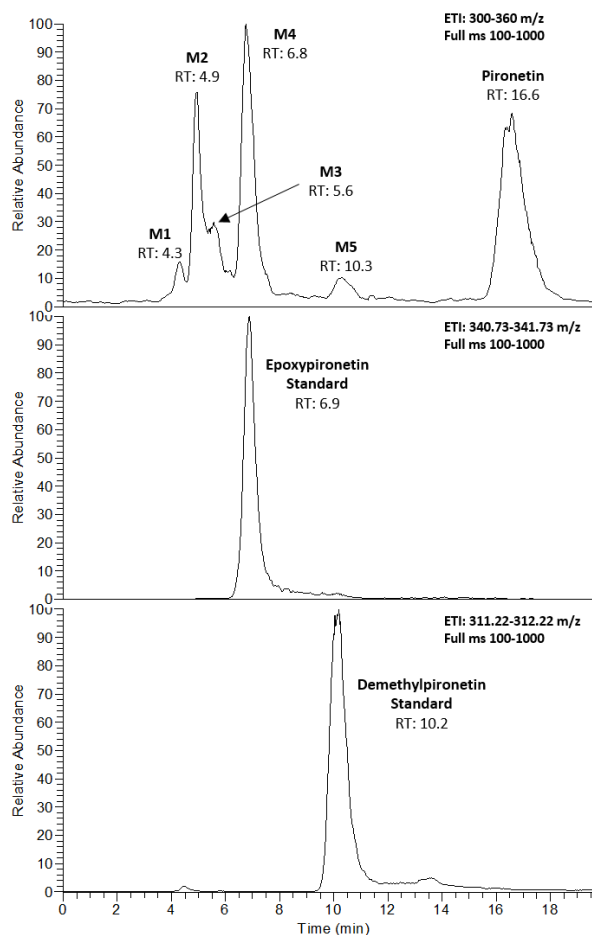


**Figure 2.4.** LC traces of human liver microsome reaction (top) compared to the synthesized epoxy pironetin (**M4**, middle) and demethylpironetin (**M5**, bottom) standards.

## 2.5 Biological Evaluation

We determined the antiproliferative activity of pironetin, demethylpironetin, and epoxyronetin against chemotherapeutic sensitive and resistant ovarian cancer cell lines (Table 2.3).<sup>90</sup> Epoxyronetin was previously synthesized from pironetin and demethylpironetin was previously isolated from pironetin producing bacteria strains.<sup>39,91</sup> These derivatives were shown to be approximately 25-fold less effective and equipotent, respectively, than pironetin in arresting 3Y1 rat fibroblast cells at the G2/M phase.<sup>39</sup> Additionally, epoxyronetin was found to have a minimum inhibitory concentration against A2780 sensitive ovarian cancer cells of 540 nM (as compared to pironetin's 26 nM).<sup>91</sup>

**Table 2.3.** In vitro cytotoxicity evaluation of pironetin, epoxyronetin, and demethylpironetin

	GI50 (nM) <sup>a</sup>	
	A2780 <sup>b</sup>	A2780CP <sup>c</sup>
Pironetin ( <b>1.1</b> )	22.2 ± 1.0	22.3 ± 3.0
Epoxyronetin ( <b>M4</b> )	218.2 ± 1.8	1014.9 ± 1.3
Demethylpironetin ( <b>M5</b> )	29.6 ± 1.4	82.3 ± 1.9

<sup>a</sup> Each measurement is in triplicate on a minimum of two separate experiments

<sup>b</sup> Drug-sensitive ovarian cancer cell line

<sup>c</sup> Cisplatin-resistant ovarian cancer A2780 cell line

A2780 is a sensitive ovarian cancer cell line that was harvested from the tumor tissue of an untreated patient.<sup>92</sup> A2780CP was derived from chronic exposure of the sensitive A2780 strain to cisplatin, rendering this strain resistant to cisplatin treatment.<sup>93</sup> Our data is consistent with previous reports and confirms that pironetin and demethylpironetin display

similar cytotoxicity against the A2780 sensitive ovarian cancer cell line, while epoxyronetin is approximately 20-fold less cytotoxic than pironetin. Additionally, our data shows that both demethylpironetin and epoxyronetin are four times and 46-fold less cytotoxic than pironetin in A2780CP cells, respectively.

## 2.6 Discussion and Conclusion

Our data establishes that pironetin is rapidly and extensively metabolized, primarily to epoxyronetin, which displays significantly reduced cytotoxicity. It is probable that the epoxide has a short half-life *in vivo* due to its high electrophilicity. The liver contains a high concentration of nucleophilic glutathione (GSH) (~7 mM) as well as microsomal and soluble epoxide hydrolases (EH), which catalyze the hydration of epoxides to form the diol. Neither GSH or EH were present in the human liver microsome preparations utilized here, however both reactions are common detoxification methods which could further explain the marginal *in vivo* efficacy.<sup>94, 95</sup>

In summary of this chapter, we have shown that the natural product pironetin is rapidly metabolized to several metabolites in human liver microsomes. We identified the major site of metabolism of the natural product pironetin to be the unconjugated olefin, as well as found several minor labile sites along the backbone. Further investigation revealed the major metabolite to be epoxyronetin (**M4**), which was confirmed when the synthesized epoxyronetin standard matched the retention time and fragmentation pattern of the major metabolite formed. Epoxyronetin loses between 20- and 50-fold activity against the two ovarian cancer cell lines tested. Epoxyronetin is further oxidized along the eastern portion of the molecule to generate the second major metabolite. Additionally, two minor, isomeric

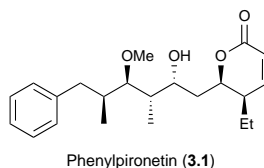
metabolites are formed by the dual oxidation of the eastern portion, and the demethylation of C9 leads to the minor metabolite demethylpironetin (**M5**), as determined by semisynthesis.

These results were partially predicted by the use of the SMARTCyp software, which predicted metabolism along most of the aliphatic backbone. Pironetin was also shown to slightly inhibit metabolism of midazolam and testosterone, both metabolized by Cyp3A4. As pironetin has nM cytotoxicity and is rapidly metabolized, it is unlikely that the concentration of pironetin will ever be high enough to affect drug metabolism through Cyp3A4. These data show that pironetin has several major metabolic liabilities which need to be addressed in order for a lead molecule to emerge. Further, our work provides an explanation for the marginal in vivo efficacy of pironetin. In summary, we have shown that the natural product pironetin is rapidly metabolized to several metabolites. We identified the major site of metabolism of the natural product pironetin to be the unconjugated olefin in human liver microsomes, as well as found several labile sites along the backbone. Further investigation suggests the major metabolite in HLM to be epoxy pironetin (**M4**), which was independently synthesized and found to have matching retention time and fragmentation pattern to the major pironetin metabolite formed in both microsomal preparations.

## Chapter 3: Total Synthesis and Evaluation of a Metabolically Stabilized Pironetin Analog

### 3.1 Introduction

We have shown that pironetin is rapidly metabolized by human liver microsomes (HLMs) to epoxy-pironetin (**M4**) and several additional metabolites with reduced potency and the presumed ability to be detoxified or form adducts.<sup>49</sup> We therefore were interested in determining if blocking the unconjugated olefin site of metabolism would improve the metabolic stability while maintaining potency. In addition, we and others have reported that demethylpironetin, a natural product isolated from pironetin producing bacteria strains, has similar potency to pironetin against sensitive and resistant ovarian cancer cell lines. We were therefore interested in developing the first synthetic route towards demethylated analogs. To begin to address the first hypothesis, Dr. David Huang first synthesized



	Phenylpironetin
GI <sub>50</sub> (OVCAR5 <sup>a</sup> )	57 nM
GI <sub>50</sub> (A2780 <sup>a</sup> )	68 nM
Liver Microsome Half-Life (Human) <sup>b</sup>	5 min
Liver Microsome Half-Life (Mouse) <sup>b</sup>	4 min

<sup>a</sup> Drug-sensitive ovarian cancer cell line.

<sup>b</sup> Performed by CEREP.

**Figure 3.1.** Cytotoxicity and metabolism evaluation of phenylpironetin (**3.1**) in cells and liver microsomes. Synthesis and cellular evaluation performed by Dr. Huang.

phenylpironetin (**3.1**) and evaluated it against sensitive ovarian cancer cells lines and for metabolic half-life in human and mouse liver microsomes (Figure 3.1, unpublished data).

Dr. Huang showed that while cytotoxicity was maintained, the metabolism was not improved over pironetin. To continue analog exploration towards improved metabolic stability while also developing the first route towards demethylated pironetin analogs, we sought to synthesize 4-fluorophenyldemethylpironetin. We report here efforts towards the total synthesis and biological evaluation of 4-fluorophenyldemethylpironetin (**3.2**, Figure 3.2) in which the unconjugated olefin has been replaced to improve metabolic stability.

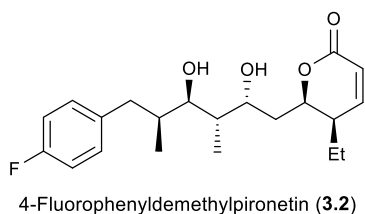


**Figure 3.2.** Structure of target molecule 4-fluorophenyldemethylpironetin.

## 3.2 Synthesis of 4-Fluorophenyldemethylpironetin (**3.2**)

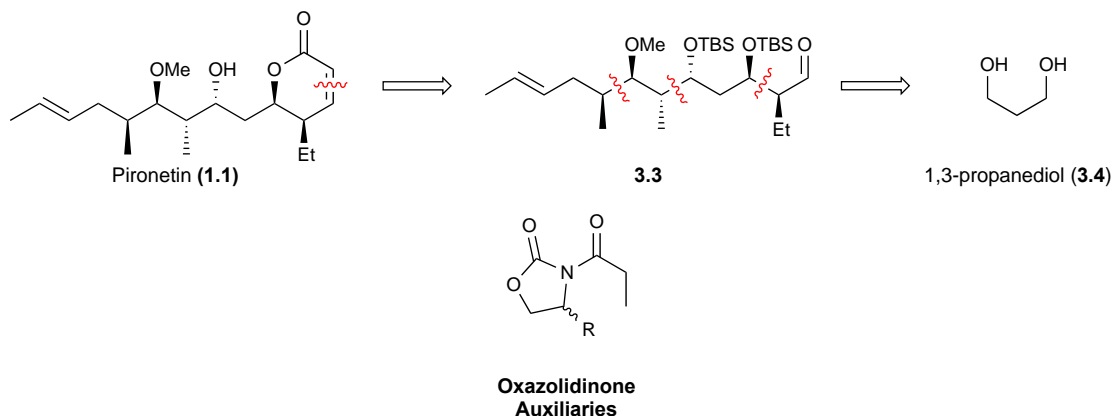
### 3.2.1 Route Design

At the time of initiation of this synthesis, no route towards demethylated pironetin derivatives had been published. To address this, we initially embarked on the total synthesis utilizing similar chemistry and disconnects adapted from the phenylpironetin (**3.1**) synthesis. However, during our exploration towards synthesizing 4-fluorophenylpironetin, it became evident that the presence of fluorine significantly hindered several stages of this chemistry, including the deoxygenation and debenzoylation following Grignard addition and the final aldol condensation. Due to these insurmountable issues, we moved through a few routes before settling instead to an iterative aldol route that would allow for rather late

stage incorporation of the desired olefin replacement and allow for greater flexibility in synthesizing additional molecules of interest. We turned to the literature to find potential starting materials and auxiliaries.

As described in the introduction, Dias and coworkers published the total synthesis of pironetin, outlined in Scheme 3.1, which utilized three iterative aldol condensations through intermediate and disconnects **3.3**, with Evans' oxazolidinone auxiliaries and a tosylate displacement to install the unconjugated olefin, starting from 1,3-propanediol (**3.4**).

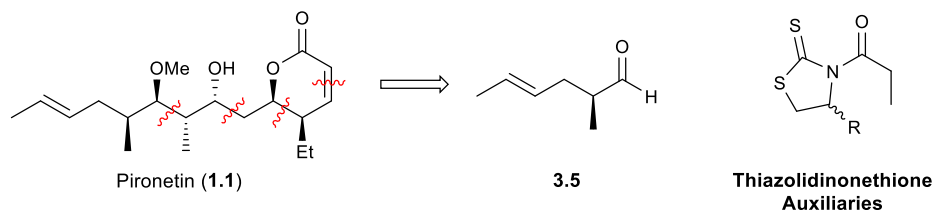
**Scheme 3.1.** Retrosynthesis of Dias's total synthesis using Evans' oxazolidinone auxiliaries starting from 1,3-propane diol<sup>63</sup>



We found this route to be a good starting point, however due to the inability to cleave the oxazolidinone directly to the corresponding aldehyde, thus adding unnecessary steps and chromatography, we decided to instead use Crimmins' thiazolidinonethione auxiliaries.<sup>65, 96, 97</sup> These were employed in his group's total synthesis of pironetin, highlighted in the introduction and shown briefly in Scheme 3.2.<sup>66</sup> Aldehyde **3.5** was prepared in eight steps from crotyl bromide and ethyl acetate. Additionally, several

different auxiliaries were utilized (R=benzyl, tri-methylated benzyl, isopropyl) and we were interested in investigating whether a single pair of non-acylated enantiomeric auxiliaries could efficiently yield the desired diastereomers. Most importantly, in contrast to the oxazolidinone auxiliaries, the thiazolidinonethiones can be cleaved directly to the aldehyde using DIBAL-H. Further, the un-acylated auxiliary can be recovered and reused, providing sustainability.

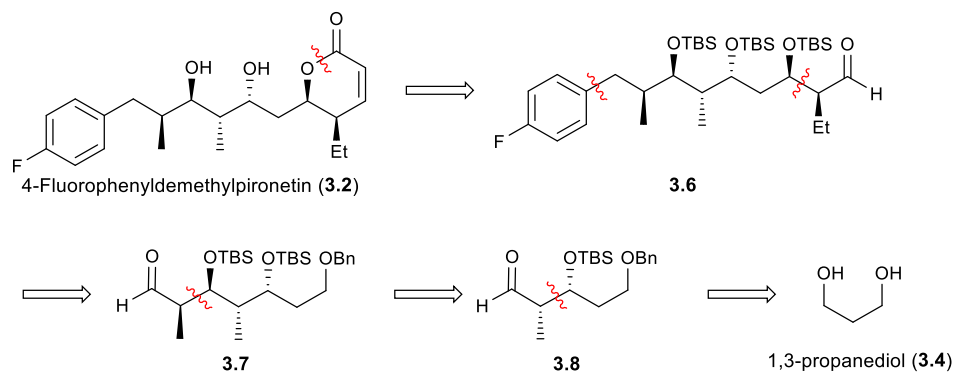
**Scheme 3.2.** Crimmins' total synthesis utilized thiazolidinonethione auxiliaries<sup>66</sup>



### 3.2.2 Retrosynthesis and Synthesis of Auxiliaries

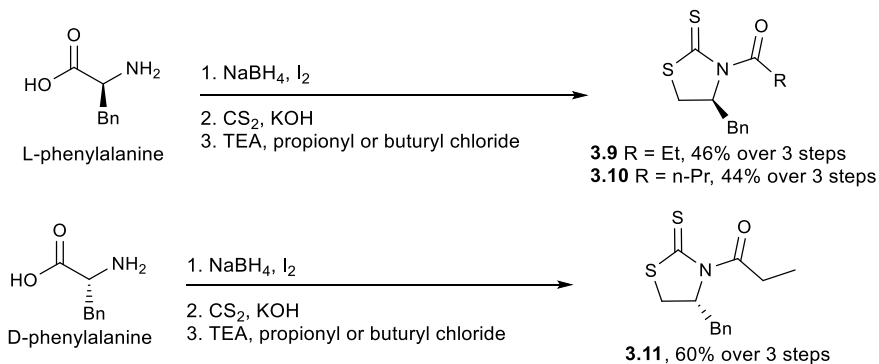
Utilizing the starting material and general disconnects from Dias' total synthesis and the Crimmins' auxiliary, the retrosynthetic analysis of 4-fluorophenyl-demethylpironetin (**3.13**) is outlined in Scheme 3.3. We envisioned formation of the  $\alpha,\beta$ -unsaturated lactone through a cis-selective Horner-Wadsworth Emmons reaction with aldehyde **3.6** followed by treatment with acid to yield **3.2**. Aldehyde **3.6** can be obtained from the sequential Grignard addition, deoxygenation, and aldol condensation with aldehyde **3.7**, which can be derived from iterative aldols going through aldehyde **3.8**. The starting material, 1,3-propane diol (**3.4**) is readily available and the aldol condensations can easily be scaled up to several gram quantities. To begin our synthesis, we decided to use phenylalanine-derived chiral auxiliaries as one of the aldol intermediates was already published and characterized

### Scheme 3.3. Retrosynthesis of 4-fluorophenyldemethylpironetin



and we found the chemistry to be highly reproducible.<sup>98</sup> These auxiliaries were easily synthesized in large quantities from D- or L-phenylalanine in three steps, Scheme 3.4.<sup>65</sup>

### Scheme 3.4. Synthesis of thiazolidinone thione chiral auxiliaries



#### 3.2.3 Synthesis of Alcohol Intermediate 3.18

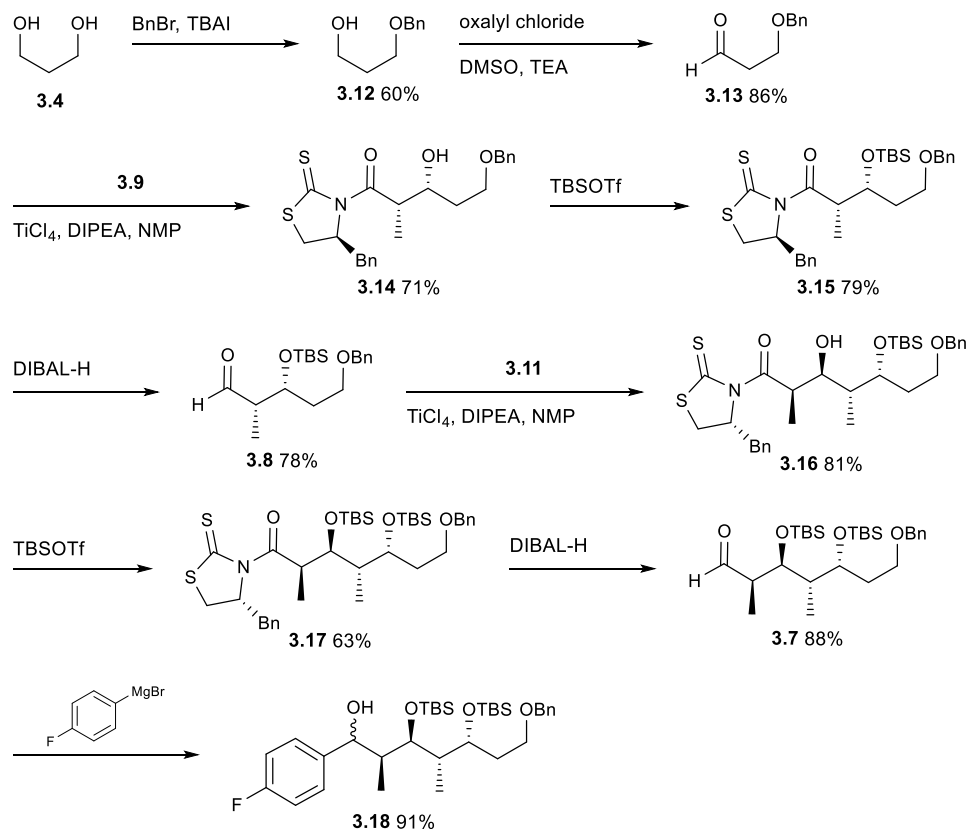
In the forward direction (Scheme 3.5), 1,3-propanediol (**3.4**) was treated with TBAI followed by benzyl bromide to yield benzyl ether **3.12**. Swern oxidation of **3.12** to aldehyde **3.13** set up for the first aldol condensation with thiazolidinonethione **3.9** via the uncoordinated titanium enolate to yield the Evan's syn alcohol **3.14**. Silyl protection led to **3.15** and removal of the chiral auxiliary with DIBAL-H generated aldehyde **3.8**, which was used for the second aldol condensation with thiazolidinonethione **3.11**. Subsequent silyl

protection to **3.17** and removal of the auxiliary revealed aldehyde **3.7**. Addition of 4-fluorophenyl magnesium bromide yielded alcohol **3.18** as a pair of diastereomers, which were both carried forward.

It was envisioned that benzylic deoxygenation and debenzylation could occur in a similar way as accomplished in the phenylpironetin synthesis by Dr. Huang (Scheme 3.6).<sup>99, 100</sup>

Alcohol **3.19** was oxidized to the corresponding aldehyde and then subjected to Grignard addition to provide secondary alcohol **3.20**, which activated with trifluoroacetic anhydride and deoxygenated with Pd/C and H<sub>2</sub> under a balloon. This concurrently deoxygenated and debenzylated the molecule to furnish alcohol **3.21** (Dr. Huang's unpublished results).

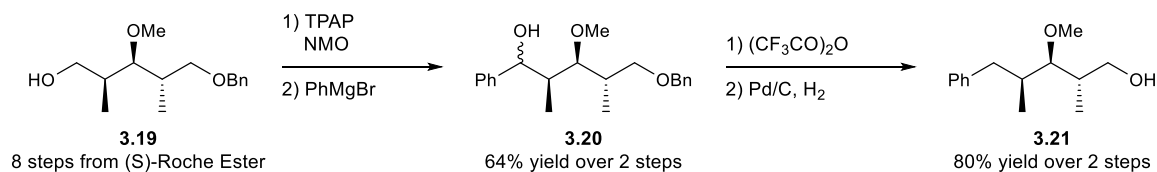
**Scheme 3.5.** First half of the synthesis of 4-fluorophenyl demethylpironetin



### 3.2.4 Deoxygenation and Debonylation Optimization

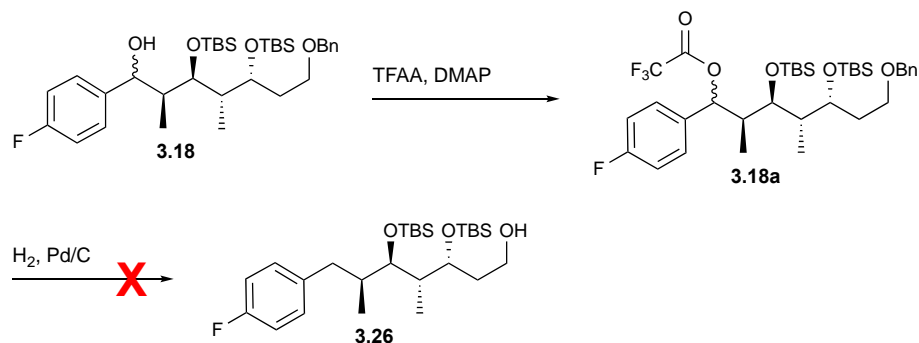
Attempts to accomplish the same deoxygenation and debonylation sequence with the 4-fluorophenyl demethylpironetin derivative failed, Scheme 3.7. Conversion of alcohol **3.18** to trifluoroacetate **3.18a** proceeded cleanly and fully. However, neither the deoxygenation nor the debonylation would readily occur. Initially, we believed that the Pd was getting quenched due to the various reactions involving sulfur-containing molecules in the synthesis leading up to **3.18**, however even when filtering and adding

#### Scheme 3.6. Key conversion in the phenylpironetin synthesis



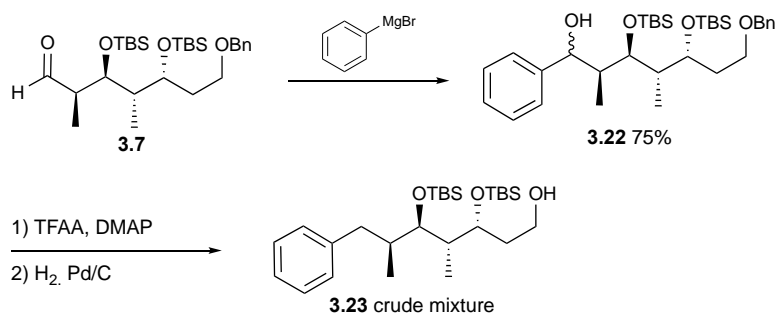
fresh Pd (up to stoichiometric amounts) the reaction never went to completion. Altering the solvent resulted in partial or full TBS deprotection, increasing the pressure for short periods of time led to starting material and TBS deprotection.

#### Scheme 3.7. Initial attempt at deoxygenation and debonylation



To evaluate whether the fluorine or the route was the issue, the phenyldemethylpironetin intermediate was synthesized (**3.23**) from aldehyde intermediate **3.7** (Scheme 3.8). A crude and small-scale conversion to the trifluoroacetate followed by Pd/C and H<sub>2</sub> led to about 50% deoxygenation and debenzylation over a few hours, suggesting that the fluorine was inhibiting reactivity. Additionally, the 4-chlorophenyl precursor was synthesized, and the deoxygenation and debenzylation was sluggish and low yielding, further suggesting that addition of an electron withdrawing group, such as

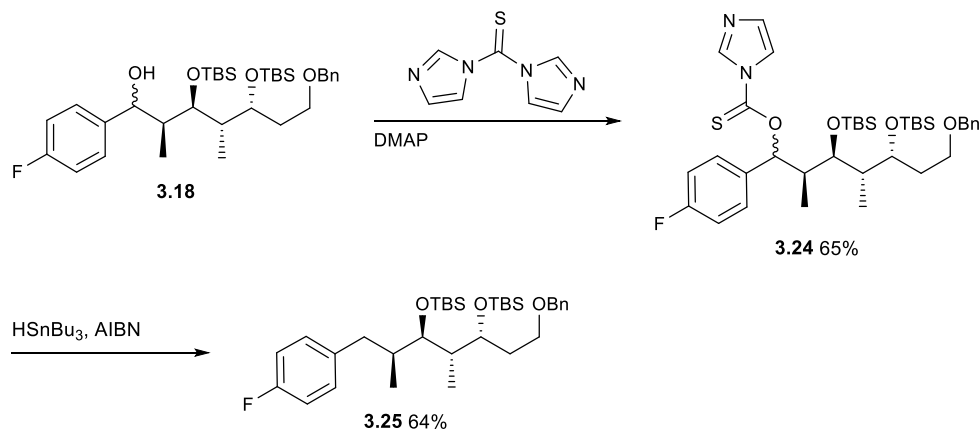
**Scheme 3.8.** Test scheme with phenyldemethylpironetin derivative



fluorine, was causing the loss of reactivity. As expected, the time and temperature required for the Grignard additions of phenyl, 4-chlorophenyl, and 4-fluorophenyl were remarkably different – from 40 minutes at 0 °C to 1.5 h at 0 °C to 18 h at room temperature. Altering the concentration of the reaction did not affect reaction progress, changing solvents led to TBS deprotection, and quantitative recovery of starting material alluded that these were not the issues. Alternatively, insertion into the C-O bond by the palladium species might have been significantly hampered due to the increased bond strength. Most puzzling, though, is the inability to debenzylate the alcohol on the opposite end of the molecule using Pd/C.

As a workaround, the Barton McCombie deoxygenation sequence was attempted (Scheme 3.9). The Barton McCombie begins with conversion of the alcohol into the thiocarbonate, followed by radical-mediated deoxygenation. This sequence is traditionally used for deoxygenation of secondary alkyl hydroxyl groups with few published examples of benzylic alcohol deoxygenation.<sup>101-103</sup> Activation of the benzylic alcohol was accomplished with 1,1'-thiocarbonyldiimidazole to give carbothioate **3.24**, and heating with HSnBu<sub>3</sub> and AIBN in toluene completed the deoxygenation, yielding **3.25**.

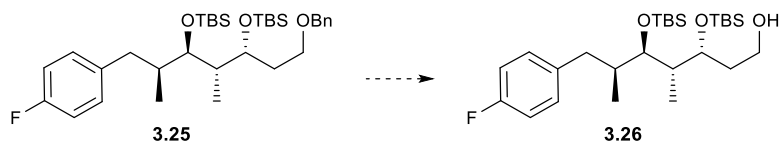
**Scheme 3.9.** Barton McCombie deoxygenation



The next challenge was the benzyl ether deprotection. Initially, the Pd/C and H<sub>2</sub> hydrogenolysis was successful, however after this old bottle of Pd/C rapidly ran out and a new bottle was used, the chemistry no longer worked (Entry 1). Table 3.1 describes the optimization. As treatment with Pd/C in EtOAc was giving very low yields after long amounts of time at atm and high pressures, EtOH/EtOAc mixtures and straight EtOH (Entries 2 and 3) were used as the solvent, however this led to no improvement as the TBS groups started to come off. Switching to Pd(OH)<sub>2</sub> worked decently one time on very small scale (Entry 4), however further attempts were unsuccessful. Throughout all of the Pd

usage, the solvent and starting material were stirred with activated charcoal for one hour and up to overnight in an attempt to remove anything which would quench the palladium. Additionally, the unfinished reaction was filtered to remove the Pd/C and fresh Pd/C was added. In addition to Pd species, in situ generated Li-naphthalide was added (Entry 5), however this resulted in complete recovery of starting material.<sup>104</sup> Further, utilizing ammonium formate as a hydrogen transfer reagent in the presence of catalytic Pd/C (Entry 6) was also unsuccessful.<sup>105</sup>

**Table 3.1.** Optimization of benzyl ether deprotection

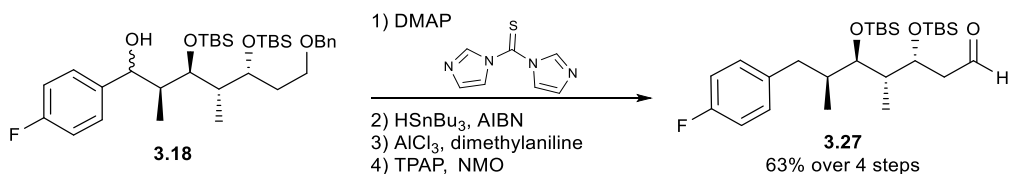


Entry	Conditions	Temperature	Yield	Comments
1	Pd/C in EtOAc	RT	5-80%	Inconsistent, altering pressure gives no change, takes >1 week to get any conversion
2	Pd/C in EtOAc/EtOH (various mixtures)	RT	0-40%	Inconsistent, takes >1 week Increasing pressure removes TBS
3	Pd/C in EtOH	RT	0%	TBS gone
4	Pd(OH) <sub>2</sub>	RT	10-60%	Inconsistent, takes > 1 week
5	Li-Naphthalide	0 °C to RT	0%	Complete recovery of SM
6	Ammonium formate, Pd/C EtOAc/MeOH (1:1)	Up to 70 °C in sealed container	0%	Complete recovery of SM
7	AlCl <sub>3</sub> , N,N-dimethylaniline	RT	85%	Consistent, good on scale up

Finally, AlCl<sub>3</sub> and dimethylaniline were added, which was successful and reproducible (Entry 7). This reaction likely proceeds by initial coordination of the AlCl<sub>3</sub> to the ether

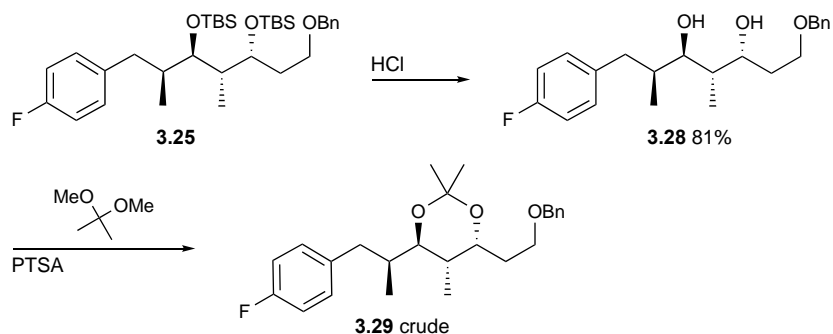
oxygen followed by attack of the dimethylaniline to the benzylic carbon.<sup>106, 107</sup> Overall, the deoxygenation, debenzylation, and oxidation sequence was improved from an inconsistent 0-18% yield over several weeks, to a generally consistent 63% over several days (Scheme 3.10).

**Scheme 3.10.** Final optimization of deoxygenation and debenzylation chemistry



The relative anti-configuration of alcohol **3.25** was confirmed by silyl deprotection (**3.28**) followed by conversion to acetonide **3.29**, shown in Scheme 3.11. Using the <sup>13</sup>C chemical shift analysis published by Rychnovsky and coworkers in 1990 and expanded upon by Evans and coworkers in the same year, the <sup>13</sup>C NMR of crude **3.29** revealed the acetonide peaks at 25.3 and 24.0, consistent with the anti-diol. A syn-diol would show peaks at 19 and 30 ppm.<sup>108, 109</sup>

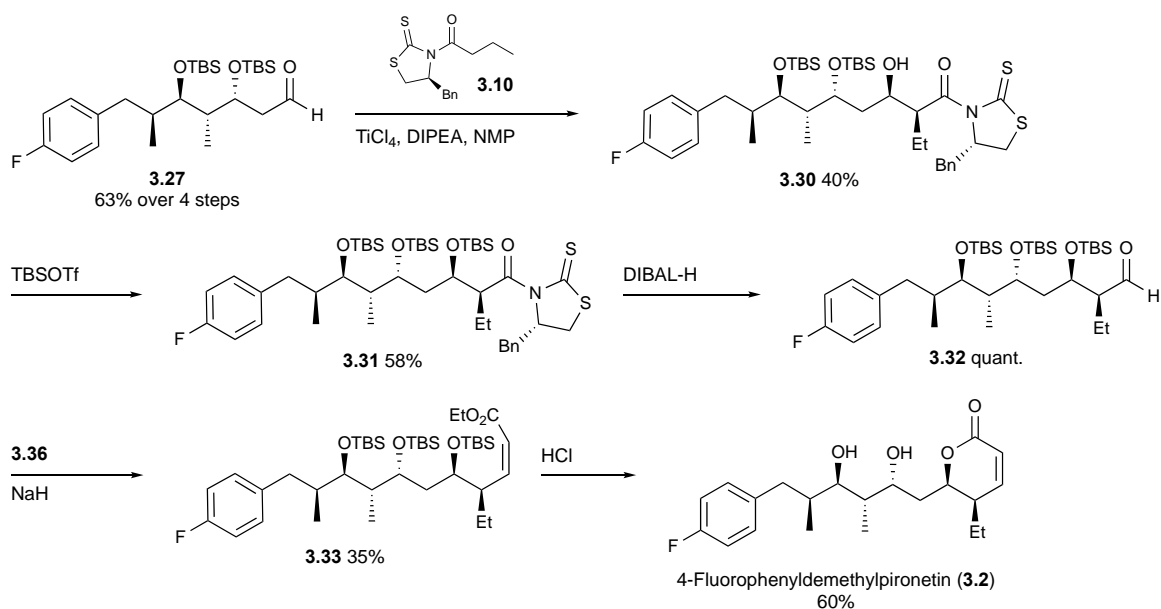
**Scheme 3.11.** Synthesis of the ketal for confirmation of the anti-diol



### 3.2.5 Completion of the Synthesis

The final steps of the total synthesis are shown in Scheme 3.12. Reaction of aldehyde **3.27** with auxiliary **3.11** generated syn aldol product **3.30**, generating alcohol **3.30**. Subsequent silyl protection to **3.31** was followed by DIBAL-H cleavage to yield aldehyde **3.32**, which underwent a Z-selective Horner-Wadsworth Emmons reaction with phosphonate **3.36** (synthesis shown in Scheme 3.13) to generate the intermediate cis-alkene (**3.33**).<sup>64</sup> Treatment with acid allowed for global deprotection and lactone formation, generating the target molecule, 4-fluorophenylidemethylpironetin **3.2**. The Z-selective Horner-Wadsworth Emmons followed by lactonization by acid treatment has been utilized in several total syntheses of pironetin and analogs.<sup>44, 45, 62</sup> Thus, in 19 linear steps and 31 total steps including synthesis of the auxiliaries and phosphonate, the target molecule was obtained.

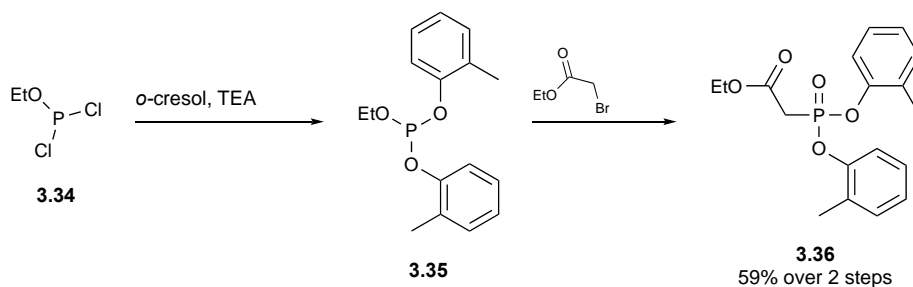
**Scheme 3.12.** Completion of 4-fluorophenylidemethylpironetin



### 3.3 Discussion and Future Directions

In conclusion, we synthesized 4-fluorophenyldemethylpironetin in an attempt to improve pironetin's metabolic stability and maintain potency. Our synthesis represents the first reported total synthesis of a demethylpironetin analog, however improvement is still necessary. At this time, the difficulties encountered whilst removing grease from the final compound have proven insurmountable to obtaining finalized NMRs and biological data.

**Scheme 3.13.** Preparation of phosphonate **3.36**



Further, pironetin does not ionize well by ESI, and so obtaining mass confirmation of the final product is delayed until APCI can be utilized on the Orbitrap, which also requires removal of grease. These disappointing set-backs will be overcome. We are currently performing an even larger scale up of the synthesis (>20 g of intermediate **3.17**) and exploring alternative routes to avoid problematic transformations on scale, including the deoxygenation steps. Additionally, we are re-exploring the order in which the western and eastern portions of the molecule are assembled. While our initial attempts at elongating the eastern portion before derivatizing the western side were unsuccessful many years ago, it is certainly worth revisiting.

As the western olefin was identified as the major site of pironetin metabolism, phenylpironetin (**3.1**) was first synthesized by Dr. David Huang to investigate the utility of replacing the olefin. This synthesis was completed about half way through the total synthesis of 4-fluorophenyldemethylpironetin. While phenylpironetin (**3.1**) showed similar potency as compared to pironetin, phenylpironetin (**3.1**) did not show any improvements in metabolic stability. When phenylpironetin (**3.1**) was sent to Pharmaron for metabolite identification, 17 metabolites were identified after a 15-minute incubation period (Dr. Huang, unpublished results). Incorporation of the phenyl group enhanced oxidative metabolism around the entire molecule, especially around the lactone. Oxidation of nearly every carbon was observed by mass spectrometry, and many observed metabolites contained multiple oxidations. While it is highly unlikely that incorporation of a single fluorine atom will reverse and improve these results, completion of the biological and metabolic evaluations of 4-fluorophenyldemethylpironetin (**3.2**) is required and will be completed as material is available.

One can envision a number of next generation small molecule analogs in which the phenyl has been decorated further or the terminal western methyl is replaced with a trifluoromethyl group. Before these molecules are synthesized, a better understanding of pironetin's proclivity towards oxidative metabolism is critical. The evaluation of 4-fluorophenyldemethylpironetin should provide highly useful information in this regard. Furthermore, due to the synthetic complexity and the seeming requirement for each stereocenter, methodology for the semisynthesis of olefin replacements should be investigated further. Additionally, total synthesis of the pironetin lactam, instead of the

lactone, would be an intriguing molecule to evaluate, and it is also feasible that replacement of some of the methyl pendants with trifluoromethyl would significantly alter metabolic stability.

## Chapter 4: Synthesis and Evaluation of Pironetin-Folate Conjugates

### 4.1 Introduction

While tubulin-binding chemotherapeutics have potent anti-proliferative activity, treatment with these agents has undesired side effects, especially neurological and bone marrow toxicities.<sup>33, 34</sup> Since pironetin forms a covalent bond with cysteine 316 of  $\alpha$ -tubulin, it is our hypothesis that the severe weight loss reported in the previous *in vivo* study could be caused by covalent off-target binding. Indeed, upon incubation of pironetin with the ethyl ester of glutathione, a 1:1 ratio of pironetin to glutathione-pironetin adduct was detected by LC-MS/MS, suggesting that pironetin can form covalent adducts with other proteins.<sup>45</sup> In addition to conjugate addition of pironetin with Cys316, it is possible that epoxy-pironetin, the major metabolite, is a suitable electrophile for a broad scheme of nucleophiles found *in vivo*. To decrease these potential side effects and improve efficacy, we proposed to establish a proof-of-concept method for the targeted delivery of pironetin to ovarian cancer cells.

The idea of selectively delivering a cytotoxic agent to a cancer cell using a targeting agent was first described in 1913 by Paul Ehrlich.<sup>110</sup> The goal of targeted drug delivery is to selectively deliver a compound of interest to a specific cell to minimize unwanted effects on other cells. A multitude of techniques have been employed with varying success rates to accomplish this, including conjugation to proteins, small molecules, peptides, nanoparticles, liposomes, or some combination of these.

Antibody drug conjugates (ADCs) are a rapidly growing class of therapeutics that has required half a century of research to see FDA approval.<sup>111</sup> So far, all approved ADCs are anticancer therapies, however clinical trials are ongoing for other indications, including rheumatoid arthritis. After the first approved ADC was withdrawn from the market in 2010 due to increased toxicity over chemotherapy with the free drug alone, the next FDA approvals came in 2011 and 2013 for second generation ADCs brentuximab vedotin (Adcetris) and ado-trastuzumab emtansine (Kadcyla), respectively.<sup>112, 113</sup> In 2017, both inotuzumab ozogamicin (Besponsa) and gemtuzumab ozogamicin (Mylotarg) were approved.<sup>114, 115</sup> Many of these conjugates are approved for multiple cancer indications.

There are currently more than 100 clinical trials at various stages investigating an ADC (accessed from [clinicaltrials.gov](http://clinicaltrials.gov)). Many of these contain microtubule targeting agent warheads, some of which are too toxic to use without the targeting moiety. ADCs consist of a monoclonal antibody (mAb) linked to a cytotoxic agent. When the mAb recognizes a specific antigen, the ADC is internalized, usually through receptor-mediated endocytosis, and delivered to the lysosome. The ADC undergoes subsequent proteolytic degradation in the lysosome, releasing the cytotoxic agent. There are several generations of ADCs, and the evolution has addressed the understanding of topics such as the linker and its cleavage, off target effects, the bystander effect, warhead choice, and drug-to-antibody ratio.<sup>111</sup>

While ADCs are the most well studied and represented of the tumor targeting agents, we decided to instead focus on a small molecule approach to remain within our laboratory's and the ITDD's capabilities. To address this preference, we chose folate conjugation. Conjugation to folic acid is an attractive approach because malignant tissues overexpress

the folate receptors as compared to normal tissue, particularly in ovarian, lung, breast, kidney, brain, and myeloid cancers.<sup>116, 117</sup> Folate conjugated radio imaging agents have been shown to preferentially label solid tumors and the kidneys in patients over normal tissue.<sup>118</sup> The folate-vinca alkaloid conjugate EC145/Vintafolide (**4.1**, Figure 4.1) advanced into phase III clinical trials against ovarian cancer, however the trial was halted

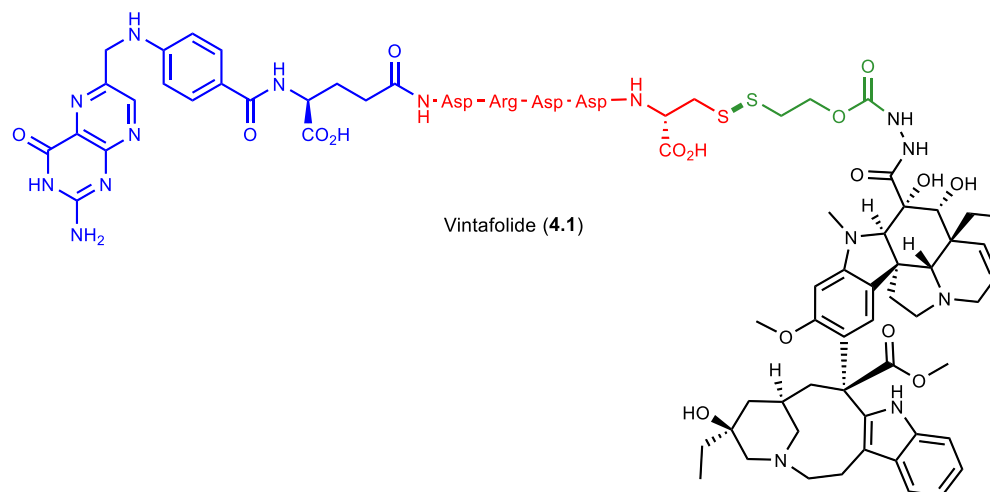


**Figure 4.1.** Structure of the most advanced folate conjugate, Vintafolide, which utilizes desacetylvinblastine hydrazide (DAVLBH), a microtubule targeting agent too potent to use alone.

in 2014 due to lack of improvement in progression-free survival.<sup>119, 120</sup> Based on the evolution required, and still ongoing, for the development of successful ADCs, it is rather unsurprising that the first small molecule folate conjugate to enter clinical trials failed.<sup>111</sup>

The membrane associated folate receptors (FR) are transporters used to bring folates and reduced folates into cells for use in one carbon metabolism for purine, pyrimidine, and amino acid biosynthesis. FRs exist as four isoforms ( $\alpha$ ,  $\beta$ ,  $\gamma$ , and  $\delta$ ) and are identified by their varied expression patterns.<sup>121</sup> FR $\alpha$  is anchored to the membrane by glycosylphosphatidylinositol (GPI) and is found in epithelial cells of the kidney, lung,

mammary ducts, and choroid plexus.<sup>122</sup> FR $\beta$  is likewise membrane associated through GPI and found on activated myeloid cells, including spleen, placenta, and macrophages.<sup>122-124</sup> FR $\gamma$  is a soluble protein which is thought to ensure stability and bioavailability of reduced folates as it is nearly undetectable in normal serum and upregulated in folate deficient states.<sup>125</sup> FR $\delta$ , now called Juno, is anchored to mammalian egg cells and facilitates fertilization by recognizing IZUMO1 on sperm and was found to not bind folic acid.<sup>126</sup> The unique expression pattern of the folate receptors is enhanced in malignant states. FR $\alpha$  is dramatically overexpressed in most ovarian and uterine cancers while FR $\beta$  is overexpressed in most myeloid leukemias as well as macrophages associated with tumors and inflammatory diseases.<sup>117, 127-131</sup> Preparation of several radiopharmaceutical folate conjugates has demonstrated that the biodistribution in humans is primarily at the tumor site and the kidney, but other normal tissues were largely untouched.<sup>132</sup> Additionally, folate conjugates were found at sites of macrophage activation (inflammation in arthritis).<sup>133</sup> Therefore, if a molecule that does not display toxicity at the kidney is found, the conjugate should be safe. As such, utilizing the FR to selectively target human malignancies has been a burgeoning field for close to three decades.

Folic acid (also known as folate or vitamin B9) binds to FR $\alpha$ ,  $\beta$ , and  $\gamma$  with similar high affinity ( $K_d = 1.0, 1.0$  and  $0.4$  nM, respectively).<sup>125, 134</sup> Binding triggers internalization of the ligand-bound receptors into the endosome, which has a unique environment. Folate receptor (or folate conjugate) containing endosomes are mildly acidic (pH  $\sim 5$ ) and contain a high concentration of reducing thiols.<sup>135-137</sup> It was soon discovered that folic acid tethered to a small molecule, liposomes loaded with small molecules, or proteins could get

internalized to the endosome.<sup>138, 139</sup> Internalization was dependent upon free FR localized to the membrane, and so adding high concentrations of folic acid to the media or adding a phospholipase to cleave GPI, which holds the folate receptor at the membrane, resulted in elimination of internalization.<sup>140</sup> Once inside the endosome, a slight drop in pH leads to conformational change to the receptor, releasing the ligand and detaching the folic acid from the conjugate. The warhead can then be separated from the rest of the molecule via an acid or thiol labile linker and diffuse across the endosomal membrane to exert its effect within the cell. Concurrently, the folate receptor makes its way back to the membrane, where it can again engage with folic acid or another conjugate molecule.<sup>141</sup> This cycle is

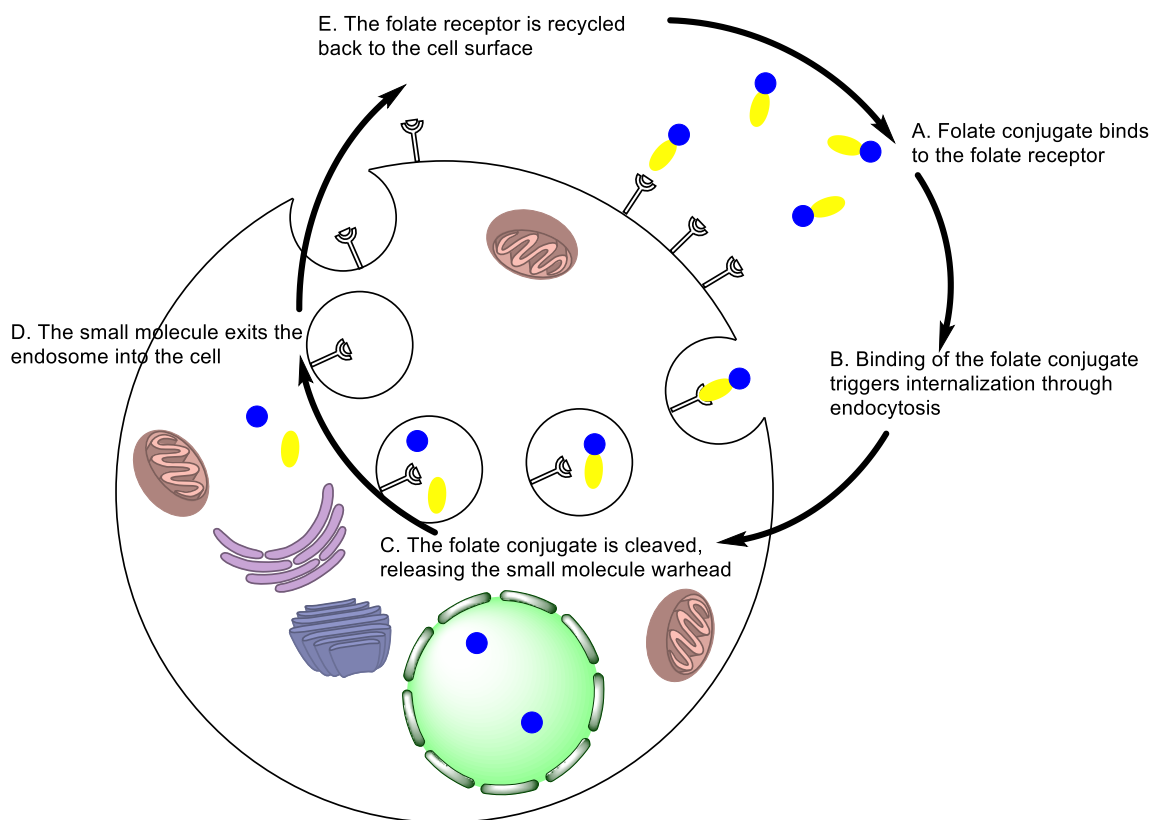


**Figure 4.2.** Mechanism of cellular internalization and cleavage of a folate conjugate. The folic acid moiety is in yellow and the small molecule warhead in blue.

depicted in Figure 4.2.

Folate conjugates have evolved to consist of four parts: the targeting folate moiety (blue), a spacer (red), a self-immolative linker (green), and the small molecule warhead (black), as shown in Figure 4.3. The spacer is selected to enhance hydrophilicity, therefore

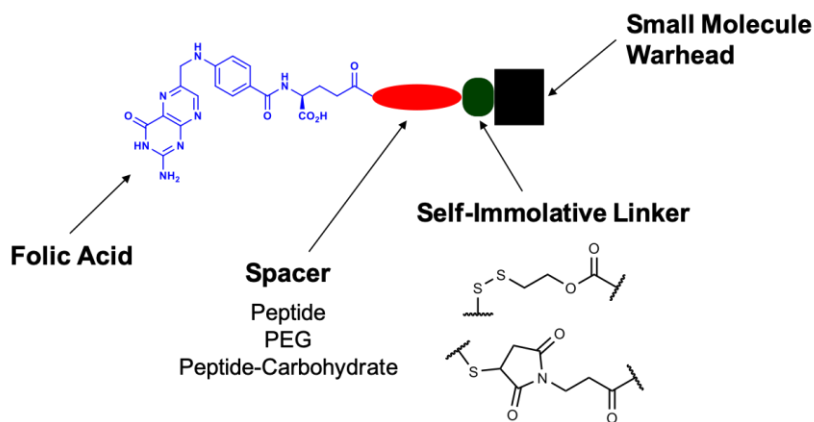


**Figure 4.3.** General structure of a folate conjugate. In blue is the folic acid, the targeting moiety, red is the spacer, green is the cleavable linker, and black is the small molecule payload. Upon endocytosis, the self-immolative linker is cleaved, releasing the unmodified small molecule.

halting passive diffusion of naturally greasy chemotherapeutics and, theoretically, ensuring that the conjugate will selectively enter only folate positive cells through the folate receptor. Peptide-, polyethyleneglycol- (PEG), or carbohydrate-based spacers, and combinations of these, have been successful in vitro and in vivo. The best spacer choice is quite warhead dependent as it affects the binding affinity of the conjugate to the folate receptor in addition to altering the chemical and physiochemical properties of the molecule.<sup>142</sup> The spacer has also been shown to contribute to hepatic clearance and therefore maximum tolerated dose and safety.<sup>143</sup>

Extensive work optimizing the linker has concluded that a self-immolative disulfide generally works best for high serum stability but rapid and selective cleavage in the thiol

rich endosome. When disulfide linkers were utilized, full cell killing was observed, but when acid labile linkers were used, often times it was found that the mildly acidic environment of the endosome was not enough to fully release small molecule or liposomal payloads.<sup>137</sup>

Finally, it is of the utmost importance to select the right cytotoxic agent for conjugation. Due to the limited number of folate receptors on the cell surface and the recycle time required, there is a limit to the concentration of small molecule that will accumulate within a cell. Further, it's been shown that even upon internalization, tritiated folic acid or folate conjugates do not always unload and are often recycled back to the surface, further limiting the concentration of compound to reach the cell.<sup>144</sup> Endocyte has reported unpublished results in which they measured only 1-5  $\mu\text{M}$  of various cytotoxic agents within cells, meaning that molecules must have low to sub-nanomolar potencies in order to affect cellular activity.<sup>142</sup> With such a multifaceted mechanism of internalization, there are many processes that must be correctly balanced in order to achieve an active molecule. When molecules do not display the desired activity, often it is difficult to logically improve the outcome.<sup>145,146</sup>

## **4.2 Design and Synthesis of the First Generation Pironetin-Folate Conjugate and a Camptothecin-Conjugate Positive Control**

Our first proof-of-concept pironetin conjugate **4.2** is based on the design of Vintafolide. Utilizing the spacer and a similar disulfide containing linker adapted to release the alcohol rather than a hydrazide, our proposed conjugate is shown in Figure 4.4. The conjugate contains folic acid (blue), a peptide spacer (red), a cleavable linker (green), and pironetin

(black). The synthesis of the peptide and activated pironetin is shown in Scheme 4.1. Folate peptide **4.3** was synthesized as previously reported using solid phase peptide synthesis on cysteine modified Wang resin at room temperature with PyBOP as the coupling reagent.<sup>147</sup>

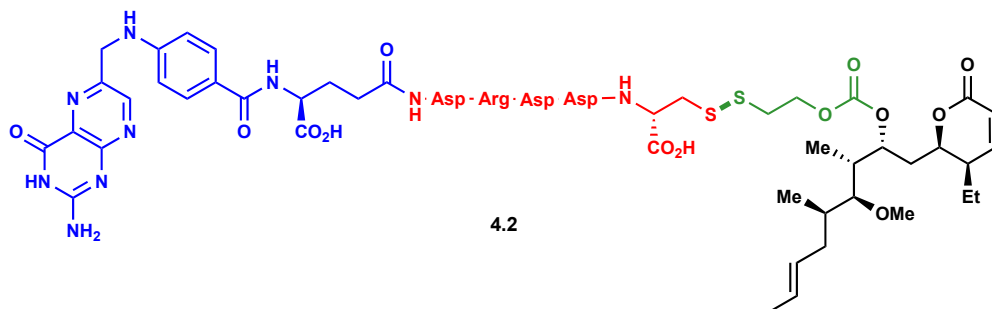
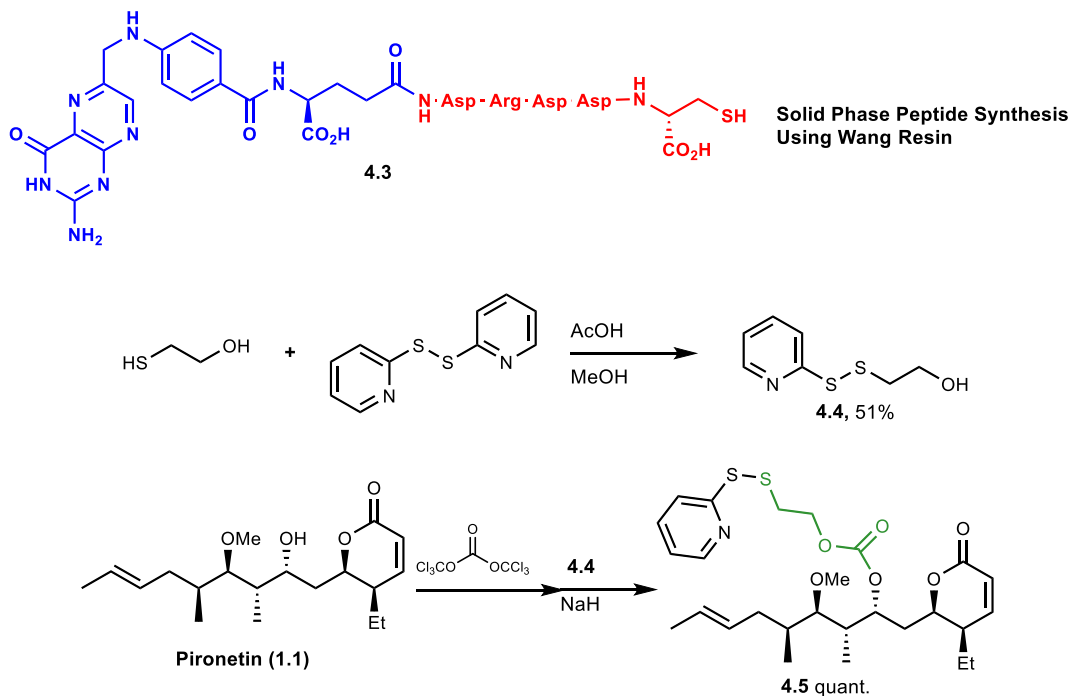


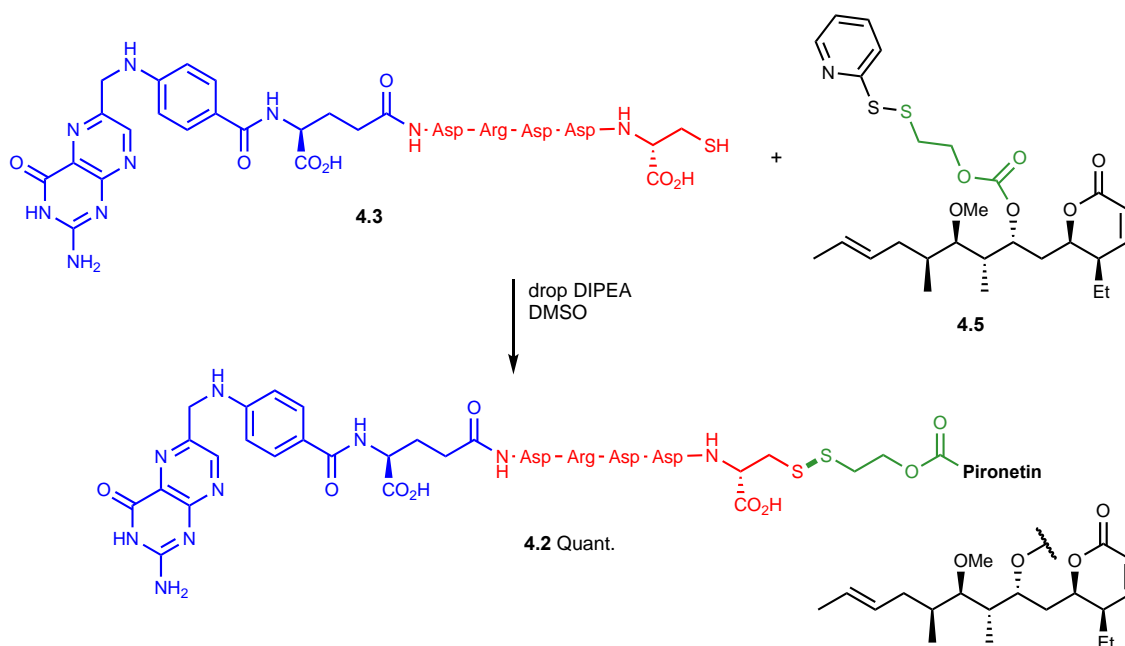
**Figure 4.4.** First generation pironetin conjugate **4.2** is made of folic acid (blue), a peptide spacer (red), the self-immolative disulfide linker (green), and pironetin (black).

**Scheme 4.1.** Synthesis of the folate peptide and activated pironetin



The mixed disulfide **4.4** was synthesized by treating aldrithiol with  $\beta$ -mercaptoethanol.<sup>147</sup> Treatment of pironetin with triphosgene followed by disulfide **4.4** yielded activated pironetin carbonate **4.5**. The pironetin conjugate (**4.2**) was synthesized by combining peptide **4.3** with activated pironetin **4.5** with a drop of base as shown in Scheme 4.2.

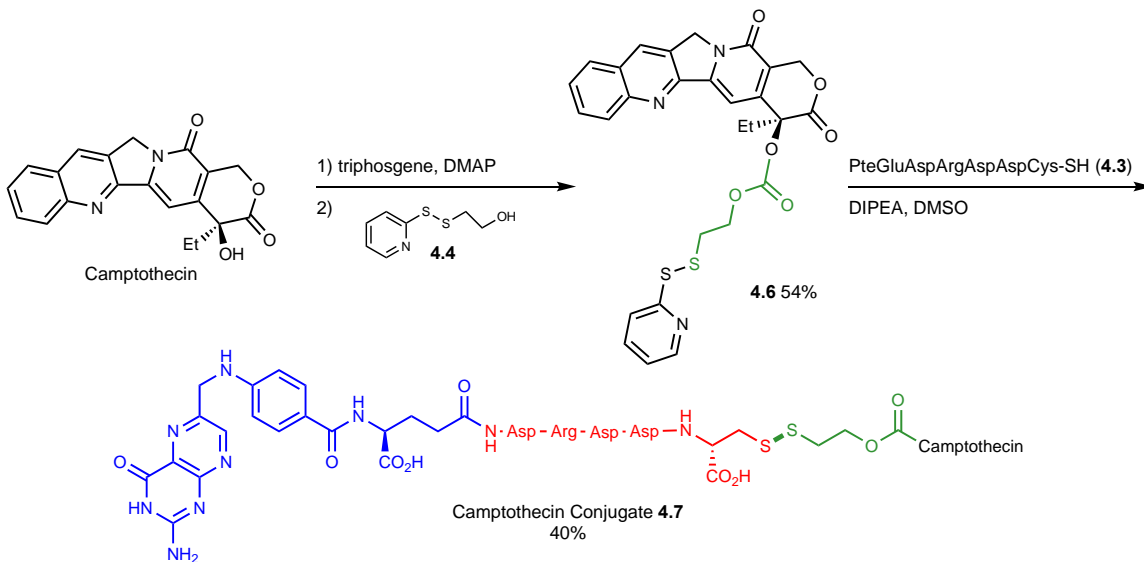
**Scheme 4.2.** Convergent synthesis of pironetin conjugate **4.2**



Following synthesis of the first pironetin conjugate, we desired a positive control which would allow us to judge whether the cell system and assay were working. We turned to the literature and decided upon a camptothecin conjugate which was already published and utilized the same linker and spacer as our pironetin conjugate design.<sup>147</sup> Camptothecin induces apoptosis by inhibiting topoisomerase 1. The synthesis of camptothecin conjugate **4.7** is shown in Scheme 4.3. Camptothecin was treated with DMAP followed by

triphosgene. Upon clearing of the cloudy reaction, alcohol **4.4** was added. Following purification, peptide **4.3** and a drop of DIPEA were combined with activated camptothecin carbonate **4.6** to yield the camptothecin conjugate **4.7**.

**Scheme 4.3.** Synthesis of positive control camptothecin conjugate 4.7



### 4.3 Characterization of Pironetin Release

With the first-generation conjugate in hand, the first step was to check whether pironetin would in fact be released in an unmodified form when exposed to free thiol, the conditions found in the endosome. Based on literature precedence, we chose to incubate the pironetin-folate conjugate with a 10x excess of DTT and monitor by HPLC. The results are shown in Figure 4.5. After one hour, the peptide and conjugate were observed, and by eight hours, the conjugate was undetected and only peptide remained. Pironetin is only weakly UV active and was not observed significantly at 280 nm, so we therefore repeated the experiment and monitored by LC-MS to confirm unmodified pironetin release, Figure 4.6. The masses and fragmentation patterns for the peptide, conjugate, and pironetin match

the standards. Additionally, as pironetin forms a covalent adduct with cysteine of  $\alpha$ -tubulin and GSH, we also incubated pironetin with DTT as a control and saw very minimal to no adduct formation by UV (monitored at 220, Figure 4.7).

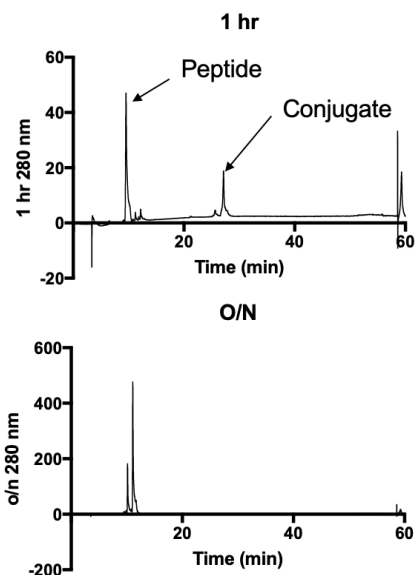


**Figure 4.5.** Conversion of conjugate to peptide is rapid, but pironetin is not UV active.

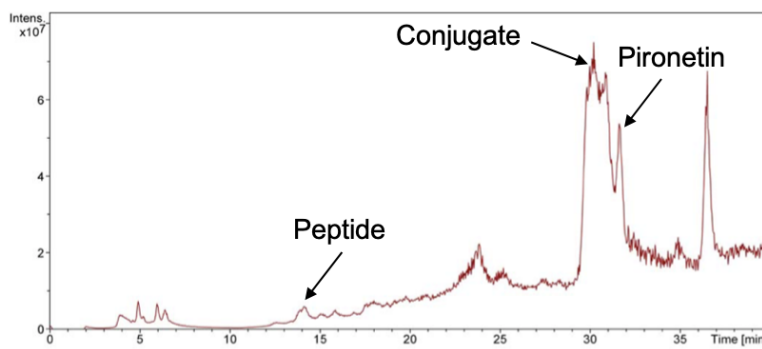


**Figure 4.6.** Pironetin is released from the conjugate upon incubation with DTT as confirmed by LC-MS.

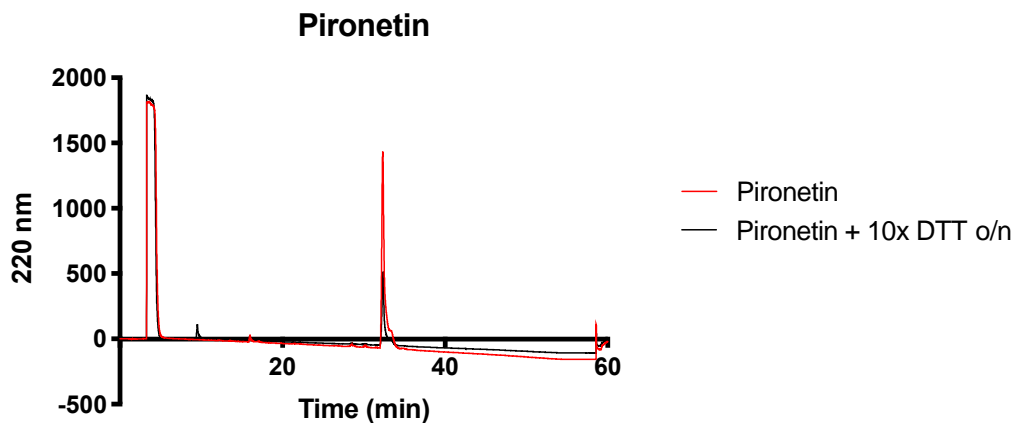


**Figure 4.7.** Pironetin, when treated with 10x excess DTT, forms a very minor new peak after an overnight incubation.

#### 4.4 Selection and Characterization of Cell Lines for Folate Conjugate Evaluation

With the knowledge that unmodified pironetin is released from the conjugate under reducing conditions *in vitro*, the next question was whether the conjugate would be internalized by binding to the folate receptor, leading to endocytosis and pironetin release. We chose two ovarian cancer cell lines with a reported range of folate receptor expression: IGROV-1 with very high folate receptor expression and SK-OV-3 with low levels.<sup>148, 149</sup> As internalization by the folate receptor is expected to be competitively inhibited by excess folic acid, we adapted these cells to survive under folate-free conditions over six months. Normal RPMI 1640 media + 10% FBS + pen/strep contains 2.3  $\mu\text{M}$  folic acid, and the binding affinity of FR $\alpha$  for folic acid is < 1 nM. After adaptation to folate free (FF) conditions, the media with the additives contained < 1 nM of folic acid, which is near the folic acid concentration in serum (0.3 nM). Additionally, it's been reported that FR $\alpha$  is saturated at folic acid concentrations above 50 nM (under equilibrium conditions) and that under non-equilibrium conditions, 120 nM folic acid is enough to saturate the receptor.<sup>122,</sup>

<sup>150</sup> In the next sections, cell lines which were adapted to folate free (FF) media (IGROV-1 and SK-OV-3) will be notated as FF IGROV and FF SKOV.

Following adaptation, we attempted to confirm the relative levels of folate receptor expression using Western blot and an ELISA kit from cell lysates. Unfortunately, these efforts were unsuccessful. A suitable antibody for Western blotting was not identified and the ELISA kits were inconsistent across multiple attempts, leading to data which both confirmed and contradicted literature reports from the same samples. Reproducibly detecting FR $\alpha$  in cells and tissues remains a challenge in the field. While many detection methods have been developed, FR $\alpha$  is marked by a complex secondary structure and a set of post-translational modifications leading to a reduction in reproducibility. We thus carried forward with the assumption that IGROV-1 had very high levels of FR and SKOV-3 had low levels.

#### **4.5 Confirmation of Camptothecin Conjugate Activity and Internalization**

The camptothecin conjugate (4.7) was evaluated in IGROV and SKOV cell lines which were adapted to FF conditions (FF IGROV and FF SKOV) utilizing the MTT assay. To assess FR mediated internalization, 50  $\mu$ M of folic acid was added to the media. Results are shown in Figure 4.8. In IGROV cells, the camptothecin conjugate shows similar activity as compared to camptothecin, and most importantly, this activity is significantly decreased when 50  $\mu$ M folic acid (FA) is added. To further support receptor mediated internalization, when the camptothecin conjugate is dosed for one hour, activity was partially maintained. This supports the internalization dynamics of the folate receptor. When IGROV and SKOV cells were treated with tritiated folic acid, rapid internalization

was observed followed by steady state internalization. Consistent with previous studies monitoring folic acid intake, the majority of the labeled folic acid remained bound to the receptor and was not released into the cell.<sup>144</sup> This can be extrapolated to folate conjugates and is another reason that conjugates require such high potency to achieve activity. Nonetheless, our camptothecin conjugate maintained some activity when dosed for only an hour, further indicating receptor mediated internalization.

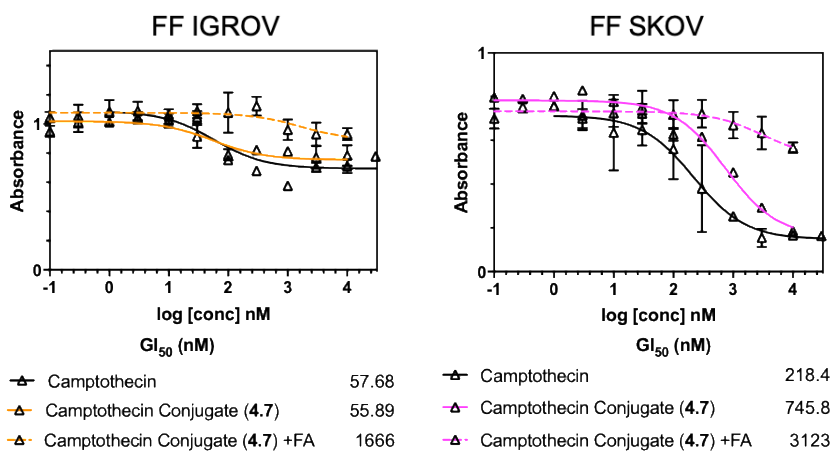


**Figure 4.8.** Camptothecin conjugate 4.7 shows folate receptor mediated activity. FA competition assays were performed with 50 μM FA.

#### 4.6 First Generation Pironetin Conjugate Activity

With the knowledge that our positive control was performing as expected, we began evaluating the first pironetin conjugate for cytotoxicity. The results are shown in Figure 4.9. In both cell lines, the conjugate lost a significant amount of activity, but more concerning is that addition of 250 μM FA does not alter activity, indicating non-folate receptor mediated internalization.

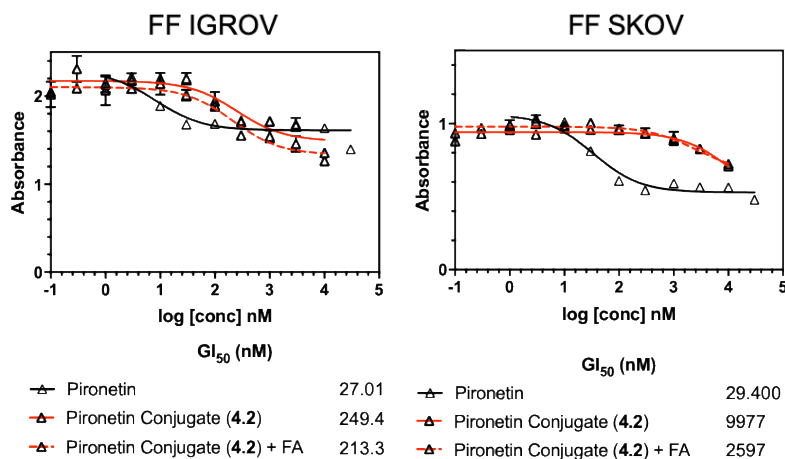


**Figure 4.9.** Evaluation of pironetin conjugate **4.2** in FF adapted cells. FA competition assays were performed with 250  $\mu$ M FA.

We also showed that treatment with folic acid concurrently with pironetin did not alter the activity (Figure 4.10). Finally, we set up a qualitative assay looking for internalization and release of pironetin and the conjugate utilizing tandem mass spectrometry. Regardless of folate receptor mediated internalization or not, we were seeing some activity in the IGROV cell line upon dosing, indicating that a xenobiotic was entering the cell, and therefore we needed to determine that pironetin was being released and not a modified, inactive version of pironetin. One of our concerns upon engaging in pironetin-folate conjugate research was specifically putting pironetin, a Michael acceptor, into a thiol rich environment, like the endosome. Our group has previously reported that pironetin does react with glutathione, but it is reversible.<sup>45</sup> In order to answer some of these questions, pironetin (**1.1**) and the pironetin conjugate (**4.2**) were dosed to cells at the high concentration utilized in the dose response. As a control, cells were treated with FF media

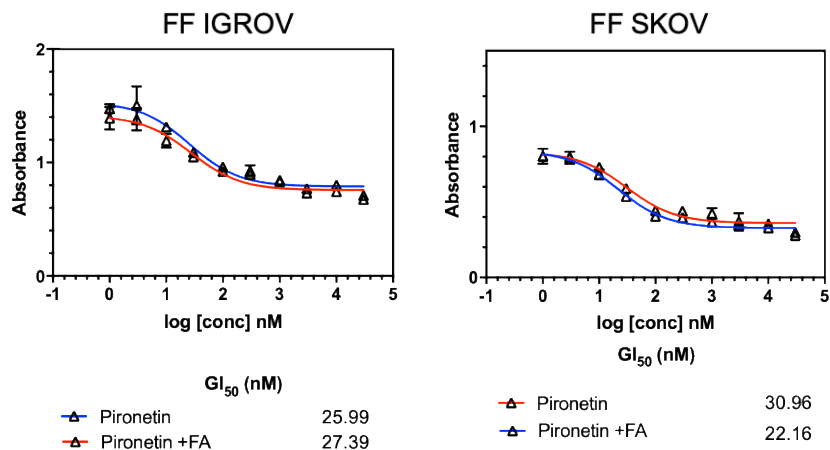


**Figure 4.10.** Confirmation that addition of 50  $\mu$ M FA does not alter the activity of pironetin (n=1).

containing the same concentration of DMSO. Samples were then worked up as described in the SI and injected onto the Orbitrap Velos using a targeted method looking specifically for pironetin, the folate conjugate, the folate peptide, and the pironetin mono-ethyl GSH adduct. The data is shown in Figure 4.11.

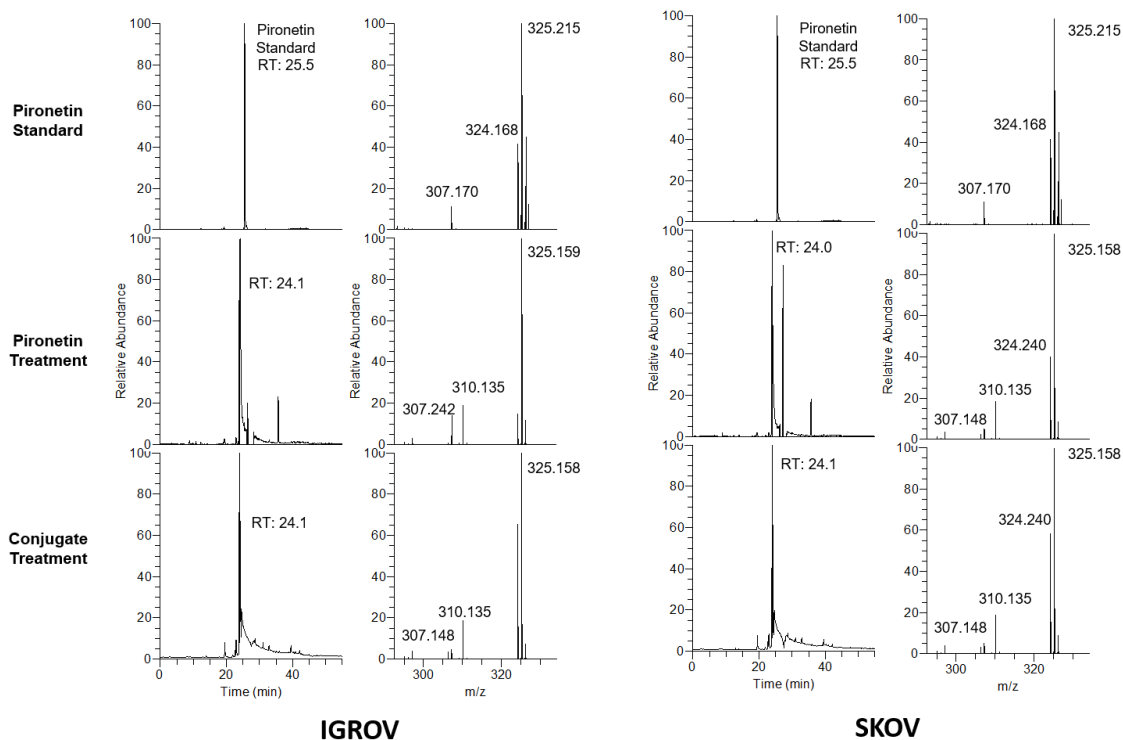


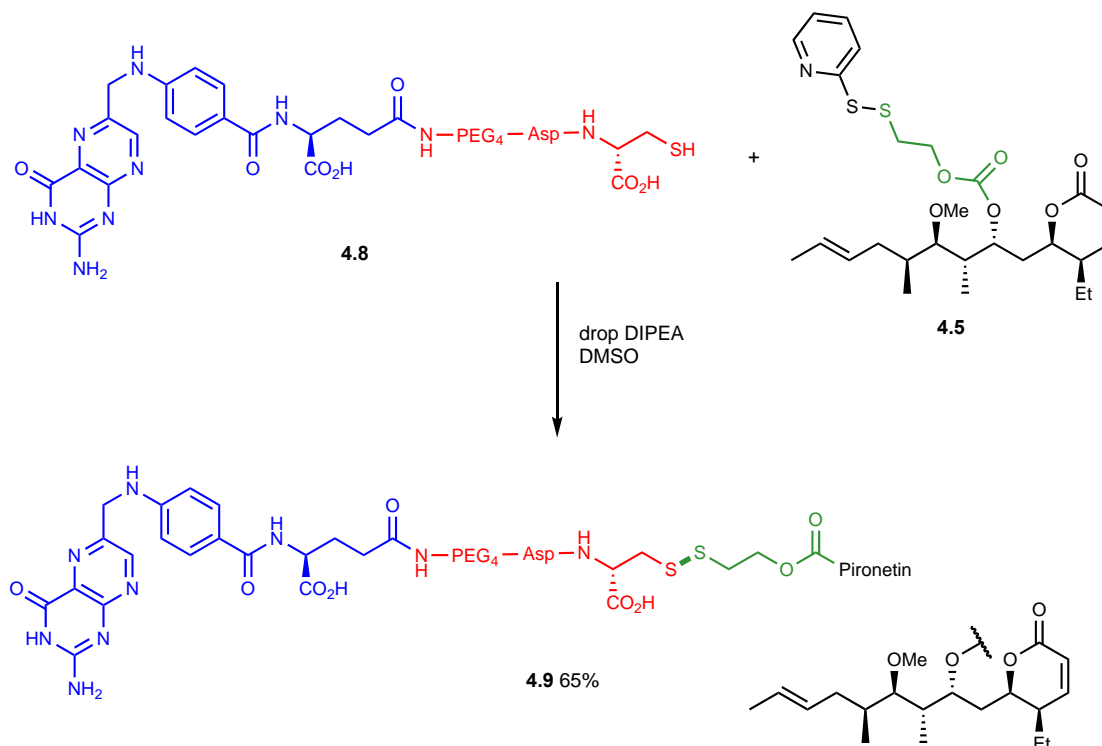
**Figure 4.11.** Internalization of pironetin conjugate. Pironetin is seen after treatment alone and after conjugate treatment. Retention times are slightly different due to solubility of the crude cell samples.

As expected, when cells are treated with pironetin, pironetin is observed inside the cell. When the pironetin conjugate is dosed, the masses corresponding to pironetin, the conjugate, and the pironetin-glutathione adduct are observed. Although this was a rather messy assay, this tells us that the activity we see in the cell-based assays is due to pironetin getting released internally in an unmodified form. However, internalization is not folate receptor mediated, meaning further exploration was necessary.

## 4.7 Second Generation Pironetin Conjugate Synthesis and Activity

Previous folate conjugate SAR published by the Low group and Endocyte highlighted the importance of the spacer unit for controlling receptor mediated endocytosis. In addition to improving solubility, the spacer physically separates folic acid from the

**Scheme 4.4.** Synthesis of the second-generation pironetin conjugate **4.9**



warhead, encouraging the binding affinity of the conjugate to remain close to that of folic acid. To address our internalization problem, we synthesized a second-generation conjugate (**4.9**) with a PEG4 spacer. The synthesis is shown in Scheme 4.4. Peptide **4.8** was synthesized on solid phase and coupled with the activated pironetin carbonate **4.5** with a drop of base to yield conjugate **4.9**. Following purification, the second-generation

conjugate was evaluated in the IGROV and SKOV cell lines in the presence and absence of excess folic acid. These results are shown in Figure 4.12.

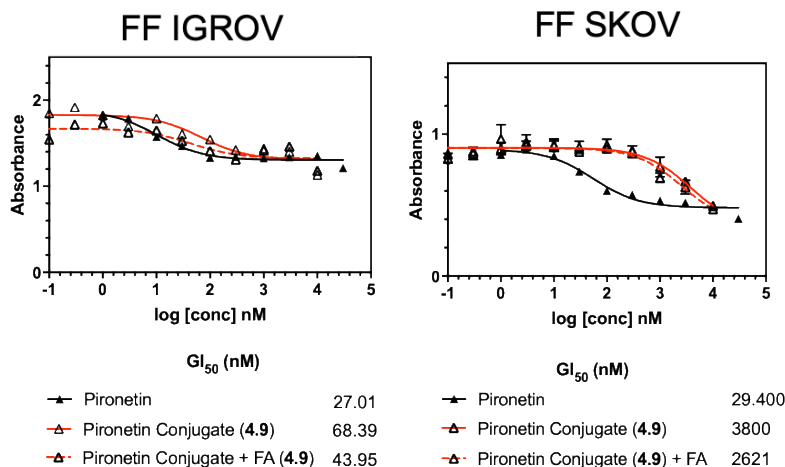


**Figure 4.12.** Evaluation of the second-generation conjugate (**4.9**). FA competition assays were performed with 250  $\mu$ M FA.

We observed similar results for conjugate **4.9** compared to the full peptide spacer conjugate **4.2**. When dosed in the absence of folic acid, the PEG4 conjugate displayed similar potency as compared with pironetin in the IGROV cell line but lost about 1000x activity against the SKOV cell line. When 250  $\mu$ M of FA was added, no change was observed in either cell line.

## 4.8 Discussion

As a proof of concept tumor targeting approach utilizing pironetin, we synthesized two folate conjugates. The folate receptor is overexpressed in most ovarian cancers and by targeting this, we hypothesized that the off-target effects which culminated in weight loss in the reported mouse in vivo study could be minimized.<sup>39</sup> This was also the first endeavor to utilize a covalent modifying compound as the warhead utilizing the folate conjugate

approach, to our knowledge. Unfortunately, both our conjugates showed significantly decreased activity as compared to pironetin. Further, this activity was not diminished by excess folic acid, suggesting that internalization was occurring by a non-folate receptor mediated pathway.

Our pironetin conjugate data is strikingly similar to that of an early folate small molecule conjugate. In 2001, the Low group published the synthesis and evaluation of several paclitaxel folate conjugates with the goal of improving solubility and PK properties. While the linker strategy was different and less selective for endosomal release, the results were the same as for the pironetin conjugates. The paclitaxel conjugate maintained most of the binding affinity for the folate receptor and mostly released in the endosome, but it failed to kill cells (or reduce tumor burden in mice) in a folate receptor specific manner. Addition of high concentrations of folic acid did not reduce activity, and the conjugate showed no preference for high FR $\alpha$  expressing cells over low FR $\alpha$  expressing cells. The authors concluded that the conjugate was still too hydrophobic, allowing for non-specific binding and non-receptor specific internalization. Simply altering the spacer would likely not address this issue, thus necessitating a more careful selection of small molecule warhead for the conjugates.<sup>151</sup> Pironetin does display low water solubility,<sup>152</sup> and so it possible, as with the paclitaxel conjugate, adding a hydrophilic spacer does not remedy this, therefore requiring an alternative targeting strategy.

Other studies have also generated inactive or non-specific folate conjugates. In an SAR of Vintafolide's development, it was found that while keeping the linker and spacer the same, changing the vinca alkaloid warhead from deacetylvinblastine hydrazide

(DAVLBH) to other vinca analogs, including some with increased or equivalent potency on their own, led to completely inactive conjugates. While the reasons behind this are still not understood, the authors hypothesized that the actual compound released in the endosome was not what they expected. Further, it is possible that once released in the endosome, the small molecules become trapped or altered by the slightly acidic environment.<sup>153</sup> While we did see release of pironetin in the cells by LC-MS/MS, it is difficult to say whether pironetin was also getting modified and impossible to say (from this experiment) if pironetin was getting stuck in the endosome. Current efforts are focused on determining the relative affinity of the pironetin conjugates (**4.2** and **4.9**) as compared to folic acid utilizing a FITC-folate conjugate.

Possible next steps include moving away from the folate conjugate to another targeted approach, specifically an ADC. One can envision conjugating pironetin to a mAb specific for the folate receptor, HER2, or Muc16, all of which are overexpressed in many ovarian cancers.<sup>154-157</sup> Due to the potent cytotoxicity and the novel mechanism of action, pironetin remains an extremely interesting compound with unmet potential.

## **4.9 General Summary and Future Directions**

Pironetin is the only natural product known to target  $\alpha$ -tubulin; however, despite its novel mechanism of action, pironetin is still far from being a useful drug-like molecule due to poor pharmacokinetic properties and significant off-target effects. The work presented herein documented an attempt to improve the PK and drug-like utility of pironetin first by identifying the sites of metabolism, blocking the metabolism through total synthesis, and

characterizing a targeted pironetin-conjugate. This work demonstrated that pironetin is extremely metabolically labile and primarily metabolized to epoxypironetin. Our attempts to improve the metabolic stability by blocking epoxidation were ultimately unsuccessful, leading to extensive and increased metabolism along the rest of the molecule. Additional work to complete the biological and metabolic evaluation of 4-fluorophenyldemethylpironetin is ongoing, however barring exceedingly positive results, the total synthesis approach does not appear the most efficient or promising.

Our second approach to improve pironetin's utility focused on minimizing the off-target toxicity, as pironetin is a covalent modifier and a microtubule targeting agent. Our proof-of-concept pironetin-folate conjugates were designed to selectively release pironetin inside cells which overexpress the folate receptor, however we found that the pironetin conjugates showed a significant decrease in cytotoxicity as compared to pironetin in the cell lines tested. This work showed that the activity was not diminished by excess folic acid, suggesting that internalization was occurring by a non-folate receptor mediated pathway, necessitating investigation of another targeting approach.

## Chapter 5: Experimental Data

### 5.1 General Chemistry Procedures

All reactions were run under an inert atmosphere of N<sub>2</sub> gas. Reaction solvents were anhydrous and of HPLC quality. All other reagents were purchased from Sigma or Fischer and used without further purification. Yields were calculated for material judged homogeneous by thin layer chromatography (TLC), nuclear magnetic resonance (NMR), and high performance liquid chromatography (HPLC) for final compounds. TLC was performed on 250 micron plates, eluting with the solvent indicated, visualized by a 254 nm UV lamp, and stained with potassium permanganate solution. Glassware for reactions was oven dried at 140 °C prior to use. Column flash chromatography was performed using silica gel, 60 Å, 230-400 mesh. NMR spectra were acquired on a 400 MHz instrument for <sup>1</sup>H and a 100 MHz instrument for <sup>13</sup>C unless otherwise noted. Chemical shifts for <sup>1</sup>H NMR spectra are reported in parts per million (ppm) and referenced to the signal of residual nondeuterated solvent (7.26 ppm for CDCl<sub>3</sub> and 7.16 for C<sub>6</sub>D<sub>6</sub>). Chemical shifts for <sup>13</sup>C NMR are reported in parts per million (ppm) and referenced to the centerline of the deuterated solvent (77.2 ppm for CDCl<sub>3</sub> and 128.1 for C<sub>6</sub>D<sub>6</sub>). High resolution mass spectrometry data were acquired on a Bruker BioTOF II ESI unless otherwise noted. Matrix assisted laser desorption/ionization (MALDI) for peptides and conjugates was collected on an AB-Sciex 5800 MALDI/TOF-MS using α-cyano-4-hydroxycinnamic acid as the matrix.

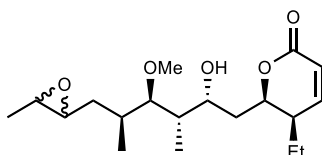
## 5.2 Chapter 2 Metabolite Identification

### 5.2.1 Pironetin Extraction

Pironetin was obtained from the fermentation broth of *Streptomyces prunicolor* strain PA-48153 in a similar manner as reported in the patent by Kurokawa and coworkers following a 200L fermentation harvest (performed by the Biotechnology Resource Center at UMN), yielding 61 kg of cell paste and 129 kg of supernatant.<sup>158</sup>

### 5.2.2 Synthesis of Epoxypironetin and Demethylpironetin.

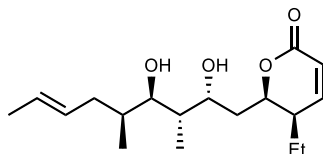
**(5*R*,6*R*)-5-Ethyl-6-((2*R*,3*S*,4*R*,5*S*)-2-hydroxy-4-methoxy-3,5-dimethyl-6-(3-methyloxiran-2-yl)hexyl)-5,6-dihydro-2H-pyran-2-one (epoxypironetin, M4).**



To a solution of pironetin (3.0 mg, 9.3  $\mu\text{mol}$ ) and  $\text{NaHCO}_3$  (0.77 mg, 9.3  $\mu\text{mol}$ ) at 0  $^\circ\text{C}$  in DCM (0.22 mL, 0.043 M) was added mCPBA (4.2 mg, 0.025 mmol). Upon consumption of pironetin (3 h), the reaction was diluted with DCM (3 mL) and then quenched with saturated aqueous  $\text{Na}_2\text{S}_2\text{O}_3$  (1 mL) and poured into aqueous  $\text{NaHCO}_3$  (1 mL, 10 wt % in water). The organic layer was washed with saturated aqueous  $\text{NaHCO}_3$  (3 mL), water (3 mL), and then dried over  $\text{Na}_2\text{SO}_4$ , filtered, and concentrated under reduced pressure to yield crude powder, which was purified by flash column chromatography ( $\text{SiO}_2$ ) in 10% EtOAc in hexanes to yield epoxypironetin, **M4**, a pair of inseparable diastereomers, as a white viscous oil (2.9 mg, 92%).  $^1\text{H}$  NMR (400 MHz,  $\text{CDCl}_3$ )  $\delta$  7.00 (dd,  $J = 9.8, 6.0$  Hz, 1H), 6.02 (d,  $J = 9.8$  Hz, 1H), 4.73 (dt,  $J = 9.4, 3.5$  Hz, 1H), 4.26 – 4.13 (m, 1H), 3.48 (d,  $J = 10.4$  Hz, 3H), 3.10 – 3.03 (m, 1H), 2.79 – 2.63 (m, 2H), 2.28 (dp,  $J = 10.2, 5.5$  Hz, 1H),

2.07 (td,  $J = 11.3, 10.3, 6.8$  Hz, 1H), 1.84 – 1.72 (m, 2H), 1.72 – 1.58 (m, 3H), 1.55 – 1.46 (m, 1H), 1.41 (ddd,  $J = 14.2, 9.6, 5.3$  Hz, 1H), 1.31 (d,  $J = 5.2$  Hz, 3H), 1.14 – 0.92 (m, 9H).  $^{13}\text{C}$  NMR (100 MHz,  $\text{CDCl}_3$ )  $\delta$  164.8, 150.8, 121.0, 91.6, 90.9, 77.4, 77.9, 67.9, 67.1, 61.9, 61.4, 58.6, 58.2, 55.6, 54.3, 39.2, 38.9, 37.1, 36.8, 36.7, 36.2, 34.8, 33.9, 21.0, 17.7, 16.1, 15.3, 12.5, 12.2, 11.2, 11.1. HRMS calc'd for  $\text{C}_{19}\text{H}_{32}\text{O}_5$  ( $\text{M}+\text{Na}$ ) $^+$  363.4498, found ( $\text{M}+\text{Na}$ ) $^+$  363.2143.  $^1\text{H}$  NMR chemical shifts are consistent with reported values ( $^{13}\text{C}$  not reported).<sup>58</sup> Epoxypironetin was found to be >95% pure by HPLC analysis.

**(5*R*,6*R*)-6-((2*R*,3*S*,4*R*,5*S*,*E*)-2,4-Dihydroxy-3,5-dimethylnon-7-en-1-yl)-5-ethyl-5,6-dihydro-2*H*-pyran-2-one (demethylpironetin, M5).**



Demethylpironetin was prepared as previously described.<sup>58</sup> To a solution of pironetin (11.4 mg, 0.035 mmol) in DCM (1.8 mL, 0.02 M) at  $-78$  °C was added a 15-crown-5 solution (0.3 M in DCM, 0.54 mL, 0.20 mmol) saturated with NaI.  $\text{BBr}_3$  (1 M in DCM, 105  $\mu\text{L}$ , 0.10 mmol) was then added dropwise to the reaction at  $-78$  °C. The reaction was warmed to 0 °C over 3 h and stirred at 0 °C for 3 h. The reaction was diluted with  $\text{Et}_2\text{O}$  and quenched with saturated aqueous  $\text{NH}_4\text{Cl}$  (5 mL) and 15% sodium thiosulfate (5 mL). The organic layers were separated and the combined aqueous layers was extracted with  $\text{Et}_2\text{O}$  (4x). The combined organic extracts were washed with brine, dried over  $\text{Na}_2\text{SO}_4$ , and concentrated under reduced pressure. The crude material was dissolved in  $\text{Et}_2\text{O}$  (20 mL) and stirred overnight at rt with silica gel (1 g). This solution was filtered and the silica gel

was washed with EtOAc (5x). The organics were then washed with 15% sodium thiosulfate (20 mL), saturated NaHCO<sub>3</sub> (20 mL), brine (20 mL), dried over Na<sub>2</sub>SO<sub>4</sub>, and concentrated. The crude oil was purified by flash chromatography with 40% EtOAc in hexanes (2x) and then by C<sub>18</sub> chromatography (A: H<sub>2</sub>O with 0.1% TFA, B: AcCN, 30-70% B) to yield demethylpironetin (**M5**) (6.2 mg, 57%). <sup>1</sup>H NMR (600 MHz, CDCl<sub>3</sub>) δ 7.02 (dd, *J* = 9.8, 6.0 Hz, 1H), 6.03 (dd, *J* = 9.8, 0.9 Hz, 1H), 5.55 – 5.37 (m, 2H), 4.79 (ddd, *J* = 10.1, 3.6, 2.7 Hz, 1H), 4.16 (dt, *J* = 10.8, 2.2 Hz, 1H), 3.57 (dd, *J* = 8.5, 3.5 Hz, 1H), 2.34 – 2.26 (m, 1H), 2.12 – 2.06 (m, 1H), 2.02 – 1.94 (m, 1H), 1.92 – 1.86 (m, 1H), 1.83 (ddd, *J* = 14.2, 10.1, 2.0 Hz, 1H), 1.77 – 1.64 (m, 6H), 1.55 – 1.47 (m, 1H), 0.98 (t, *J* = 7.5 Hz, 3H), 0.89 (d, *J* = 6.8 Hz, 3H), 0.86 (d, *J* = 7.0 Hz, 3H). <sup>13</sup>C NMR (100 MHz, CDCl<sub>3</sub>) δ 164.9, 151.0, 129.4, 127.2, 120.9, 77.7 (2 overlapping), 69.9, 39.8, 39.3, 37.6, 35.4, 34.8, 21.0, 18.1, 12.4 (2 overlapping), 11.2. HRMS calc'd for C<sub>18</sub>H<sub>30</sub>O<sub>4</sub> (M+Na)<sup>+</sup> 333.2042, found (M+Na)<sup>+</sup> 333.2035. NMR chemical shifts were consistent with reported values.<sup>58, 88</sup> Demethylpironetin was found to be >95% pure by HPLC analysis.

## 5.2.3 Metabolite Identification in Human Liver Microsomes

### 5.2.3.1 Microsomal Incubation

Metabolism reactions were run in a microcentrifuge tube while shaking at 37 °C. Reaction solvents were of HPLC quality. Pooled human liver microsomes were purchased from Fisher Scientific and were of mixed gender.

The following stock solutions were created:

- 0.1 M Tris buffer, pH 7.4

- Pironetin (solubilized in DMSO and diluted with Tris buffer to 50 mM, final DMSO concentration <0.1%)
- NADPH Regeneration Buffer A (20 mg/mL glucose-6-phosphate, 20 mg/mL NADP, 13.3 mg/mL MgCl<sub>2</sub>•6 H<sub>2</sub>O) in Tris buffer
- NADPH Regeneration Buffer B (40 U/mL glucose-6-phosphate dehydrogenase, 5 mM sodium citrate) in Tris buffer
- Positive Control: verapamil (solubilized in DMSO and diluted with Tris buffer to 10 mM, final DMSO concentration <0.1%)

The following reactions were set up at 37 °C on a microshaker for pironetin and the verapamil positive control:

**Reaction 1:** Microsomes (50 µL, final concentration 1 mg/mL) were added to Tris buffer (860 µL). NADPH regeneration buffer A (50 µL) and the NADPH regeneration buffer B (20 µL) were added. The reaction was allowed to incubate at 37 °C for 15 min, at which time the reaction was stopped with the addition of ice-cold acetonitrile (200 µL).

**Reaction 2:** Microsomes (50 µL, final concentration 1 mg/mL) were added to Tris buffer (860 µL), and either pironetin or the verapamil stock solution (20 µL) was added. The reaction was allowed to incubate at 37 °C for 15 min, at which time the reaction was stopped with the addition of ice-cold acetonitrile (200 µL).

**Reaction 3:** Microsomes (100 µL, final concentration 1 mg/mL) were added to Tris buffer (1.72 mL) and either pironetin or verapamil stock solution (40 µL) was added. NADPH regeneration buffer A (100 µL) and the NADPH regeneration buffer B (40 µL) were added. The reaction was allowed to incubate at 37 °C for given amounts of time (2, 4, 8, 15, 30,

or 60 min), at which time 250  $\mu\text{L}$  was removed and quenched with ice-cold acetonitrile (150  $\mu\text{L}$ ).

**Reaction work-up:** Following protein precipitation with acetonitrile, to each above sample was added EtOAc (800  $\mu\text{L}$ ) and water (100  $\mu\text{L}$ ). The samples were vortexed and then centrifuged at 14,000 rpm for 5 min. The organic layer was then transferred to a new vial and dried under a flow of nitrogen. Samples were then taken up in 20% acetonitrile in water (150  $\mu\text{L}$ ) and filtered prior to LC-MS/MS analysis.

#### **5.2.3.2 LC-MS/MS Method**

Prepared metabolism samples were injected onto a NanoLC-Ultra 2D HPLC system equipped with a 5  $\mu\text{L}$  injection loop. Separation was performed on a C18 column (Synergi 2.5  $\mu\text{m}$  Max-RP 100 A column, 100 x 3 mm) using a mobile phase consisting of water + 0.1% formic acid (A) and acetonitrile + 0.1% formic acid (B) at a flow rate of 400  $\mu\text{L}/\text{min}$ . The elution gradient conditions are as follows: column was equilibrated in 20% B prior to injection. Following sample injection, the gradient was increased to 62% B over 20 min, and then increased to 99% B over an additional min. The gradient was held at 99% B for 1 min, after which the gradient was reduced to 50% B over an additional min. The gradient was then held for an additional 10 min at 50% B. The injected sample volume was 5  $\mu\text{L}$ . Samples were analyzed by HPLC-APCI<sup>+</sup>-MS/MS atmospheric pressure chemical ionization (APCI) in positive mode using an LTQ Orbitrap Velos instrument. The APCI source was heated at 250  $^{\circ}\text{C}$ . Source voltage was 3.7 kV, sheath gas and auxiliary gas flow rates were 30 and 5 arbitrary units, respectively; capillary temperature was 300  $^{\circ}\text{C}$ .

The LTQ Orbitrap Velos was operated with two scan events. The first scan event was a full FTMS scan in positive mode over a mass range of 50-1000  $m/z$  with a resolving power of 15000. The second scan event was HCD MS<sup>2</sup> fragmentation of the top five ions selected from the first scan event with an isolation width of 2.0  $m/z$ . Normalized collision energy was set to 50% with an activation time of 0.1 ms.

The data were processed using the XCaliber software. The masses for pironetin and its metabolites were extracted from the full scan data to identify peak retention times and then evaluated for structure using MS fragmentation patterns. Epoxypironetin was >95% pure for this analysis and demethylpironetin was found to be 86% pure for this experiment (demethylpironetin was later resynthesized and found to be >95% pure for the cell cytotoxicity studies).

#### **5.2.4 Cell Viability Assay**

Cell lines (A2780 and A2780CP) were a generous gift from the Skubitz lab at the University of Minnesota. Cells were grown in a 5% CO<sub>2</sub> atmosphere at 37 °C in tissue culture dishes. A2780 and A2780CP cells were grown in RPMI 1640 media supplemented with 10% fetal bovine serum (FBS) and 50 U/mL penicillin/streptomycin.

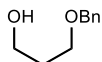
Upon ~70% growth confluence, cells were harvested by trypsin and the pellet was washed with media and spun down twice before plating 50  $\mu$ L of  $5 \times 10^4$  cells/mL in each required well of a 96-well plate. Cells were allowed to grow for 24 h, after which cells were treated with 11 concentrations of pironetin, demethylpironetin, epoxypironetin, and paclitaxel as a control. Cells were then incubated for 48 h.

Cell proliferation was analyzed following published protocol for the Non-Radioactive Cell Proliferation Assay (MTT). Following individual treatment with compounds, MTT (3-(4,5-dimethylthiazol-2-yl)-2,5-diphenyltetrazolium bromide, 15  $\mu$ L of 12 mM stock) was added to the culture medium and allowed to incubate for 4 h at 37 °C. After this time, solubilizing solution/stop mix (150  $\mu$ L, Promega) was added and the plates were set to incubate overnight at 37 °C, after which the absorbance was measured at 570 nm on a microplate reader. Each measurement was done in triplicate during each experiment on a minimum of two separate experiments.

### 5.3 Chapter 3 Total Synthesis of 4-Fluorophenyldemethylpironetin

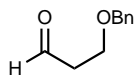
All auxiliaries and their intermediates were prepared as previously described and matched the literature NMR and OR values.<sup>159, 160</sup>

#### 3-(Benzyloxy)propan-1-ol (3.12).



To NaH (0.557 g, 23.2 mmol) dissolved in THF (28 mL, 0.5 M) was added 1,3-propanediol (1 mL, 10 mmol) dropwise. The reaction was stirred for 45 min. At this time, TBAI (2.57 g, 7.0 mmol) was added, followed by BnBr (1.657 mL, 14.0 mmol) dropwise. The reaction was allowed to stir overnight, at which time the reaction was quenched with water and extracted with DCM (3x). The organic layers were combined and washed with sodium thiosulfate followed by brine, dried over MgSO<sub>4</sub>, dried, filtered, and concentrated to yield the crude oil. The oil was purified by flash chromatography (0-30% EtOAc in hexanes) to give **3.12** as a clear oil (1.32 g, 60%). The spectral data is consistent with reported values.<sup>98</sup> <sup>1</sup>H NMR (400 MHz; CDCl<sub>3</sub>) δ 7.38 – 7.27 (m, 5H), 4.53 (s, 2H), 3.85 – 3.73 (t, *J* = 5.6 Hz, 2H), 3.72 – 3.60 (t, *J* = 5.8 Hz, 2H), 1.93 (br s, 1H), 1.88 (p, *J* = 5.7 Hz, 2H).

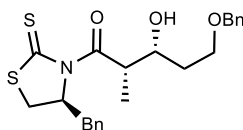
#### 3-(Benzyloxy)propanal (3.13).



To a solution of DMSO in DCM at –78 °C was added a solution of oxalyl chloride. The reaction mixture was stirred at –78 °C for 10 min, at which time 3-(benzyloxy)propan-1-ol (**3.12**) was added dropwise in DCM. After 15 min, TEA was added and the solution was

allowed to stir for 5 min before warming to room temperature. After complete consumption of the alcohol (1 h), the reaction was quenched with saturated ammonium chloride and the aqueous phase was washed with DCM (3x). The organic phase was washed with saturated sodium bicarbonate, brine, dried (Na<sub>2</sub>SO<sub>4</sub>), and concentrated *in vacuo*. The crude reaction mixture was purified (CombiFlash, 0-40% EtOAc in hexanes) to yield aldehyde (**3.13**) as a clear oil (0.854 g, 86%). The spectral data is consistent with reported values.<sup>98</sup> <sup>1</sup>H NMR (400 MHz, CDCl<sub>3</sub>) δ 9.81 (s, 1H), 7.39 – 7.28 (m, 5H), 4.55 (s, 2H), 3.83 (t, *J* = 6.1 Hz, 2H), 2.71 (td, *J* = 6.1, 1.9 Hz, 2H).

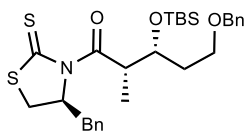
**(2*S*,3*R*)-1-((*S*)-4-Benzyl-2-thioxothiazolidin-3-yl)-5-(benzyloxy)-3-hydroxy-2-methylpentan-1-one (3.14).**



To a stirred solution of thiazolidinone thione (**3.9**, 1.95 g, 7.36 mmol) and dry DCM (5.0 mL, 1M) at 0 °C was added TiCl<sub>4</sub> (0.855 mL, 7.76 mmol) dropwise, upon which the mixture turned orange. If necessary, additional DCM (< 1 mL) was added to keep the reaction solvated. After stirring for 5 min, DIPEA (1.42 mL, 8.1 mmol) was added dropwise. The dark purple reaction mixture was allowed to stir for an additional 40 min at 0 °C, at which time NMP (N-methyl-2-pyrrolidone, 1.42 mL, 14.73 mmol) was added dropwise, and the reaction was let to stir for 15 min. At this time, the mixture was cooled to -78 °C and aldehyde (**3.13**, 0.81 g, 4.91 mmol) in 0.5 mL DCM was added dropwise. The reaction was stirred at -78 °C for 2 h, and then warmed to 0 °C and let to stir for 1 h. After complete consumption of the aldehyde, the reaction mixture was quenched with

saturated ammonium chloride. The aqueous layer was extracted with DCM (3x), and the combined organic layers were washed with brine, dried (Na<sub>2</sub>SO<sub>4</sub>), filtered, and concentrated under reduced pressure. The crude product mixture was purified by silica-gel chromatography (CombiFlash, 0-20% EtOAc in hexanes) to give the *syn* aldol product **3.14** as a yellow oil (1.5 g, 71%). The spectral data is consistent with reported values.<sup>98</sup>  $[\alpha]_D^{26} +134.5$  ( $c=1$ , CHCl<sub>3</sub>) <sup>1</sup>H NMR (400 MHz, CDCl<sub>3</sub>)  $\delta$  7.37 – 7.11 (m, 10H), 5.24 (m, 1H), 4.49 (tt,  $J = 6.9, 3.4$  Hz, 1H), 4.45 (s, 2H), 4.10 (dp,  $J = 10.2, 4.1, 3.5$  Hz, 1H), 3.71 – 3.48 (m, 2H), 3.32 (dd,  $J = 11.6, 7.1$  Hz, 1H), 3.23 (s,  $J = 2.3$  Hz, 1H), 3.18 (dd,  $J = 13.2, 3.8$  Hz, 1H), 2.98 (dd,  $J = 13.2, 10.6$  Hz, 1H), 2.82 (d,  $J = 11.5$  Hz, 1H), 1.87 – 1.58 (m, 2H), 1.21 (d,  $J = 6.8$  Hz, 3H). <sup>13</sup>C NMR (100 MHz, CDCl<sub>3</sub>)  $\delta$  201.5, 177.8, 138.0, 136.6, 129.6 (2C), 129.0 (2C), 128.6 (2C), 127.9 (2C), 127.4 (2C), 73.5, 71.8, 69.2, 68.8, 43.9, 36.8, 34.0, 32.3, 11.1. HRMS calc'd for C<sub>23</sub>H<sub>27</sub>NO<sub>3</sub>S<sub>2</sub> (M+Na)<sup>+</sup> 452.5822, found (M+Na)<sup>+</sup> 452.1318.

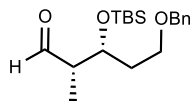
**(2*S*,3*R*)-1-((*S*)-4-Benzyl-2-thioxothiazolidin-3-yl)-5-(benzyloxy)-3-((*tert*-butyldimethylsilyl)oxy)-2-methylpentan-1-one (3.15).**



To a solution of alcohol (**3.14**, 0.99 g, 2.305 mmol) in DCM (19.70 mL, 0.117 M) at 0 °C was added 2,6-lutidine (0.537 mL, 4.61 mmol) and then TBSOTf (0.794 mL, 3.46 mmol) dropwise. The reaction was warmed to rt and upon consumption of the starting material, the mixture was quenched with sodium bicarbonate. The aqueous layer was extracted with DCM (3x), the combined organic layers were washed with brine, and then dried (Na<sub>2</sub>SO<sub>4</sub>),

filtered, and concentrated under reduced pressure. The crude oil was purified by column chromatography (CombiFlash, 0-20% EtOAc in hexanes) to yield **3.15** as a yellow oil (0.985 g, 79%).  $[\alpha]_D^{26} +131.2$  (*c* 1, CHCl<sub>3</sub>). <sup>1</sup>H NMR (400 MHz, CDCl<sub>3</sub>) δ 7.30 – 7.19 (m, 10H), 5.12 (ddd, *J* = 10.6, 7.1, 3.9 Hz, 1H), 4.54 – 4.35 (m, 3H), 4.06 (q, *J* = 5.5 Hz, 1H), 3.54 – 3.38 (m, 2H), 3.24 – 3.15 (m, 2H), 2.98 (dd, *J* = 13.2, 10.6 Hz, 1H), 2.78 (d, *J* = 11.4 Hz, 1H), 1.95 – 1.68 (m, 2H), 1.20 (d, *J* = 6.7 Hz, 3H), 0.81 (s, 9H), -0.05 (s, 6H). <sup>13</sup>C NMR (100 MHz, CDCl<sub>3</sub>) δ 201.1, 177.0, 138.6, 136.8, 129.6 (2C), 129.0 (2C), 128.5 (2C), 127.8 (2C), 127.6, 127.3, 73.2, 72.2, 69.5, 66.4, 44.7, 36.7, 35.0, 32.2, 25.9 (3C, TBS), 18.2, 13.8, -4.3, -4.5. HRMS calc'd for C<sub>29</sub>H<sub>41</sub>NO<sub>3</sub>S<sub>2</sub>Si (M+Na)<sup>+</sup> 566.8452, found (M+Na)<sup>+</sup> 566.2205.

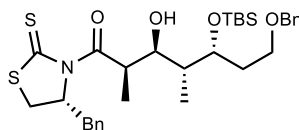
**(2*S*,3*R*)-5-(Benzyloxy)-3-((*tert*-butyldimethylsilyl)oxy)-2-methylpentanal (3.8).**



To a solution of **3.15** (129 mg, 0.237 mmol) in DCM (2.64 mL, 0.09 M) at -78 °C was added DIBAL-H (0.474 mL, 1 M in DCM) dropwise. The reaction went clear almost immediately upon addition of DIBAL-H. When clear, saturated Rochelle's Salt was added and the reaction was allowed to stir at rt for 1 hour. At this time, the aqueous layer was extracted with DCM (3x), and the combined organic layers were washed with brine, dried (Na<sub>2</sub>SO<sub>4</sub>), and concentrated under reduced pressure. The crude reaction mixture was purified by chromatography (30% EtOAc in hexanes) to yield aldehyde **3.8** as a clear oil (62 mg, 78%), which was used immediately in the next reaction. <sup>1</sup>H NMR (400 MHz, CDCl<sub>3</sub>) δ 9.71 (s, 1H), 7.27 – 7.18 (m, 5H), 4.41 (q, *J* = 11.9 Hz, 2H), 4.25 (ddd, *J* = 7.3,

5.6, 3.6 Hz, 1H), 3.45 (tq,  $J = 6.9, 3.9, 3.5$  Hz, 2H), 2.44 – 2.38 (m, 1H), 1.83 – 1.65 (m, 2H), 0.99 (d,  $J = 7.0$  Hz, 3H), 0.79 (s, 9H), -0.01 (d,  $J = 9.1$  Hz, 6H).

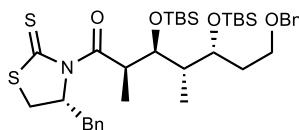
**(2*R*,3*S*,4*R*,5*R*)-1-((*R*)-4-Benzyl-2-thioxothiazolidin-3-yl)-7-(benzyloxy)-5-((*tert*-butyldimethylsilyl)oxy)-3-hydroxy-2,4-dimethylheptan-1-one (3.16).**



To a stirred solution of thiazolidinone thione (**3.11**, 0.443 g, 1.67 mmol) and dry DCM (1.12 mL, 1M) at 0 °C was added TiCl<sub>4</sub> (0.194 mL, 1.76 mmol) dropwise, upon which the mixture turned orange. If necessary, additional DCM (~ 0.2 mL) was added to keep the reaction solvated. After stirring for 5 min, DIPEA (0.320 mL, 1.83 mmol) was added dropwise. The dark purple reaction mixture was allowed to stir for an additional 40 min at 0 °C, at which time NMP (0.321 mL, 3.33 mmol) was added dropwise, and the reaction was let to stir for 15 min. At this time, the mixture was cooled to -78 °C and aldehyde (**3.8**, 0.374 g, 1.112 mmol) in 0.5 mL DCM was added dropwise. The reaction was stirred at -78 °C for 2 h, and then warmed to 0 °C and let to stir for 1 h. After complete consumption of the aldehyde, the reaction mixture was quenched with saturated ammonium chloride. The aqueous layer was extracted with DCM (3x), and the combined organic layers were washed with brine, dried (Na<sub>2</sub>SO<sub>4</sub>), filtered, and concentrated under reduced pressure. The crude product mixture was purified by silica-gel chromatography (CombiFlash, 0-20% EtOAc in hexanes) to give the *syn* aldol product **3.16** as a yellow oil (0.539 g, 81%). <sup>1</sup>H NMR (400 MHz, CDCl<sub>3</sub>) δ 7.33 – 7.26 (m, 10H), 5.34 (td,  $J = 7.0, 3.5$  Hz, 1H), 5.03 – 4.93

(m, 1H), 4.49 – 4.43 (m, 2H), 4.14 – 4.06 (m, 1H), 3.99 (td,  $J = 6.8, 2.4$  Hz, 1H), 3.46 (td,  $J = 6.8, 3.1$  Hz, 2H), 3.33 (dd,  $J = 11.5, 7.3$  Hz, 1H), 3.14 (dd,  $J = 13.2, 3.6$  Hz, 1H), 3.10 (d,  $J = 2.3$  Hz, 1H), 2.99 (ddd,  $J = 13.3, 10.5, 3.2$  Hz, 1H), 2.85 (dd,  $J = 11.6, 2.9$  Hz, 1H), 1.86 (q,  $J = 6.6$  Hz, 2H), 1.71 (td,  $J = 6.5, 2.4$  Hz, 1H), 1.26 – 1.20 (m, 3H), 1.01 (d,  $J = 6.8$  Hz, 3H), 0.88 (d,  $J = 8.0$  Hz, 9H), 0.08 (s, 6H).  $^{13}\text{C}$  NMR (100 MHz,  $\text{CDCl}_3$ )  $\delta$  201.1, 178.5, 138.5, 136.6, 129.5 (2C), 129.1 (2C), 129.0, 128.5 (2C), 127.6 (2C), 127.4, 73.5, 73.2, 72.3, 69.2, 67.4, 41.7, 39.0, 37.0, 34.9, 31.4, 26.0 (3C), 18.2, 12.5, 8.6, -3.8, -4.2. HRMS calc'd for  $\text{C}_{32}\text{H}_{47}\text{NO}_4\text{S}_2\text{Si}$  ( $\text{M}+\text{Na}$ ) $^+$  624.2608, found ( $\text{M}+\text{Na}$ ) $^+$  624.2609.

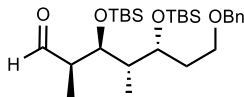
**(2*R*,3*S*,4*S*,5*R*)-1-((*R*)-4-Benzyl-2-thioxothiazolidin-3-yl)-7-(benzyloxy)-3,5-bis((*tert*-butyldimethylsilyl)oxy)-2,4-dimethylheptan-1-one (3.17).**



To a solution of alcohol (**3.16**, 1.3 g, 2.2 mmol) in DCM (19 mL, 0.12 M) at 0 °C was added 2,6-lutidine (0.50 mL, 3.2 mmol) and then TBSOTf (0.74 mL, 3.2 mmol) dropwise. The reaction was warmed to rt and upon consumption of the starting material, the mixture was quenched with sodium bicarbonate. The aqueous layer was extracted with DCM (3x), the combined organic layers were washed with brine, and then dried ( $\text{Na}_2\text{SO}_4$ ), filtered, and concentrated under reduced pressure. The crude oil was purified by chromatography (CombiFlash, 0->10% EtOAc in hexanes) to yield **3.17** as a yellow oil (0.97 g, 63%).  $[\alpha]_D^{26}$  -67.3 ( $c$  1,  $\text{CHCl}_3$ ).  $^1\text{H}$  NMR (400 MHz,  $\text{CDCl}_3$ )  $\delta$  7.35 – 7.26 (m, 10H), 5.27 (ddd,  $J = 10.6, 6.8, 3.9$  Hz, 1H), 4.77 – 4.64 (m, 1H), 4.46 (s, 2H), 4.17 (t,  $J = 5.0$  Hz, 1H), 3.69 (q,  $J = 5.7$  Hz, 1H), 3.49 (td,  $J = 6.8, 6.1, 1.9$  Hz, 2H), 3.28 – 3.13 (m, 2H), 3.00 (dd,  $J = 13.1,$

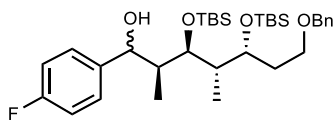
10.5 Hz, 1H), 2.76 (d,  $J = 11.5$  Hz, 1H), 1.94 – 1.72 (m, 2H), 1.67 (h,  $J = 6.8$  Hz, 1H), 1.20 (d,  $J = 6.7$  Hz, 3H), 0.90 (m, 21H), 0.09 – 0.03 (m, 12H).  $^{13}\text{C}$  NMR (100 MHz,  $\text{CDCl}_3$ )  $\delta$  200.7, 177.2, 138.6, 136.7, 129.6 (2C), 129.0 (2C), 128.5 (2C), 127.9 (2C), 127.7, 127.3, 73.8, 73.2, 70.5, 69.3, 66.8, 45.5, 41.6, 36.7, 35.7, 31.6, 26.2 (3C), 26.2 (3C), 18.5, 18.4, 13.3, 11.5, -3.5, -3.6, -3.7, -4.1. HRMS calc'd for  $\text{C}_{38}\text{H}_{61}\text{NO}_4\text{S}_2\text{Si}_2$  ( $\text{M}+\text{Na}$ ) $^+$  738.3473, found ( $\text{M}+\text{Na}$ ) $^+$  738.3488.

**(2*R*,3*S*,4*S*,5*R*)-7-(Benzyloxy)-3,5-bis(*tert*-butyldimethylsilyloxy)-2,4-dimethylheptanal (3.7).**



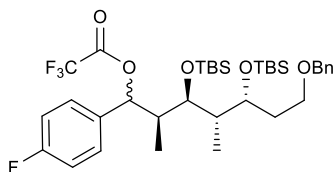
To a solution of **3.17** (585 mg, 0.817 mmol) in DCM (9.1 mL, 0.1 M) at  $-78$  °C was added DIBAL-H (1.63 mL, 1 M in DCM) dropwise. The reaction went clear almost immediately upon addition of DIBAL-H. When clear, saturated Rochelle's Salt was added and the reaction was allowed to stir at rt for 1 hour. At this time, the aqueous layer was extracted with DCM (3x), and the combined organic layers were washed with brine, dried ( $\text{Na}_2\text{SO}_4$ ), and concentrated under reduced pressure. The crude reaction mixture was purified by chromatography (0-20% EtOAc in hexanes) to yield aldehyde **3.7** as a clear oil (366 mg, 88%), which was used immediately in the next reaction.  $^1\text{H}$  NMR (400 MHz,  $\text{CDCl}_3$ )  $\delta$  9.68 (s, 1H), 7.35 – 7.26 (m, 5H), 4.48 (s, 2H), 4.32 (dd,  $J = 6.9, 1.9$  Hz, 1H), 3.99 (td,  $J = 6.2, 3.2$  Hz, 1H), 3.47 (t,  $J = 6.8$  Hz, 2H), 2.47 (qd,  $J = 6.8, 1.7$  Hz, 1H), 1.86 (q,  $J = 6.6$  Hz, 2H), 1.74 (tt,  $J = 7.4, 3.8$  Hz, 1H), 1.12 (d,  $J = 7.0$  Hz, 3H), 0.89 – 0.83 (m, 21H), 0.09 – 0.03 (m, 12H).

**(2*S*,3*R*,4*S*,5*R*)-7-(Benzyloxy)-3,5-bis(*tert*-butyldimethylsilyloxy)-1-(4-fluorophenyl)-2,4-dimethylheptan-1-ol (3.18).**



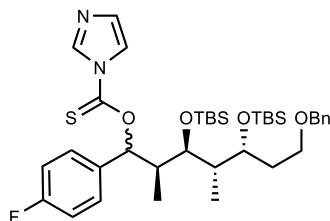
(4-Fluorophenyl)magnesium bromide (1.10 mL, 1.10 mmol, 1 M in THF) was added dropwise to a solution of aldehyde **3.7** (374 mg, 0.735 mmol) in THF (6.23 mL, 0.12 M) at 0 °C. The reaction was warmed to rt and stirred overnight, at which time saturated NH<sub>4</sub>Cl was added and the aqueous layer was extracted with EtOAc (4x). The combined organic layers were washed with brine, dried over sodium sulfate, and concentrated under reduced pressure. The crude reaction mixture was purified by chromatography (0->10% EtOAc in hexanes) to yield **3.18** as a clear oil (403 mg, 91%). <sup>1</sup>H NMR (400 MHz, CDCl<sub>3</sub>) δ 7.35 – 7.26 (m, 5H), 7.25 – 7.16 (m, 2H), 7.04 – 6.94 (m, 2H), 4.51 – 4.43 (m, 3H), 4.27 (d, *J* = 6.8 Hz, 1H), 3.91 (q, *J* = 5.5 Hz, 1H), 3.51 (t, *J* = 6.9 Hz, 2H), 2.52 (br s, 1H), 1.92 – 1.80 (m, 4H), 0.94 – 0.88 (m, 21H), 0.61 (d, *J* = 6.9 Hz, 3H), 0.16 – 0.07 (m, 12H). <sup>13</sup>C NMR (100 MHz, CDCl<sub>3</sub>) δ 179.2, 140.2 (d, <sup>4</sup>*J*<sub>CF</sub> = 3.1 Hz), 138.6, 128.6 (d, <sup>3</sup>*J*<sub>CF</sub> = 5.2 Hz, 2C), 128.5 (2C), 127.8, 127.7 (2C), 115.2 (d, <sup>2</sup>*J*<sub>CF</sub> = 21.3 Hz, 2C), 76.4, 73.2, 71.2, 67.1, 44.0, 35.6, 35.4, 26.3 (3C), 26.2 (3C), 18.6, 18.5, 11.3, 8.2, -3.3, -3.5, -3.6, -4.0. HRMS calc'd for C<sub>34</sub>H<sub>57</sub>FO<sub>4</sub>Si<sub>2</sub> (M+Na)<sup>+</sup> 627.9836, found (M+Na)<sup>+</sup> 627.3664.

**(2*S*,3*R*,4*S*,5*R*)-7-(Benzyloxy)-3,5-bis((*tert*-butyldimethylsilyl)oxy)-1-(4-fluorophenyl)-2,4-dimethylheptyl 2,2,2-trifluoroacetate (3.18a).**



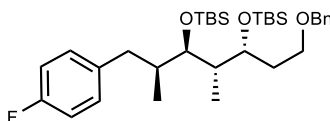
To a solution of alcohol 3.18 (138 mg, 0.228 mmol) in DCM (4.6 mL, 50 mM) was added DMAP (5.6 mg, 0.046 mmol). The reaction was cooled to 0 °C, TFAA (84  $\mu$ L, 0.593 mmol) was added dropwise, and the reaction stirred until the starting material was consumed by TLC. At this time, saturated NaHCO<sub>3</sub> was added and the reaction warmed to RT and stirred for 15 min. The reaction was then extracted 3x DCM, the organic layers were combined and washed with brine, dried over Na<sub>2</sub>SO<sub>4</sub>, and concentrated under reduced pressure. The crude oil was then passed through a plug of silica with 30% EtOAc/hexanes to yield **3.18a** as an oil (160 mg, 99%). <sup>1</sup>H NMR (400 MHz, CDCl<sub>3</sub>)  $\delta$  7.41 – 7.34 (m, 5H), 7.31 – 7.27 (m, 2H), 7.09 – 7.02 (m, 2H), 5.81 (d, *J* = 10.7 Hz, 1H), 4.47 – 4.38 (m, 2H), 3.76 (q, *J* = 5.4 Hz, 1H), 3.46 (d, *J* = 6.7 Hz, 1H), 3.37 (t, *J* = 6.8 Hz, 2H), 1.71 – 1.50 (m, 4H), 1.09 (d, *J* = 6.5 Hz, 3H), 0.98 – 0.89 (m, 18H), 0.83 (d, *J* = 7.0 Hz, 3H), 0.12 – 0.03 (m, 12H). <sup>13</sup>C NMR (100 MHz, CDCl<sub>3</sub>)  $\delta$  194.1, 164.4, 141.0, 138.5, 133.2 (2C), 130.3 (*d*, <sup>3</sup>*J*<sub>CF</sub> = 7.7 Hz, 2C), 128.5 (2C), 127.8, 127.7, 116.0 (*d*, <sup>2</sup>*J*<sub>CF</sub> = 21.8 Hz, 2C), 83.0, 73.2, 72.2, 70.2, 66.8, 43.8, 40.5, 35.6, 26.3 (3C), 25.9 (3C), 18.8, 18.3, 10.8, 10.5, -2.8, -3.4, -3.4, -4.1.

***O*-((2*S*,3*R*,4*S*,5*R*)-7-(Benzyloxy)-3,5-bis((*tert*-butyldimethylsilyl)oxy)-1-(4-fluorophenyl)-2,4-dimethylheptyl) 1*H*-imidazole-1-carbothioate (**3.24**).**



To a solution of alcohol **3.18** (403 mg, 0.666 mmol) in DCM (16.65 mL, 0.04 M) was added DMAP (8.14 mg, 0.067 mmol) and 1,1'-diimidazolethione (594 mg, 3.33 mmol). The reaction was allowed to stir at reflux until consumption of starting material (~48 h), at which time the reaction was cooled and washed with water and brine. The organic layers were dried over Na<sub>2</sub>SO<sub>4</sub>, filtered, concentrated, and purified by chromatography (0-100% EtOAc in hexanes) to yield **3.24** as a light-yellow oil (307 mg, 65%). <sup>1</sup>H NMR (400 MHz, CDCl<sub>3</sub>) δ 8.35 (s, 1H), 7.62 (s, 1H), 7.32 – 7.17 (m, 8H), 7.00 (ddt, *J* = 8.7, 4.4, 2.9 Hz, 2H), 6.11 (d, *J* = 10.4 Hz, 1H), 4.49 (s, 2H), 4.16 – 4.09 (m, 1H), 3.96 (q, *J* = 5.5 Hz, 1H), 3.53 (t, *J* = 6.5 Hz, 2H), 2.03 – 1.71 (m, 4H), 0.98 – 0.81 (m, 21H), 0.64 (d, *J* = 6.8 Hz, 3H), 0.12 – -0.01 (m, 12H).

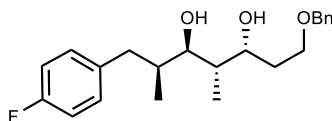
**(5*R*,6*S*,7*R*)-5-(2-(Benzyloxy)ethyl)-7-((*S*)-1-(4-fluorophenyl)propan-2-yl)-2,2,3,3,6,9,9,10,10-nonamethyl-4,8-dioxa-3,9-disilaundecane (**3.25**).**



To a solution of imidazolide **3.24** (307 mg, 0.430 mmol) in toluene (24 mL, 0.018 M) was added HSnBu<sub>3</sub> (1.29 mL, 1.29 mmol, 1 M in cyclohexane) and AIBN (21 mg, 0.130 mmol). The reaction was refluxed until the starting material was consumed (24-48 h), at which time the reaction was cooled and concentrated. The crude oil was purified by

chromatography (0-20% EtOAc in hexanes) to yield **3.25** as a clear oil (160 mg, 64%).  $[\alpha]_D^{26}$  -74.5 (*c* 0.73, CHCl<sub>3</sub>). <sup>1</sup>H NMR (400 MHz, CDCl<sub>3</sub>) δ 7.38 – 7.23 (m, 5H), 7.13 (dd, *J* = 8.3, 5.4 Hz, 2H), 6.98 (t, *J* = 8.5 Hz, 2H), 4.60 – 4.45 (m, 2H), 3.92 (q, *J* = 5.4 Hz, 1H), 3.76 (d, *J* = 6.6 Hz, 1H), 3.52 (t, *J* = 6.9 Hz, 2H), 2.68 (dd, *J* = 13.5, 5.4 Hz, 1H), 2.51 (dd, *J* = 13.5, 9.5 Hz, 1H), 1.92 (dt, *J* = 14.0, 6.6 Hz, 1H), 1.87 – 1.74 (m, 2H), 1.73 – 1.64 (m, 1H), 1.00 – 0.85 (m, 24H), 0.18 – 0.05 (m, 12H). <sup>13</sup>C NMR (100 MHz, CDCl<sub>3</sub>) δ 161.4 (<sup>1</sup>*J*<sub>CF</sub> = 243.4 Hz), 138.6, 137.2 (<sup>4</sup>*J*<sub>CF</sub> = 3.2 Hz), 130.5 (<sup>3</sup>*J*<sub>CF</sub> = 7.7 Hz, 2C), 128.4 (2C), 127.7 (2C), 127.6, 115.0 (<sup>2</sup>*J*<sub>CF</sub> = 21.0 Hz, 2C), 76.4, 73.2, 71.1, 67.0, 44.0, 41.4, 38.1, 35.7, 26.1 (3C), 26.3 (3C), 18.7, 18.4, 13.4, 11.3, -3.2, -3.4, -3.7, -3.7. HRMS calc'd for C<sub>34</sub>H<sub>57</sub>FO<sub>3</sub>Si<sub>2</sub> (M+Na)<sup>+</sup> 611.3722, found (M+Na)<sup>+</sup> 611.3742.

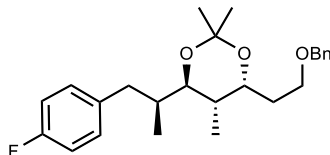
**(2*S*,3*R*,4*S*,5*R*)-7-(Benzyloxy)-1-(4-fluorophenyl)-2,4-dimethylheptane-3,5-diol (3.28).**



Silane **3.25** (15 mg, 0.025 mmol) was taken up in 1% HCl in EtOH (0.5 mL) and allowed to stir overnight. Upon completion, reaction was diluted with EtOAc and saturated NaHCO<sub>3</sub>. The aqueous layer was washed 3x EtOAc, the organic layers combine and washed with brine, dried over Na<sub>2</sub>SO<sub>4</sub>, filtered, and concentrated. The crude oil was purified by chromatography (0-100% EtOAc in hexanes) to yield **3.28** as a clear oil (7.4 mg, 81%). <sup>1</sup>H NMR (400 MHz, CDCl<sub>3</sub>) δ 7.34 – 7.18 (m, 5H), 7.08 (dd, *J* = 8.3, 5.6 Hz, 2H), 6.89 (t, *J* = 8.5 Hz, 2H), 4.48 (s, 2H), 4.08 – 3.94 (m, 1H), 3.72 (dt, *J* = 9.2, 4.5 Hz, 1H), 3.60 (td, *J* = 9.6, 3.1 Hz, 1H), 3.45 (dd, *J* = 9.1, 2.7 Hz, 1H), 2.72 – 2.40 (m, 2H), 1.96 – 1.70 (m, 3H), 1.51 (d, *J* = 14.5 Hz, 1H), 0.81 (d, *J* = 6.7 Hz, 3H), 0.70 (d, *J* = 7.1 Hz,

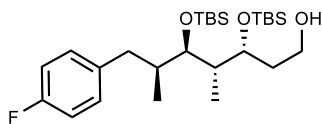
3H).  $^{13}\text{C}$  NMR (100 MHz,  $\text{CDCl}_3$ )  $\delta$  161.4 ( $^1J_{\text{CF}} = 243.1$  Hz), 137.7, 137.1 ( $^4J_{\text{CF}} = 3.2$  Hz), 130.6 ( $^3J_{\text{CF}} = 7.7$  Hz, 2C), 128.7 (2C), 128.0 (2C), 127.9, 115.0 ( $^2J_{\text{CF}} = 21.0$  Hz, 2C), 76.2, 75.4, 73.7, 70.6, 39.8, 39.5, 37.8, 31.5, 12.6, 12.2.

**(4*R*,5*S*,6*R*)-4-(2-(Benzyloxy)ethyl)-6-((*S*)-1-(4-fluorophenyl)propan-2-yl)-2,2,5-trimethyl-1,3-dioxane (3.29).**



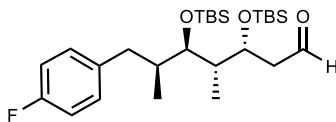
To solution of dimethoxypropane (7.55  $\mu\text{L}$ , 62  $\mu\text{mol}$ ) and PTSA (0.2 mg, 1  $\mu\text{mol}$ ) in DCM (0.05 mL) was added diol **3.28** (7.4 mg, 21  $\mu\text{mol}$ ) in DCM (0.05 mL). The reaction mixture was stirred at rt until starting material was consumed. The reaction mixture was then poured into saturated aqueous  $\text{NaHCO}_3$ , and the mixture was then extracted with EtOAc. The EtOAc extract layers were washed with brine, dried over  $\text{MgSO}_4$ , and concentrated. NMR analysis was carried out on the crude product (**3.29**) to confirm the *anti* 1,3-diol.  $^1\text{H}$  NMR (400 MHz,  $\text{CDCl}_3$ )  $\delta$  7.38 – 7.27 (m, 5H), 7.10 (dd,  $J = 8.2, 5.5$  Hz, 2H), 6.95 (t,  $J = 8.5$  Hz, 2H), 4.50 (s, 2H), 3.97 (dt,  $J = 9.2, 4.7$  Hz, 1H), 3.54 (t,  $J = 6.5$  Hz, 2H), 3.11 (dd,  $J = 7.9, 2.5$  Hz, 1H), 2.69 (dd,  $J = 13.6, 7.1$  Hz, 1H), 2.49 (dd,  $J = 13.6, 8.0$  Hz, 1H), 1.84 – 1.73 (m, 2H), 1.66 (dq,  $J = 8.9, 4.7, 4.2$  Hz, 2H), 1.27 (s, 6H), 0.90 (d,  $J = 6.7$  Hz, 3H), 0.73 (d,  $J = 6.7$  Hz, 3H).  $^{13}\text{C}$  NMR (100 MHz,  $\text{CDCl}_3$ )  $\delta$  161.4, 138.62, 137.1 ( $^4J_{\text{CF}} = 3.1$  Hz), 130.5 ( $^3J_{\text{CF}} = 7.7$  Hz, 2C), 128.5 (2C), 128.0 (2C), 127.7, 115.0 ( $^2J_{\text{CF}} = 21.1$  Hz, 2C), **100.5**, 76.3, 73.4, 67.4, 66.2, 39.5, 38.3, 36.8, 31.3, **25.3**, **24.0**, 13.9, 12.4.

**(3*R*,4*S*,5*R*,6*S*)-3,5-bis(*tert*-Butyldimethylsilyloxy)-7-(4-fluorophenyl)-4,6-dimethylheptan-1-ol (3.26).**



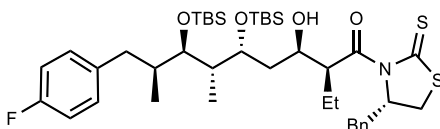
Benzyl ether **3.25** (20.0 mg, 34  $\mu$ mol) was taken up in DCM (0.290 mL, 0.118 M) and dimethylaniline (84  $\mu$ L, 0.68 mmol) was added dropwise.  $\text{AlCl}_3$  (72 mg, 0.54 mmol) was then added in one portion and the reaction was allowed to stir until starting material was consumed ( $\sim$ 1 h), at which time the reaction was cooled to 0  $^\circ\text{C}$  and slowly quenched with 1 M  $\text{NaHSO}_4$  (1 mL). The mixture was warmed to rt and partitioned between EtOAc and saturated aqueous  $\text{NaHCO}_3$  (10 mL each). The organic layer was washed with brine, dried over  $\text{MgSO}_4$ , filtered, and concentrated under vacuum. The crude oil was purified by flash chromatography (0-10% EtOAc in hexanes) to give alcohol **3.26** as a pale-yellow oil (9.4 mg, 56%).  $^1\text{H}$  NMR (400 MHz,  $\text{CDCl}_3$ )  $\delta$  7.14 – 7.03 (m, 2H), 6.96 (t,  $J = 8.7$  Hz, 2H), 3.88 – 3.70 (m, 2H), 3.69 – 3.57 (m, 2H), 2.60 (dd,  $J = 13.4, 6.0$  Hz, 1H), 2.45 (ddd,  $J = 15.2, 10.3, 5.5$  Hz, 1H), 1.78 (ddt,  $J = 22.1, 14.1, 6.3$  Hz, 3H), 1.49 (dq,  $J = 14.6, 5.0$  Hz, 1H), 0.97 – 0.83 (m, 24H), 0.13 – 0.04 (m, 12H).  $^{13}\text{C}$  NMR (100 MHz,  $\text{CDCl}_3$ )  $\delta$  161.4 (d,  $^1J_{\text{CF}} = 243.6$  Hz), 137.5 (d,  $^4J_{\text{CF}} = 3.1$  Hz), 130.6 (d,  $^3J_{\text{CF}} = 7.7$  Hz, 2C), 115.2 (d,  $^2J_{\text{CF}} = 21.1$  Hz, 2C), 75.6, 72.6, 60.0, 43.6, 41.5, 38.2, 37.0, 26.3 (3C), 26.1 (3C), 18.7, 18.3, 14.1, 12.1, -3.2, -3.6, -3.8, -4.0. HRMS calc'd for  $\text{C}_{27}\text{H}_{51}\text{FO}_3\text{Si}_2$  ( $\text{M}+\text{Na}$ ) $^+$  521.3253, found ( $\text{M}+\text{Na}$ ) $^+$  521.3243.

**(3*R*,4*S*,5*R*,6*S*)-3,5-bis((*tert*-Butyldimethylsilyl)oxy)-7-(4-fluorophenyl)-4,6-dimethylheptanal (3.27).**



To a solution of alcohol **3.26** (28 mg, 0.056 mmol) in DCM (0.45 mL, 0.125 M) was added 4 Å molecular sieves (28 mg) and NMO (7.8 mg, 0.066 mmol). The mixture was cooled to 0 °C and allowed to stir for 15 min, after which a solution of TPAP (2 mg, 0.0056 mmol) in DCM (0.1 mL) was added and allowed to stir at 0 °C. After the starting material was consumed, the reaction was diluted with 20% EtOAc in hexanes (2 mL) and filtered through silica. Aldehyde **3.27** was used without further purification in the next reaction. <sup>1</sup>H NMR (400 MHz, CDCl<sub>3</sub>) δ 9.74 – 9.53 (s, 1H), 6.98 – 6.94 (m, 2H), 6.84 – 6.79 (m, 2H), 4.01 (q, *J* = 5.5 Hz, 1H), 3.53 (td, *J* = 7.3, 6.6, 3.0 Hz, 1H), 2.52 – 2.45 (m, 1H), 2.37 – 2.25 (m, 3H), 1.70 – 1.60 (m, 2H), 0.82 – 0.73 (m, 24H), -0.01 – -0.08 (m, 12H).

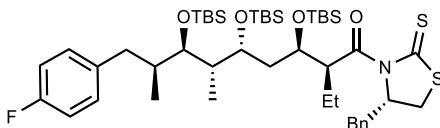
**(2*S*,3*R*,5*R*,6*S*,7*R*,8*S*)-1-((*S*)-4-Benzyl-2-thioxothiazolidin-3-yl)-5,7-bis((*tert*-butyldimethylsilyl)oxy)-2-ethyl-9-(4-fluorophenyl)-3-hydroxy-6,8-dimethylnonan-1-one (3.30).**



To a stirred solution of thiazolidinone thione (**3.10**, 52.7 mg, 0.188 mmol) and dry DCM (1 mL) at 0 °C was added TiCl<sub>4</sub> (20.6 μL, 0.188 mmol) dropwise, upon which the mixture turned orange. If necessary, additional DCM (~ 0.1 mL) was added to keep the reaction solvated. After stirring for 20 min, DIPEA (32.7 μL, 0.188 mmol) was added dropwise. The dark purple reaction mixture was allowed to stir for an additional 20 min at 0 °C, at which time NMP (18.1 μL, 0.188 mmol) was added dropwise, and the reaction was let to

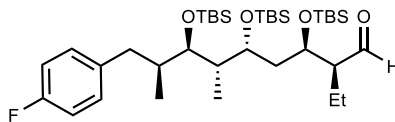
stir for 20 min. At this time, the mixture was cooled to  $-78\text{ }^{\circ}\text{C}$  and aldehyde (**3.27**, 27.3 mg, 0.055 mmol) in 0.1 mL DCM was added dropwise. The vial was washed with an additional 0.1 mL. The reaction was stirred at  $-78\text{ }^{\circ}\text{C}$  for 4 h, and then warmed to  $-50\text{ }^{\circ}\text{C}$  and allowed to stir overnight. After complete consumption of the aldehyde, the reaction mixture was quenched with saturated ammonium chloride. The aqueous layer was extracted with DCM (3x), and the combined organic layers were washed with brine, dried ( $\text{Na}_2\text{SO}_4$ ), filtered, and concentrated under reduced pressure. The crude product mixture was purified by silica-gel chromatography (10% EtOAc in hexanes) to give the *syn* aldol product **3.30** as a yellow oil (17.1 mg, 40%).  $[\alpha]_D^{26} + 32.2$  ( $c$  1,  $\text{CHCl}_3$ ).  $^1\text{H}$  NMR (400 MHz,  $\text{CDCl}_3$ )  $\delta$  7.37 – 7.26 (m, 5H), 7.07 (dd,  $J = 8.4, 5.5$  Hz, 2H), 6.95 (t,  $J = 8.6$  Hz, 2H), 5.30 (ddd,  $J = 10.7, 7.0, 4.1$  Hz, 1H), 4.88 (dt,  $J = 9.2, 4.8$  Hz, 1H), 4.27 (dd,  $J = 10.8, 5.3$  Hz, 1H), 3.87 – 3.81 (m, 1H), 3.73 (d,  $J = 5.7$  Hz, 1H), 3.27 – 3.21 (m, 2H), 3.05 (dd,  $J = 13.2, 10.6$  Hz, 1H), 2.81 (d,  $J = 11.4$  Hz, 1H), 2.62 (dd,  $J = 13.5, 5.0$  Hz, 1H), 2.45 (dd,  $J = 13.5, 9.4$  Hz, 1H), 2.05 (q,  $J = 7.2$  Hz, 1H), 1.92 (dt,  $J = 14.8, 7.7$  Hz, 1H), 1.86 – 1.67 (m, 3H), 1.63 – 1.57 (m, 1H), 1.00 – 0.88 (m, 24H), 0.83 (d,  $J = 6.5$  Hz, 3H), 0.17 – 0.05 (m, 12H).  $^{13}\text{C}$  NMR (100 MHz,  $\text{CDCl}_3$ )  $\delta$  201.8, 175.9, 161.4 (d,  $^1J_{\text{CF}} = 243.7$  Hz), 137.0 (d,  $^4J_{\text{CF}} = 3.2$ ), 136.7, 130.5 (d,  $^3J_{\text{CF}} = 7.7$  Hz, 2C), 129.5 (2C), 129.0 (2C), 127.3, 115.2 (d,  $^2J_{\text{CF}} = 21.0$  Hz, 2C), 75.2, 74.3, 70.1, 69.6, 50.5, 43.5, 42.1, 37.9, 37.1 (2C), 32.0, 26.2 (3C), 26.1 (3C), 20.4, 18.6, 18.2, 14.0, 12.8, 11.7, -3.3, -3.8, -4.0, -4.2. HRMS calc'd for  $\text{C}_{41}\text{H}_{66}\text{FNO}_4\text{S}_2\text{Si}_2$  ( $\text{M}+\text{Na}$ ) $^+$  798.3775, found ( $\text{M}+\text{Na}$ ) $^+$  798.3848.

**(2*S*,3*R*,5*R*,6*S*,7*R*,8*S*)-1-((*S*)-4-Benzyl-2-thioxothiazolidin-3-yl)-3,5,7-tris((tert-butyl-dimethylsilyloxy)-2-ethyl-9-(4-fluorophenyl)-6,8-dimethylnonan-1-one (3.31).**



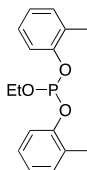
To alcohol **3.30** (8 mg, 0.01 mmol) at 0 °C in DCM (88  $\mu$ L, 0.1 M) was added 2,6-lutidine (2.4  $\mu$ L, .021 mmol) followed by TBSOTf (3.6  $\mu$ L, 0.016 mmol) dropwise. The reaction was warmed to RT and stirred until starting material was consumed, at which time the reaction was quenched with saturated NaHCO<sub>3</sub> and extracted 3x DCM. The combined organic layers were dried over Na<sub>2</sub>SO<sub>4</sub>, filtered, and concentrated under reduced pressure. The crude oil was purified via flash chromatography (0-20% EtOAc in hexanes) to give **3.31** as a yellow oil (5.2 mg, 58% yield). <sup>1</sup>H NMR (400 MHz, CDCl<sub>3</sub>)  $\delta$  7.37 – 7.26 (m, 5H), 7.12 (dd,  $J$  = 8.2, 5.6 Hz, 2H), 6.92 (t,  $J$  = 8.5 Hz, 2H), 5.21 (ddd,  $J$  = 10.7, 6.9, 3.4 Hz, 1H), 4.80 (dt,  $J$  = 8.7, 4.4 Hz, 1H), 4.00 – 3.89 (m, 2H), 3.85 (d,  $J$  = 6.9 Hz, 1H), 3.29 (dd,  $J$  = 13.3, 3.7 Hz, 1H), 3.22 (dd,  $J$  = 11.4, 6.9 Hz, 1H), 3.04 (dd,  $J$  = 13.1, 10.7 Hz, 1H), 2.82 (d,  $J$  = 11.3 Hz, 1H), 2.73 (dd,  $J$  = 13.3, 4.2 Hz, 1H), 2.48 (dd,  $J$  = 13.2, 10.6 Hz, 1H), 1.99 (ddd,  $J$  = 16.4, 13.6, 6.4 Hz, 2H), 1.91 (t,  $J$  = 6.7 Hz, 2H), 1.82 (td,  $J$  = 7.2, 2.9 Hz, 1H), 1.61 (dd,  $J$  = 13.8, 6.9 Hz, 1H), 0.92 – 0.83 (m, 36H), 0.09 (d,  $J$  = 8.6 Hz, 18H). <sup>13</sup>C NMR (100 MHz, CDCl<sub>3</sub>)  $\delta$  201.0, 175.1, 161.3 (d, <sup>1</sup> $J_{CF}$  = 242.9 Hz), 137.4, (d, <sup>4</sup> $J_{CF}$  = 3.1 Hz), 136.9, 130.7 (d, <sup>3</sup> $J_{CF}$  = 7.7 Hz, 2C), 129.6 (2C), 129.0 (2C), 127.3, 114.9 (d, <sup>2</sup> $J_{CF}$  = 21.0 Hz, 2C), 77.4, 71.0, 70.7, 69.8, 51.1, 43.6, 41.7, 41.1, 38.0, 36.8, 31.8, 26.5 (3C), 26.3 (3C), 25.9 (3C), 20.5, 18.8, 18.6, 18.1, 13.2, 12.1, 9.9, -2.8, -3.0, -3.1, -3.9, -4.0, -4.3.

**(2*S*,3*R*,5*R*,6*S*,7*R*,8*S*)-3,5,7-tris((*tert*-Butyldimethylsilyl)oxy)-2-ethyl-9-(4-fluorophenyl)-6,8-dimethylnonanal (3.32).**



To a solution of **3.31** (12.8 mg, .014 mmol) in DCM (0.160 mL, 0.1 M) at  $-78\text{ }^{\circ}\text{C}$  was added DIBAL-H (29  $\mu\text{L}$ , 1 M in DCM) dropwise. The reaction went clear almost immediately upon addition of DIBAL-H. When clear, saturated Rochelle's Salt was added and the reaction was allowed to stir at rt for 1 hour. At this time, the aqueous layer was extracted with DCM (3x), and the combined organic layers were washed with brine, dried ( $\text{Na}_2\text{SO}_4$ ), and concentrated under reduced pressure. The crude reaction mixture was purified by manual chromatography (20% EtOAc in hexanes) to yield aldehyde **3.32** as a clear oil (9.8 mg, quant.), which was used immediately in the next reaction.  $^1\text{H}$  NMR (400 MHz,  $\text{CDCl}_3$ )  $\delta$  9.63 (s, 1H), 7.05 – 6.96 (m, 2H), 6.90 – 6.83 (m, 2H), 3.95 (ddd,  $J = 8.1, 5.5, 2.4$  Hz, 1H), 3.86 – 3.77 (m, 1H), 3.65 (dd,  $J = 8.0, 1.5$  Hz, 1H), 2.57 (dd,  $J = 13.4, 4.8$  Hz, 1H), 2.40 (dd,  $J = 13.3, 10.3$  Hz, 1H), 2.04 (ddt,  $J = 10.0, 4.0, 2.0$  Hz, 1H), 1.90 – 1.65 (m, 5H), 1.52 (d,  $J = 7.0$  Hz, 1H), 0.81 – 0.70 (m, 36H), -0.06 (d,  $J = 1.8$  Hz, 18H).

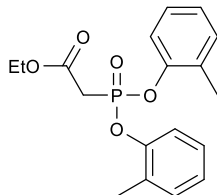
**Ethyl di-*o*-Tolyl Phosphite (3.35).**



A solution of *o*-cresol (6.26 mL, 60.7 mmol) and TEA (8.89 mL, 63.8 mmol) in toluene (46.4 mL, 0.67 M) was cooled to  $0\text{ }^{\circ}\text{C}$ . Dichloro(ethoxy)phosphane (3.55 mL, 1.67 M in diethyl ether, 31.1 mmol) was cannula transferred dropwise. After the addition was

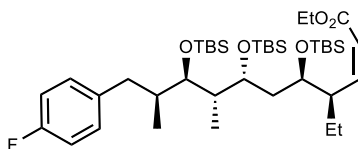
complete, the reaction was warmed to rt and allowed to stir overnight. The reaction was then filtered through celite, concentrated, and used crude in the next reaction.

**Ethyl 2-(bis(*o*-Tolyloxy)phosphoryl)acetate (3.36).**



To phosphite **3.35** at 120 °C was added ethyl bromoacetate (5.19 mL, 46.7 mmol) over 15 min. The reaction was allowed to stir for 48 h at which time the reaction was cooled, concentrated, and purified by CombiFlash (5-25% EtOAc in hexanes) to yield **3.36** as a yellow oil (6.344 g, 59 %). NMRs are consistent with reported values.<sup>161</sup> <sup>1</sup>H NMR (400 MHz, CDCl<sub>3</sub>) δ 7.29 (d, *J* = 8.0 Hz, 2H), 7.19 (d, *J* = 7.3 Hz, 2H), 7.15 – 7.05 (m, 4H), 4.22 (q, *J* = 7.1 Hz, 2H), 3.33 (d, *J* = 21.8 Hz, 2H), 2.25 (s, 6H), 1.27 (t, *J* = 7.1 Hz, 3H). <sup>13</sup>C NMR (100 MHz, CDCl<sub>3</sub>) δ 165.1, 149.0, 131.6, 129.7, 127.3, 125.5, 120.5, 62.1, 35.5, 16.5, 14.2.

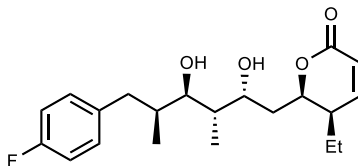
**Ethyl (4*R*,5*R*,7*R*,8*S*,9*R*,10*S*,*Z*)-5,7,9-tris((*tert*-Butyldimethylsilyl)oxy)-4-ethyl-11-(4-fluorophenyl)-8,10-dimethylundec-2-enoate (3.33).**



To phosphonate ester (33 mg, .095 mmol) at 0 °C in THF (1.0 mL, 7.57 mM) was added NaH (3.8 mg, .095 mmol). The slurry was allowed to stir for 15 min, at which time the reaction was cooled to -78 °C and aldehyde **3.32** (6.3 mg, 9.2 μmol in 0.2 mL THF) was added dropwise. The reaction was slowly warmed to 0 °C over 2 h. Following consumption

of starting material, the reaction was quenched with  $\text{NH}_4\text{Cl}$  and extracted with 3x EtOAc. The combined organic layers were washed with brine, dried over  $\text{MgSO}_4$ , filtered, and concentrated. The crude oil was purified by flash chromatography (5% EtOAc in hexanes) to yield **3.33** as a clear oil (2.4 mg, 35%).  $^1\text{H}$  NMR (400 MHz,  $\text{CDCl}_3$ )  $\delta$  7.10 (q,  $J = 7.1$ , 5.8 Hz, 2H), 6.95 (td,  $J = 8.8$ , 3.7 Hz, 2H), 6.12 (dddt,  $J = 35.1$ , 16.2, 10.0, 1.0, 0.5 Hz, 1H), 5.83 (d,  $J = 11.7$  Hz, 1H), 4.86 – 4.74 (m, 1H), 4.04 – 3.94 (m, 1H), 3.91 – 3.63 (m, 3H), 3.55 – 3.35 (m, 1H), 2.74 – 2.61 (m, 1H), 2.54 – 2.43 (m, 1H), 2.43 – 2.34 (m, 1H), 2.00 – 1.85 (m, 3H), 0.07 (s, 18H). Grease is obscuring signals between 1.8 and 0.4. Efforts to remove grease were unsuccessful. Attempts to collect a  $^{13}\text{C}$  NMR were unsuccessful on 400 and 700 MHz NMR instruments. Attempts to collect HRMS were unsuccessful. All of these characterization data will be completed upon generation of more material.

**(5*R*,6*R*)-5-Ethyl-6-((2*R*,3*S*,4*R*,5*S*)-6-(4-fluorophenyl)-2,4-dihydroxy-3,5-dimethylhexyl)-5,6-dihydro-2H-pyran-2-one (4-fluorophenyldemethylpironetin, **3.2**)**



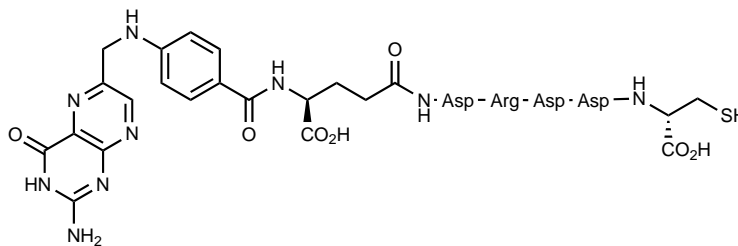
To alkene **3.33** (2.4 mg, 2.66  $\mu\text{mol}$ ) was added 1% HCl in EtOH (60  $\mu\text{L}$ ). The reaction was allowed to stir overnight at which time it was diluted with DCM and quenched with saturated sodium bicarbonate. The aqueous layer was washed 3 additional times with DCM, the combined organic layers washed with brine, dried over  $\text{MgSO}_4$ , filtered, concentrated, and purified by flash chromatography (5% EtOAc in hexanes) to yield the target molecule, 4-fluorophenyldemethylpironetin (**3.2**, 0.7 mg, 60%).  $^1\text{H}$  NMR (400 MHz,  $\text{CDCl}_3$ )  $\delta$  7.16 – 7.10 (m, 2H), 6.98 – 6.91 (m, 2H), 6.39 – 6.31 (m, 1H), 6.25 – 6.16

(m, 1H), 4.72 – 4.66 (m, 1H), 3.68 – 3.62 (m, 2H), 3.28 – 3.20 (m, 1H). Grease is obscuring signals between 2.4 and 0.4. Extensive efforts to remove grease were unsuccessful. All characterization data will be completed upon generation of more material.

## 5.4 Chapter 4 Synthesis and Evaluation of Pironetin Conjugates

### 5.4.1 Synthesis of Conjugates

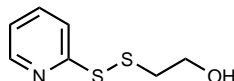
**N2-(4-(((2-Amino-4-oxo-3,4-dihydropteridin-6-yl)methyl)amino)benzoyl)-N5-(((S)-3-carboxy-1-(((S)-1-(((S)-3-carboxy-1-(((S)-3-carboxy-1-(((S)-1-carboxy-2-mercaptoethyl)amino)-1-oxopropan-2-yl)amino)-1-oxopropan-2-yl)amino)-5-guanidino-1-oxopentan-2-yl)amino)-1-oxopropan-2-yl)amino)-L-glutamine (4.3).**



Folic acid peptide **4.3** was synthesized by solid phase peptide synthesis at rt starting from cysteine modified Wang resin as previously described.<sup>147</sup> Briefly, the resin was Fmoc deprotected with 20% piperidine in DMF (3x3mL, 5 min each), washed with DMF, and swelled with DCM. This allowed for coupling in DMF (3 mL) with PyBop (0.22 mmol), DIPEA (0.44 mmol), HoBt (0.22 mmol) and the amino acid of interest (0.22 mmol): Fmoc-Asp(OtBu)-OH, Fmoc-Asp(OtBu)-OH, Fmoc-Arg(Pbf)-OH, Fmoc-Asp(OtBu)-OH, and Fmoc-Glu(OtBu). Couplings were followed by Fmoc deprotection, both monitored by the Kaiser test. Following successful Glu coupling and Fmoc deprotection, N<sub>10</sub>-TFA pteroinic acid (N<sub>10</sub>-TFA Pte, 0.44 mmol) was coupled. The resulting peptide was treated with hydrazine (2% in DMF, 3 mL, 3x5 min) followed by global deprotection and cleavage from the resin (92.5% TFA, 2.5% TIPS, 2.5% EDT, 2.5% H<sub>2</sub>O). After stirring for 1.5 h, the cleaved peptide was drained into ice cold Et<sub>2</sub>O and allowed to precipitate overnight at -20 °C. Following precipitation, the peptide was pelleted by centrifugation, decanted, and

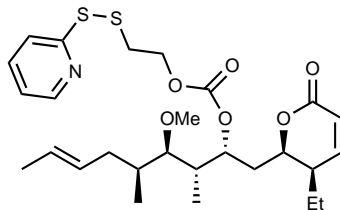
immediately purified by preparative HPLC (A: H<sub>2</sub>O with 0.1% TFA; B: ACN). MALDI calc'd for C<sub>40</sub>H<sub>51</sub>N<sub>15</sub>O<sub>17</sub>S 1046.00, found 1046.43.

**2-(Pyridin-2-yl)disulfaneyl)ethan-1-ol (4.4).**



To alditiol (1 g, 5 mmol) in 10 mL MeOH at rt was added a few drops of acetic acid.  $\beta$ -Mercaptoethanol (0.160 mL, 2.27 mmol in 4 mL MeOH) was added dropwise and the reaction was allowed to stir overnight. The next day, the reaction was concentrated under reduced pressure and purified by flash chromatography to yield alcohol **4.4** as a yellow solid (462.1 mg, 51%). NMR characterization is consistent with reported values.<sup>147</sup> <sup>1</sup>H NMR (400 MHz, CDCl<sub>3</sub>)  $\delta$  8.51 (d,  $J$  = 4.9 Hz, 1H), 7.58 (td,  $J$  = 7.7, 1.6 Hz, 1H), 7.40 (d,  $J$  = 8.1 Hz, 1H), 7.15 (m, 1H), 5.70 (bs, 1H), 3.80 (t,  $J$  = 5.1 Hz, 2H), 2.95 (m, 2H). HRMS calc'd for C<sub>7</sub>H<sub>9</sub>NOS<sub>2</sub> (M+Na)<sup>+</sup> 210.0126, found (M+Na)<sup>+</sup> 210.0009.

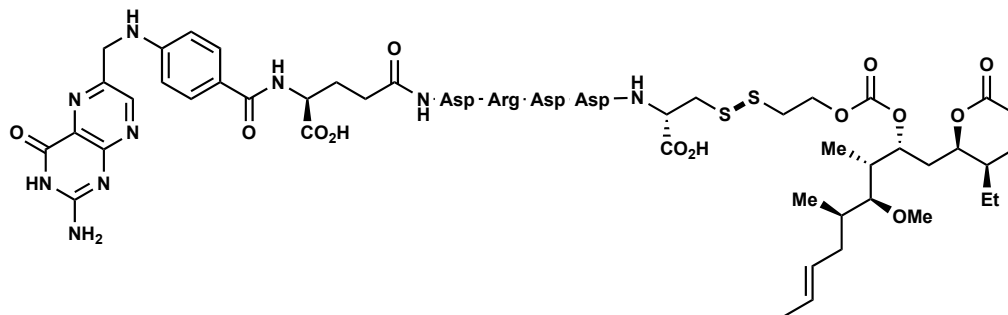
**(2*R*,3*S*,4*R*,5*S*,*E*)-1-((2*R*,3*R*)-3-Ethyl-6-oxo-3,6-dihydro-2*H*-pyran-2-yl)-4-methoxy-3,5-dimethylnon-7-en-2-yl (2-(pyridin-2-yl)disulfaneyl)ethyl) Carbonate (4.5).**



To a solution of pironetin (**1.1**, 10.0 mg, 0.031 mmol) in DCM (0.350 mL) was added DMAP (23.0 mg, 0.18 mmol) in one portion. Triphosgene (3.2 mg, 0.011 mmol) was carefully added and the reaction immediately turned cloudy. After the reaction went clear (about 1 h), alcohol **4.4** (5.8 mg, 0.031 mmol) in DCM (0.150 mL, final concentration 0.06

M) was added dropwise. The reaction was allowed to stir at rt overnight, at which time the crude reaction was concentrated under reduced pressure and purified by flash chromatography (0-20% EtOAc in DCM) to yield activated pironetin (**4.5**) as a yellow solid (16.2 mg, 98% yield). <sup>1</sup>H NMR (400 MHz, CDCl<sub>3</sub>) δ 8.49 (d, *J* = 4.9 Hz, 1H), 7.74 – 7.61 (m, 2H), 7.13 (td, *J* = 5.6, 4.9, 2.3 Hz, 1H), 7.00 (dd, *J* = 9.8, 6.0 Hz, 1H), 6.02 (d, *J* = 9.7 Hz, 1H), 5.51 – 5.33 (m, 2H), 5.19 (td, *J* = 6.8, 2.0 Hz, 1H), 4.50 (dt, *J* = 8.4, 4.3 Hz, 1H), 4.42 (t, *J* = 6.4 Hz, 2H), 3.41 (s, 3H), 3.08 (t, *J* = 6.5 Hz, 2H), 2.96 (dd, *J* = 9.3, 2.3 Hz, 1H), 2.25 (dt, *J* = 9.9, 5.1 Hz, 1H), 2.11 (ddt, *J* = 22.0, 14.8, 6.7 Hz, 2H), 2.03 – 1.93 (m, 2H), 1.75 (ddd, *J* = 13.1, 6.5, 2.8 Hz, 2H), 1.65 (s, 3H), 1.51 (ddd, *J* = 13.5, 8.3, 4.6 Hz, 2H), 0.96 (d, *J* = 7.5 Hz, 3H), 0.90 (d, *J* = 7.0 Hz, 3H), 0.82 (d, *J* = 6.8 Hz, 3H). <sup>13</sup>C NMR (100 MHz, CDCl<sub>3</sub>) δ 164.2, 154.9, 150.5, 149.4, 137.8, 130.2, 129.0, 126.7, 121.3, 121.0, 120.5, 85.3, 77.4, 75.7, 65.4, 61.4, 39.7, 38.5, 37.3, 36.0, 34.5, 29.8, 20.7, 18.2, 12.6, 11.1, 10.5. HRMS calc'd for C<sub>27</sub>H<sub>39</sub>NO<sub>6</sub>S<sub>2</sub> (M+Na)<sup>+</sup> 560.2219, found (M+Na)<sup>+</sup> 560.2111.

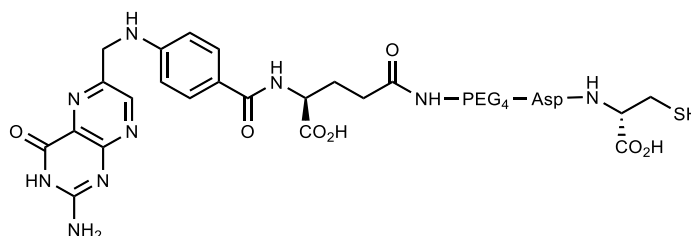
#### First Generation Pironetin Conjugate (**4.2**).



To a solution of peptide **4.3** (2.21 mg, 2.1 μmol) in DMSO (30 μL, 0.07 M final concentration) was added activated pironetin **4.5** (1.3 mg, 2.4 μmol) in DMSO (10 μL) and DIPEA (0.82 μL, 4.7 μmol) by Wiretrol. The reaction was allowed to stir overnight at RT

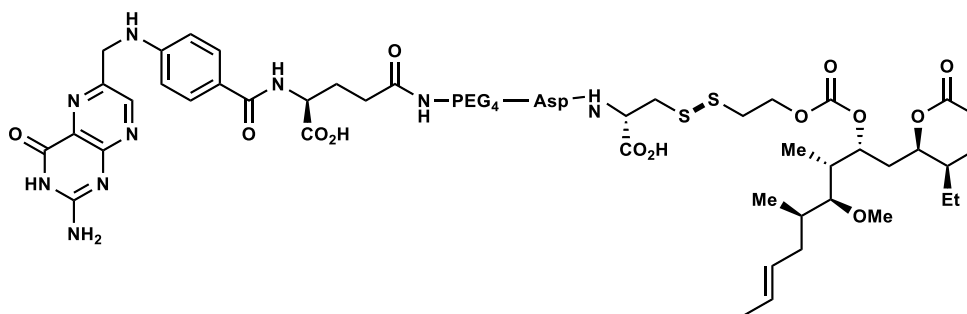
at which time the reaction was quenched with 10% HCl, diluted with ACN until solution was clear, and purified by preparative HPLC (A: H<sub>2</sub>O + 0.1% TFA B: ACN). MALDI calc'd for C<sub>62</sub>H<sub>85</sub>N<sub>15</sub>O<sub>23</sub>S<sub>2</sub> 1472.56, found 1472.85.

**(2*S*,5*S*,23*S*)-23-(4-(((2-Amino-4-oxo-3,4-dihydropteridin-6-yl)methyl)amino)benzamido)-5-(carboxymethyl)-2-(mercaptomethyl)-6,20-dioxo-9,12,15,18-tetraoxa-3,4,19-triazatetracosanedioic Acid (4.8).**



Peptide **4.8** was synthesized in the same way as peptide **4.3** except replacing Fmoc-N-amido-PEG<sub>4</sub>-acid for Asp-Arg-Asp. Following precipitation, the peptide was pelleted by centrifugation, decanted, and immediately purified by preparative HPLC (A: H<sub>2</sub>O with 0.1% TFA; B: ACN). MALDI calc'd for C<sub>37</sub>H<sub>50</sub>N<sub>10</sub>O<sub>15</sub>S (M+Na) 929.92, found 929.54.

**Second Generation Pironetin Conjugate (4.9).**



Conjugate **4.9** was synthesized in the same way as conjugate **4.2** except using peptide **4.8**. The reaction was allowed to stir overnight at RT at which time the reaction was quenched with 10% HCl, diluted with ACN until solution was clear, and purified by preparative

HPLC (A: H<sub>2</sub>O + 0.1% TFA; B: ACN). MALDI calc'd for C<sub>59</sub>H<sub>84</sub>N<sub>10</sub>O<sub>21</sub>S<sub>2</sub> (M+Na) 1355.49, found 1355.60.

#### **Camptothecin Conjugate 4.7.**

Synthesis of intermediates and the final conjugate were done according to the literature and each compound matched the reported characterization.<sup>147</sup>

#### **5.4.2 Characterization of Pironetin Release**

Pironetin or conjugate **4.2** was treated with 10x molar excess of DTT in H<sub>2</sub>O. After 1 h and 8 h, the crude sample (50 µL) was injected onto an HPLC equipped with a 5 µm C<sub>18</sub> 100 Å, LC Column (150 x 4.6 mm) using (A) water and (B) acetonitrile. Samples were maintained at 10 °C and the column was maintained at 25 °C. For analysis, the column was allowed to equilibrate at 30% B prior to the injection of sample. Following sample injection, the gradient was increased to 99% B over 30 min and held for an additional 6 min at 99% before reducing to 30% B over 15 min. The gradient was held at 30% B for an additional 10 min. Absorbance was monitored at 220, 280, and 354 nm.

The samples were also injected onto an Agilent MSD SL LC-MS using (A) water + 0.1% TFA and (B) acetonitrile. Samples were maintained at 10 °C and the column was maintained at 25 °C. For analysis, the column was allowed to equilibrate at 30% B prior to the injection of sample. Following sample injection, the gradient was increased to 99% B over 30 min and held for an additional 6 min at 99% before reducing to 30% B over 15 min. The gradient was held at 30% B for an additional 10 min. Samples were monitored by MS and by absorbance at 220, 280, and 354 nm.

### **5.4.3 Cell Adaptation to FF Conditions**

IGROV and SKOV cells were acquired from the NIH cell repository and cultured in RPMI 1640 media supplemented with 10% FBS and pen/strep (+FA media). To adapt to FF conditions (FF media), cells were passaged four times at six ratios of +FA media in FF media: 100% +FA media, 80% +FA media, 60% +FA media, 40% +FA media, 20% +FA media, and 100% FF media (0% +FA media).

### **5.4.4 Cell Viability Assay**

Cells (IGROV FF and SKOV FF) were grown in a 5% CO<sub>2</sub> atmosphere at 37 °C in tissue culture dishes. Cells were grown in Folate Free RPMI 1640 media supplemented with 10% fetal bovine serum (FBS) and 50 U/mL penicillin/streptomycin.

Upon ~70% growth confluence, cells were harvested by trypsin and the pellet was washed with media and spun down twice before plating 50 µL of 3x10<sup>4</sup> cells/mL in each required well of a 96-well plate. Cells were allowed to grow for 24 h, after which cells were treated with 11 concentrations of compound of interest and pironetin as a control. For experiments in which FA was added, FA was added to the drug stock solution and the dosing media. Cells were then incubated for 1 h and FA containing experiments had media replaced with FF media and then incubated for 72 h, or just incubated for 72 h.

Cell proliferation was analyzed following published protocol for the Non-Radioactive Cell Proliferation Assay (MTT). Following individual treatment with compounds, MTT (3-(4,5-dimethylthiazol-2-yl)-2,5-diphenyltetrazolium bromide, 15 µL of 12 mM stock) was added to the culture medium and allowed to incubate for 4 h at 37 °C. After this time, solubilizing

solution/stop mix (150  $\mu$ L, Promega) was added and the plates were set to incubate overnight at 37  $^{\circ}$ C, after which the absorbance was measured at 570 nm on a microplate reader. Each measurement was done in triplicate during each experiment on a minimum of two separate experiments.

#### **5.4.5 Internalization Assay**

Upon ~70% growth confluence, IGROV FF and SKOV FF cells were harvested by trypsin and the pellet was washed with media and spun down twice before plating 2 mL of  $3 \times 10^4$  cells/mL in each required well of a 6-well plate. Cells were allowed to grow for 24 h, after which cells were treated with conjugate, pironetin, or no treatment. Cells were allowed to incubate for 2 h, at which time the media was removed, the cells were washed 2x PBS buffer (pH 7.4), and lysed (RIPA buffer containing PMSF and protease inhibitor following Promega protocol). The cells were scraped into a centrifuge tube, spun down at  $20,000 \times g$  and the supernatant was collected and extracted 4x EtOAc. The organic layers were dried under nitrogen and taken up in 30% acetonitrile in water and immediately injected onto the Orbitrap Velos for analysis.

Prepared metabolism samples were injected onto a NanoLC-Ultra 2D HPLC system equipped with a 15  $\mu$ L injection loop. Separation was performed on a  $C_{18}$  column (Synergi 2.5  $\mu$ m Max-RP 100  $\text{\AA}$  column, 100 x 3 mm) using a mobile phase consisting of water + 0.1% formic acid (A) and acetonitrile + 0.1% formic acid (B) at a flow rate of 400  $\mu$ L/min. The elution gradient conditions are as follows: column was equilibrated in 5% B prior to injection. Following sample injection, the gradient was held at 5% B for 1 min and then increased to 99% B over 38 min, and then held at 99% B over an additional 4 min. The

gradient was reduced to 5% B over an additional min. The gradient was then held for an additional 10 min at 5% B. The injected sample volume was 5  $\mu$ L.

Samples were analyzed by HPLC-APCI<sup>+</sup>-MS/MS atmospheric pressure chemical ionization (APCI) in positive mode using an LTQ Orbitrap Velos instrument. The APCI source was heated at 250 °C. Source voltage was 3.7 kV, sheath gas and auxiliary gas flow rates were 30 and 5 arbitrary units, respectively; capillary temperature was 300 °C.

The LTQ Orbitrap Velos was operated with four scan events. The first scan event was a full FTMS scan in positive mode over a mass range of 300-1600  $m/z$  with a resolving power of 7500. The second scan event was HCD MS<sup>2</sup> fragmentation of the conjugate mass (1473.3000  $m/z$ ) over a mass range of 200-1500  $m/z$  and with a resolving power of 15000. The third scan event was HCD MS<sup>2</sup> fragmentation of the pironetin mass (325.2500  $m/z$ ) over a mass range of 50-400  $m/z$  and with a resolving power of 15000. The third scan event was HCD MS<sup>2</sup> fragmentation of the pironetin-GSH adduct mass (632.2000  $m/z$ ) over a mass range of 100-700  $m/z$  and with a resolving power of 15000. Normalized collision energy was set to 50% with an activation time of 0.1 ms. The data were processed using the XCaliber software.

## 5.5 References

1. Cairns, R. A.; Harris, I. S.; Mak, T. W. Regulation of cancer cell metabolism. *Nat. Rev. Cancer* **2011**, *11*, 85-95.
2. Hanahan, D.; Weinberg, R. A. The hallmarks of cancer. *Cell* **2000**, *100*, 57-70.
3. Hanahan, D.; Weinberg, R. A. Hallmarks of cancer: the next generation. *Cell* **2011**, *144*, 646-674.
4. Nowell, P. C. The clonal evolution of tumor cell populations. *Science* **1976**, *194*, 23.
5. Noone, A. M.; Howlander, N.; Krapcho, M.; Miller, D.; Brest, A.; Yu, M.; Ruhl, J.; Tatalovich, Z.; Mariotto, A.; Lewis, D. R.; Chen, H. S.; Feuer, E. J.; Cronin, K. A. SEER Cancer Statistics Review, 1975-2015, National Cancer Institute. .
6. Agarwal, R.; Kaye, S. B. Ovarian cancer: Strategies for overcoming resistance to chemotherapy. *Nat. Rev. Cancer* **2003**, *3*, 502-516.
7. Desai, A.; Mitchison, T. J. Microtubule polymerization dynamics. *Annu. Rev. Cell Dev. Biol.* **1997**, *13*, 83-117.
8. Dumontet, C.; Jordan, M. A. Microtubule-binding agents: A dynamic field of cancer therapeutics. *Nat. Rev. Drug Discov.* **2010**, *9*, 790-803.
9. Jordan, M. A.; Wilson, L. Microtubules as a target for anticancer drugs. *Nat. Rev. Cancer* **2004**, *4*, 253-265.
10. Fennell, B. J.; Naughton, J. A.; Barlow, J.; Brennan, G.; Fairweather, I.; Hoey, E.; McFerran, N.; Trudgett, A.; Bell, A. Microtubules as antiparasitic drug targets. *Expert Opin. Drug Discov.* **2008**, *3*, 501-518.
11. Chatterji, B. P.; Jindal, B.; Srivastava, S.; Panda, D. Microtubules as antifungal and antiparasitic drug targets. *Expert Opin. Drug Discov.* **2011**, *21*, 167-186.
12. Emmerson, B. T. The management of gout. *New Engl. J. Med.* **1996**, *334*, 445-451.
13. Cerguaglia, C.; Diaco, M.; Nucera, G.; La Regina, M.; Montalto, M.; Manna, R. Pharmacological and clinical basis of treatment of familial mediterranean fever (FMF) with colchicine or analogues: an update. *Curr. Drug Targets: Inflammation Allergy* **2005**, *4*, 117-124.
14. Varidaki, A.; Hong, Y.; Coffey, E. T. Repositioning microtubule stabilizing drugs for brain disorders. *Front. Cell. Neurosci.* **2018**, *12*, 1-15.
15. Perez, E. A. Microtubule inhibitors: Differentiating tubulin-inhibiting agents based on mechanisms of action, clinical activity, and resistance. *Mol. Cancer Ther.* **2009**, *8*, 2086-2095.
16. Steinmetz, M. O.; Prota, A. E. Microtubule-targeting agents: Strategies to hijack the cytoskeleton. *Trends Cell Biol.* **2018**, *28*, 776-792.
17. Manka, S.; Moores, C. Microtubule structure by cryo-EM: snapshots of dynamic instability. *Essays in Biochemistry* **2018**, *62*, 737-751.
18. Prota, A. E.; Bargsten, K.; Northcote, P. T.; Marsh, M.; Altmann, K.-H.; Miller, J. H.; Fernando Diaz, J.; Steinmetz, M. O. Structural basis of microtubule stabilization by laulimalide and peloruside A. *Angew. Chem. Int. Ed.* **2014**, *53*, 1621-1625.
19. Elie-Caille, C.; Severin, F.; Helenius, J.; Howard, J.; Muller, D. J.; Hyman, A. A. Straight GDP-tubulin protofilaments form in the presence of taxol. *Curr. Biol.* **2007**, *17*, 1765-1770.

20. Prota, A. E.; Bargsten, K.; Redondo-Horcajo, M.; Smith, A. B.; Yang, C. H.; McDaid, H. M.; Paterson, I.; Horwitz, S. B.; Díaz, J. F.; Steinmetz, M. O. Structural basis of microtubule stabilization by discodermolide. *ChemBioChem* **2017**, *18*, 905-909.
21. Dorléans, A.; Gigant, B.; Ravelli, R. B. G.; Mailliet, P.; Mikol, V.; Knossow, M. Variations in the colchicine-binding domain provide insight into the structural switch of tubulin. *Proc. Natl. Acad. Sci.* **2009**, *106*, 13775-13779.
22. Wang, Y.; Benz, F. W.; Wu, Y.; Wang, Q.; Chen, Y.; Chen, X.; Li, H.; Zhang, Y.; Zhang, R.; Yang, J. Structural insights into the pharmacophore of vinca domain inhibitors of microtubules. *Mol. Pharmacol.* **2016**, *89*, 233-242.
23. Prota, A. E.; Bargsten, K.; Fernando Diaz, J.; Marsh, M.; Cuevas, C.; Liniger, M.; Neuhaus, C.; Andreu, J. M.; Altmann, K.-H.; Steinmetz, M. O. A new tubulin-binding site and pharmacophore for microtubule-destabilizing anticancer drugs. *Proc. Natl. Acad. Sci. USA* **2014**, *111*, 13817-13821.
24. Jordan, M. A.; Wilson, L. Microtubules as a target for anticancer drugs. *Nature Reviews Cancer* **2004**, *4*, 253-265.
25. Kavallaris, M. Microtubules and resistance to tubulin-binding agents. *Nat. Rev. Cancer* **2010**, *10*, 194-204.
26. Krishna, R.; Mayer, L. D. Multidrug resistance (MDR) in cancer: Mechanisms, reversal using modulators of MDR and the role of MDR modulators in influencing the pharmacokinetics of anticancer drugs. *Eur. J. Pharm. Sci.* **2000**, *11*, 265-283.
27. Bradley, G.; Ling, V. P-glycoprotein, multidrug resistance and tumor progression. *Cancer Metastasis Rev.* **1994**, *13*, 223-233.
28. Mechetner, E.; Kyshtoobayeva, A.; Zonis, S.; Kim, H.; Stroup, R.; Garcia, R.; Parker, R. J.; Freuhauf, J. P. Levels of multidrug resistance (MDR1) P-glycoprotein expressing by human breast cancer correlate with in vitro resistance to taxol and doxorubicin. *Clin. Cancer. Res.* **1998**, *4*, 389-398.
29. Kavallaris, M.; Kuo, D. Y. S.; Burkhart, C. A.; Regl, D. L.; Norris, M. D.; Haber, M.; Horwitz, S. B. Taxol-resistant epithelial ovarian tumors are associated with altered expression of specific beta-tubulin isotypes. *J. Clin. Invest.* **1997**, *100*, 1282-1293.
30. Balaguer, F. d. A.; Mühlethaler, T.; Estévez-Gallego, J.; Calvo, E.; Giménez-Abián, J. F.; Risinger, A. L.; Sorensen, E. J.; Vanderwal, C. D.; Altmann, K. H.; Mooberry, S. L.; Steinmetz, M. O.; Oliva, M. Á.; Prota, A. E.; Díaz, J. F. Crystal structure of the cyclostreptin-tubulin adduct: Implications for tubulin activation by taxane-site ligands. *Int. J. Mol. Sci.* **2019**, *20*, 1392-1408.
31. Orr, G. A.; Verdier-Pinard, P.; McDaid, H.; Horwitz, S. B. Mechanisms of Taxol resistance related to microtubules. *Oncogene* **2003**, *22*, 7280-7295.
32. Monzo, M.; Rosell, R.; Sanchez, J. J.; Lee, J. S.; O'Brate, A.; Gonzalez-Larriba, J. L.; Alberola, V.; Lorenzo, J. C.; Nunez, L.; Ro, J. Y.; Martin, C. Paclitaxel resistance in non-small-cell lung cancer associated with beta-tubulin gene mutations. *J. Clin. Oncol.* **1999**, *17*, 1786-1793.
33. Canta, A.; Chiorazzi, A.; Cavaletti, G. Tubulin: A target for antineoplastic drugs into the cancer cells but also in the peripheral nervous system. *Curr. Med. Chem.* **2009**, *16*, 1315-1324.

34. Carlson, K.; Ocean, A. J. Peripheral neuropathy with microtubule-targeting agents: Occurrence and management approach. *Clin. Breast Cancer* **2011**, *11*, 73-81.
35. Nikas, J. B.; Boylan, K. L.; Skubitz, A. P.; Low, W. C. Mathematical prognostic biomarker models for treatment response and survival in epithelial ovarian cancer. *Cancer Inform.* **2011**, *10*, 233-247.
36. Kobayashi, S.; Tsuchiya, K.; Harada, T.; Nishide, M.; Kurokawa, T.; Nakagawa, T.; Shimada, N.; Kobayashi, K. Pironetin, a novel plant growth regulator produced by *Streptomyces* sp. NK10958. I. Taxonomy, production, isolation and preliminary characterization. *J. Antibiot.* **1994**, *47*, 697-702.
37. Kobayashi, S.; Tsuchiya, K.; Kurokawa, T.; Nakagawa, T.; Shimada, N. Pironetin, a novel plant growth regulator produced by *Streptomyces* sp. NK10958. II. Structural elucidation. *J. Antibiot.* **1994**, *47*, 703-707.
38. Kurokawa, T.; Kobayashi, K.; Tsucha, K.; Hayaoka, T.; Shida, A.; Masui, A.; Nakagawa, T. Antibiotic NK10958 Manufacture with *Streptomyces* as Agrochemical. JP05025189A, 1993.
39. Kondoh, M.; Usui, T.; Kobayashi, S.; Tsuchiya, K.; Nishikawa, K.; Nishikiori, T.; Mayumi, T.; Osada, H. Cell cycle arrest and antitumor activity of pironetin and its derivatives. *Cancer Lett.* **1998**, *126*, 29-32.
40. Usui, T.; Watanabe, H.; Nakayama, H.; Tada, Y.; Kanoh, N.; Kondoh, M.; Asao, T.; Takio, K.; Watanabe, H.; Nishikawa, K.; Kitahara, T.; Osada, H. The anticancer natural product pironetin selectively targets Lys352 of alpha-tubulin. *Chem. Biol.* **2004**, *11*, 799-806.
41. Yang, J.; Wang, Y.; Wang, T.; Jiang, J.; Botting, C. H.; Liu, H.; Chen, Q.; Yang, J.; Naismith, J. H.; Zhu, X.; Chen, L. Pironetin reacts covalently with cysteine-316 of  $\alpha$ -tubulin to destabilize microtubule. *Nat. Commun.* **2016**, *7*, 1-9.
42. Prota, A. E.; Setter, J.; Waight, A. B.; Bargsten, K.; Murga, J.; Diaz, J. F.; Steinmetz, M. O. Pironetin binds covalently to  $\alpha$ Cys316 and perturbs a major loop and helix of  $\alpha$ -tubulin to inhibit microtubule formation. *J. Mol. Biol.* **2016**, *2016*, 2981-2988.
43. Wang, C.; Cormier, A.; Gigant, B.; Knossow, M. Insight into the GTPase activity of tubulin from complexes with stathin-like domains. *Biochemistry* **2007**, *46*, 10595-10602.
44. Huang, D. S.; Wong, H. L.; Georg, G. I. Synthesis and cytotoxicity evaluation of C4- and C5-modified analogues of the  $\alpha,\beta$ -unsaturated lactone of pironetin. *ChemMedChem* **2017**, *12*, 520-528.
45. Huang, D. S.; Wong, H. L.; Georg, G. I. Synthesis and evaluation of C2 functionalized analogs of the  $\alpha$ -tubulin-binding natural product pironetin. *Bioorg. Med. Chem. Lett.* **2018**, *28*, 2789-2793.
46. Vogt, A.; McPherson, P. A.; Shen, X.; Balachandran, R.; Zhu, G.; Raccor, B. S.; Nelson, S. G.; Tsang, M.; Day, B. W. High-content analysis of cancer-cell-specific apoptosis and inhibition of in vivo angiogenesis by synthetic (-)-pironetin and analogs. *Chem. Biol. Drug Des.* **2009**, *74*, 358-368.
47. Kondoh, M.; Usui, T.; Nishikiori, T.; Mayumi, T.; Osada, H. Apoptosis induction via microtubule disassembly by an antitumour compound, pironetin. *Biochem. J.* **1999**, *340*, 411-416.

48. Yoshida, M.; Matsui, Y.; Ikarashi, Y.; Usui, T.; Osada, H.; Wakasugi, H. Antiproliferating activity of the mitotic inhibitor pironetin against vindesine- and paclitaxel-resistant human small cell lung cancer H69 cells. *Anticancer Res.* **2007**, *27*, 729-736.
49. Coulup, S. K.; Huang, D. S.; Wong, H. L.; Georg, G. I. Identification of the metabolic profile of the  $\alpha$ -tubulin-binding natural product (-)-pironetin. *J. Med. Chem.* **2019**, *62*, 1684-1689.
50. Yasui, K.; Tamura, Y.; Nakatani, T.; Horibe, I.; Kawada, K.; Koizumi, K.; Suzuki, R.; Ohtani, M. Chemical modification of PA-48153C, a novel immunosuppressant isolated from streptomyces prunicolor PA-48153. *J. Antibiot.* **1996**, *49*, 173-80.
51. Tamura, Y.; Simizu, S.; Muroi, M.; Takagi, S.; Kawatani, M.; Watanabe, N.; Osada, H. Polo-like kinase 1 phosphorylates and regulates Bcl-xL during pironetin-induced apoptosis. *Oncogene* **2009**, *28*, 107-116.
52. Yasui, K.; Tamura, Y.; Nakatani, T.; Kawada, K.; Ohtani, M. Total synthesis of (-)-PA-48153C, a novel immunosuppressive 2-pyranone derivative. *J. Org. Chem.* **1995**, *60*, 7567-74.
53. Gurjar, M. K.; Henri, J. T.; Bose, D. S.; Rao, A. V. R. Total synthesis of a potent immunosuppressant pironetin. *Tetrahedron Lett.* **1996**, *37*, 6615-6618.
54. Rao, A. V. R.; Dhar, T. G. M.; Bose, D. S.; Chakraborty, T. K.; Gurjar, M. K. A versatile approach for beta-hydroxy-alpha-amino acids: An application to (4R)-4-[(E)-2-butenyl]-4,N-dimethyl-L-threonine (MeBmt). *Tetrahedron* **1989**, *45*, 7361-7370.
55. Gurjar, M. K.; Chakrabarti, A.; Rao, A. V. R. A stereocontrolled synthesis of pironetin. *Heterocycles* **1997**, *45*, 7-10.
56. Chida, N.; Yoshinaga, M.; Tobe, T.; Ogawa, S. Total synthesis of (-)-PA-48153C (pironetin) utilizing L-quebrachitol as a chiral building block. *Chem. Commun.* **1997**, 1043-1044.
57. Watanabe, H.; Watanabe, H.; Kitahara, T. Total synthesis of (-)-pironetin. *Tetrahedron Lett.* **1998**, *39*, 8313-8316.
58. Watanabe, H.; Watanabe, H.; Bando, M.; Kido, M.; Kitahara, T. An efficient synthesis of pironetins employing a useful chiral building block, (1S, 5S, 6R)-5-hydroxybicyclo[4.1.0]heptan-2-one. *Tetrahedron* **1999**, *55*, 9755-9776.
59. Keck, G. E.; Savin, K. A.; Cressman, E. N. K.; Abbott, D. E. Effects of olefin geometry on the stereochemistry of Lewis acid mediated additions of crotylstannanes to aldehydes. *J. Org. Chem.* **1994**, *59*, 7889-7896.
60. Keck, G. E.; Wagner, C. A.; Sell, T.; Wager, T. T. An especially convenient stereoselective reduction of  $\beta$ -hydroxy ketones to anti 1,3 diols using samarium diiodide. *J. Org. Chem.* **1999**, *64*, 2172-2173.
61. Keck, G. E.; Li, X. Y.; Knutson, C. E. A versatile preparation of alpha,beta-unsaturated lactones from homoallylic alcohols. *Org. Lett.* **1999**, *1*, 411-413.
62. Keck, G. E.; Knutson, C. E.; Wiles, S. A. Total synthesis of the immunosuppressant (-)-pironetin (PA48153C). *Org. Lett.* **2001**, *3*, 707-710.
63. Dias, L. C.; de Oliveira, L. G.; de Sousa, M. A. Total synthesis of (-)-pironetin. *Org. Lett.* **2003**, *5*, 265-268.

64. Ando, K. Highly selective synthesis of Z-unsaturated esters by using new Horner-Emmons reagents, ethyl (diarylphosphono)acetates. *J. Org. Chem.* **1997**, *62*, 1934-1939.
65. Crimmins, M. T.; Chaudhary, K. Titanium enolates of thiazolidinethione chiral auxiliaries: Versatile tools for asymmetric aldol additions. *Org. Lett.* **2000**, *2*, 775-777.
66. Crimmins, M. T.; Dechert, A.-M. R. Enantioselective total synthesis of (-)-pironetin: Iterative aldol reactions of thiazolidinethiones. *Org. Lett.* **2009**, *11*, 1635-1638.
67. Nelson, S. G.; Zhu, C.; Shen, X. Catalytic asymmetric acyl halide-aldehyde cyclocondensation reactions of substituted ketenes. *J. Am. Chem. Soc.* **2004**, *126*, 14-15.
68. Shen, X.; Wasmuth, A. S.; Zhao, J.; Zhu, C.; Nelson, S. G. Catalytic asymmetric assembly of stereodefined propionate units: An enantioselective total synthesis of (-)-pironetin. *J. Am. Chem. Soc.* **2006**, *128*, 7438-7439.
69. Enders, D.; Dhulut, S.; Steinbusch, D.; Herrbach, A. Asymmetric total synthesis of (-)-pironetin employing the SAMP/RAMP hydrazone methodology. *Chem. Eur. J.* **2007**, *13*, 3942-3949.
70. Bressy, C.; Vors, J. P.; Hillebrand, S.; Arseniyadis, S.; Cossy, J. Asymmetric total synthesis of the immunosuppressant (-)-pironetin. *Angew. Chem., Int. Ed.* **2008**, *47*, 10137-10140.
71. Yadav, J. S.; Ather, H.; Rao, N. V.; Reddy, M. S.; Prasad, A. R. Stereoselective synthesis of (-)-pironetin by an iterative Prins cyclisation and reductive cleavage strategy. *Synlett* **2010**, *8*, 1205-1208.
72. Sarabia, F.; Garcia-Castro, M.; Chammaa, S.; Sanchez-Ruiz, A. The chiron approach to pironetins: synthesis of the  $\delta$ -lactonic fragment and modified building blocks from D-glucal. *J. Carbohydr. Chem.* **2006**, *25*, 267-280.
73. Watanabe, H.; Watanabe, H.; Usui, T.; Kondoh, M.; Osada, H.; Kitahara, T. Synthesis of pironetin and related analogs: studies on structure-activity relationships as tubulin assembly inhibitors. *J. Antibiot.* **2000**, *53*, 540-545.
74. Marco, J. A.; Garcia-Pla, J.; Carda, M.; Murga, J.; Falomir, E.; Trigili, C.; Notararigo, S.; Diaz, J. F.; Barasoain, I. Design and synthesis of pironetin analogs with simplified structure and study of their interactions with microtubules. *Eur. J. Med. Chem.* **2011**, *46*, 1630-1637.
75. Panos, J.; Diaz-Oltra, S.; Sanchez-Peris, M.; Garcia-Pla, J.; Murga, J.; Falomir, E.; Carda, M.; Redondo-Horcajo, M.; Diaz, J. F.; Barasoain, I.; Marco, J. A. Synthesis and biological evaluation of truncated  $\alpha$ -tubulin-binding pironetin analogues lacking alkyl pendants in the side chain or the dihydropyrone ring. *Org. Biomol. Chem.* **2013**, *11*, 5809-5826.
76. Roldán, S.; Cardona, A.; Conesa, L.; Murga, J.; Falomir, E.; Carda, M.; Marco, J. A. Synthesis and biological evaluation of simplified pironetin analogues with modifications in the side chain and the lactone ring. *Org. Biomol. Chem.* **2017**, *15*, 220-232.
77. Serafimova, I. M.; Pufall, M. A.; Krishnan, S.; Duda, K.; Cohen, M. S.; Maglathlin, R. L.; McFarland, J. M.; Miller, R. M.; Frodin, M.; Taunton, J. Reversible targeting of noncatalytic cysteines with chemically tuned electrophiles. *Nat. Chem. Biol.* **2012**, *8*, 471-476.

78. Krishnan, S.; Miller, R. M.; Tian, B.; Mullins, R. D.; Jacobson, M. P.; Taunton, J. Design of reversible, cysteine-targeted Michael acceptors guided by kinetic and computational analysis. *J. Am. Chem. Soc.* **2014**, *136*, 12624-12630.
79. Carda, M.; Murga, J.; Diaz-Oltra, S.; Garcia-Pla, J.; Panos, J.; Falomir, E.; Trigili, C.; Diaz, J. F.; Barasoain, I.; Marco, J. A. Synthesis and biological evaluation of  $\alpha$ -tubulin-binding pironetin analogues with enhanced lipophilicity. *Eur. J. Org. Chem.* **2013**, *2013*, 1116-1123.
80. Fura, A.; Shu, Y. Z.; Zhu, M. S.; Hanson, R. L.; Roongta, V.; Humphreys, W. G. Discovering drugs through biological transformation: Role of pharmacologically active metabolites in drug discovery. *J. Med. Chem.* **2004**, *47*, 4339-4351.
81. Baillie, T. A.; Cayen, M. N.; Fouda, H.; Gerson, R. J.; Green, J. D.; Grossman, S. J.; Klunk, L. J.; LeBlanc, B.; Perkins, D. G.; Shipley, L. A. Drug metabolites in safety testing. *Toxicol. Appl. Pharmacol.* **2002**, *182*, 188-196.
82. Obach, R. S. Drug-drug interactions: An important negative attribute in drugs. *Drugs of Today* **2003**, *39*, 301-338.
83. Anari, M. R.; Baillie, T. A. Bridging cheminformatic metabolite prediction and tandem mass spectrometry. *Drug Discov. Today* **2005**, *10*, 711-717.
84. Prakash, C.; Shaffer, C. L.; Nedderman, A. Analytical strategies for identifying drug metabolites. *Mass Spectrom. Rev.* **2007**, *26*, 340-369.
85. Covey, T. R.; Lee, E. D.; Bruins, A. P.; Henion, J. D. Liquid-chromatography mass spectrometry. *Anal. Chem.* **1986**, *58*, 1451-1461.
86. Clarke, N. J. R., Diane; Kormacher, Walter A.; Cox, Kathleen A. Systematic LC/MS metabolite identification in drug discovery. *Anal. Chem.* **2001**, *73*, 430A - 439A.
87. Rydberg, P.; Gloriam, D. E.; Zaretski, J.; Breneman, C.; Olsen, L. SMARTCyp: A 2D method for prediction of cytochrome P450-mediated drug metabolism. *ACS Med. Chem. Lett.* **2010**, *1*, 96-100.
88. Tsuchiya, K.; Kobayashi, S.; Nishikiori, T.; Nakagawa, T.; Tatsuta, K. NK10958P, a novel plant growth regulator produced by *Streptomyces* sp. *J. Antibiot.* **1997**, *50*, 259-260.
89. Niwa, H.; Hida, T.; Yamada, K. A new method for cleavage of aliphatic methyl ethers. *Tetrahedron Lett.* **1981**, *22*, 4239-4240.
90. Twentyman, P. R.; Luscombe, M. A study of some variables in a tetrazolium dye (MTT) based assay for cell growth and chemosensitivity. *Br. J. Cancer* **1987**, *56*, 279-285.
91. Nagata, H.; Usui, T.; Kobayashi, S.; Tsuchiya, K.; Nishikawa, K. Pironetin Analogs as Tubulin Polymerization Inhibitors, Cell Cycle Inhibitors and Antitumor Agents. JP11001434A, 1999.
92. Hamilton, T. C.; Young, R. C.; Ozols, R. F. Experimental model systems of ovarian cancer: Applications to the design and evaluation of new treatment approaches. *Semin. Oncol.* **1984**, *11*, 285-298.
93. Behrens, B. C.; Hamilton, T. C.; Masuda, H.; Grotzinger, K. R.; Whang-Peng, J.; Louie, K. G.; Knutsen, T.; McKoy, W. M.; Young, R. C.; Ozols, R. F. Characterization of a cis-diamminedichloroplatinum(II)-resistant human ovarian cancer cell line and its use in evaluation of platinum analogues. *Cancer Res.* **1987**, *47*, 414-418.

94. Richman, P. G.; Meister, A. Regulation of  $\gamma$ -glutamyl-cysteine synthetase by nonallosteric feedback inhibition by glutathione. *J. Biol. Chem.* **1975**, *250*, 1422-1426.
95. El-Sherbeni, A. A.; El-Kadi, A. O. S. The role of epoxide hydrolases in health and disease. *Arch. Toxicol.* **2014**, *88*, 2013-2032.
96. Crimmins, M. T.; King, B. W.; Tabet, E. A.; Chaudhary, K. Asymmetric aldol additions: Use of titanium tetrachloride and (-)-sparteine for the soft enolization of N-acyl oxazolidinones, oxazolidinethiones, and thiazolidinethiones. *J. Org. Chem.* **2001**, *66*, 894-902.
97. Ager, D. J.; Prakash, I.; Schaad, D. R. 1,2-Amino alcohols and their heterocyclic derivatives as chiral auxiliaries in asymmetric synthesis. *Chem. Rev.* **1996**, *96*, 835-875.
98. Dechert-Schmitt, A. M. R.; Schmitt, D. C.; Krische, M. J. Protecting-group-free diastereoselective C-C coupling of 1,3-glycols and allyl acetate through site-selective primary alcohol dehydrogenation. *Angew. Chem. Int. Ed.* **2013**, *52*, 3195-3198.
99. Goulet, M. T.; Sinclair, P. J.; Wong, F.; Staruch, M. J.; Dumont, F. J.; Cryan, J. G.; Wiederrecht, G. J.; Wyvratt, M. J.; Parsons, W. H. C32-O-phenalkyl ether derivatives of the immunosuppressant ascomycin: a tether length study. *Bioorg. Med. Chem. Lett.* **1999**, *9*, 2085-2088.
100. Robichaud, A. J.; Berger, G. D.; Evans, D. A. The asymmetric syntheses of the C-1 sidechains of zaragozic acid A and zaragozic acid C. *Tetrahedron Lett.* **1993**, *34*, 8403-8406.
101. Shibatomi, K.; Okimi, T.; Abe, Y.; Narayama, A.; Nakamura, N.; Iwasa, S. Organocatalytic asymmetric fluorination of  $\alpha$ -chloroaldehydes involving kinetic resolution. *Beilstein J. Org. Chem.* **2014**, *10*, 323-331.
102. Jana, C. K.; Studer, A. Divergent reactions for racemates: catalytic, enantioselective, and regiodivergent nitroso Diels–Alder reactions. *Angew. Chem. Int. Ed.* **2007**, *46*, 6542-6544.
103. Chenneberg, L.; Baralle, A.; Daniel, M.; Fensterbank, L.; Goddard, J.; Ollivier, C. Visible light photocatalytic reduction of O-thiocarbamates: Development of a tin-free Barton–McCombie deoxygenation reaction. *Adv. Synth. Catal.* **2014**, *356*, 2756-2762.
104. Liu, H.; Yip, J.; Shia, K. Reductive cleavage of benzyl ethers with lithium naphthalenide. A convenient method for debenzylolation. *Tetrahedron Lett.* **1997**, *38*, 2253-2256.
105. Kelly, R. C.; Gebhard, I.; Wicienski, N.; Aristoff, P. A.; Johnson, P. D.; Martin, D. G. Coupling of cyclopropapyrroloindole (CPI) derivatives. The preparation of CC-1065, ent-CC-1065, and analogs. *J. Am. Chem. Soc.* **1987**, *109*, 6837-6838.
106. Akiyama, T.; Hirofuji, H.; Ozaki, S. AlCl<sub>3</sub>-N,N-dimethylaniline: A new benzyl and allyl ether cleavage reagent. *Tetrahedron Lett.* **1991**, *32*, 1321-1324.
107. Takahiko, A.; Hajimu, H.; Shoichiro, O. AlCl<sub>3</sub>-N,N-Dimethylaniline: A novel benzyl and allyl ether cleavage reagent. *Bull. Chem. Soc. Jpn.* **1992**, *65*, 1932-1938.
108. Evans, D. A.; Rieger, D. L.; Gage, J. R. <sup>13</sup>C NMR chemical shift correlations in 1,3-diol acetonides. Implications for the stereochemical assignment of propionate-derived polyols. *Tetrahedron Lett.* **1990**, *31*, 7099-7100.
109. Rychnovsky, S. D.; Skalitzky, D. J. Stereochemistry of alternating polyol chains: <sup>13</sup>C NMR analysis of 1,3-diol acetonides. *Tetrahedron Lett.* **1990**, *31*, 945-948.

110. Ehrlich, P. Address in pathology, ON CHEMIOOTHERAPY. *Br. Med. J.* **1913**, 2, 353-359.
111. Beck, A.; Goetsch, L.; Dumontet, C.; Corvaia, N. Strategies and challenges for the next generation of antibody–drug conjugates. *Nature Reviews Drug Discovery* **2017**, 16, 315.
112. Brentuximab Vedotin - National Cancer Institute. <https://www.cancer.gov/about-cancer/treatment/drugs/brentuximabvedotin>
113. Ado-Trastuzumab Emtansine - National Cancer Institute. <https://www.cancer.gov/about-cancer/treatment/drugs/ado-trastuzumab-emtansine>
114. Inotuzumab Ozogamicin - National Cancer Institute. <https://www.cancer.gov/about-cancer/treatment/drugs/inotuzumabozogamicin>
115. Gemtuzumab Ozogamicin - National Cancer Institute. <https://www.cancer.gov/about-cancer/treatment/drugs/gemtuzumabozogamicin>
116. Campbell, I. G.; Jones, T. A.; Foulkes, W. D.; Trowsdale, J. Folate-binding protein is a marker for ovarian-cancer. *Cancer Res.* **1991**, 51, 5329-5338.
117. Toffoli, G.; Cernigoi, C.; Russo, A.; Gallo, A.; Bagnoli, M.; Boiocchi, M. Overexpression of folate binding protein in ovarian cancers. *Int. J. Cancer* **1997**, 74, 193-198.
118. Low, P. S.; Henne, W. A.; Doorneweerd, D. D. Discovery and development of folic-acid-based receptor targeting for imaging and therapy of cancer and inflammatory diseases. *Acc. Chem. Res.* **2008**, 41, 120-129.
119. Clinical trials.gov. A service of the U.S. National Institutes of Health. <https://clinicaltrials.gov/> (11/09/2016).
120. Oza, A. M.; Vergote, I. B.; Gilbert, L. G.; Ghatage, P.; Lisyankaya, A.; Ghamande, S.; Chambers, S. K.; Arranz, J. A.; Provencher, D. M.; Bessette, P.; Amnon, A.; Symanowski, J.; Penson, R. T.; Naumann, R. W.; Clark, R. A randomized double-blind phase III trial comparing vintafolide (EC145) and pegylated liposomal doxorubicin (PLD/Doxil®/Caelyx®) in combination versus PLD in participants with platinum-resistant ovarian cancer (PROCEED) (NCT01170650). *Gynecol. Oncol.* **2015**, 137, 5-6.
121. Ross, J. F.; Chaudhuri, P. K.; Ratnam, M. Differential regulation of folate receptor isoforms in normal and malignant tissues in vivo and in established cell lines. Physiologic and clinical implications. *Cancer* **1994**, 73, 2432-2443.
122. Parker, N.; Turk, M. J.; Westrick, E.; Lewis, J. D.; Low, P. S.; Leamon, C. P. Folate receptor expression in carcinomas and normal tissues determined by a quantitative radioligand binding assay. *Anal. Biochem.* **2005**, 338, 284-93.
123. Reddy, J. A.; Haneline, L. S.; Srour, E. F.; Antony, A. C.; Clapp, D. W.; Low, P. S. Expression and functional characterization of the beta-isoform of the folate receptor on CD34(+) cells. *Blood* **1999**, 93, 3940-3948.
124. Shen, F.; Ross, J. F.; Wang, X.; Ratnam, M. Identification of a novel folate receptor, a truncated receptor, and receptor type .beta. in hematopoietic cells: cDNA cloning, expression, immunoreactivity, and tissue specificity. *Biochemistry* **1994**, 33, 1209-1215.
125. Shen, F.; Wu, M.; Ross, J. F.; Miller, D.; Ratnam, M. Folate receptor type gamma is primarily a secretory protein due to lack of an efficient signal for

glycosylphosphatidylinositol modification: protein characterization and cell type specificity. *Biochemistry* **1995**, *34*, 5660-5665.

126. Bianchi, E.; Doe, B.; Goulding, D.; Wright, G. J. Juno is the egg Izumo receptor and is essential for mammalian fertilization. *Nature* **2014**, *508*, 483-487.

127. Booger, L. S.; Boonstra, M. C.; Beck, A. J.; Charehbili, A.; Hoogstins, C. E.; Prevoo, H. A.; Singhal, S.; Low, P. S.; van de Velde, C. J.; Vahrmeijer, A. L. Concordance of folate receptor- $\alpha$  expression between biopsy, primary tumor and metastasis in breast cancer and lung cancer patients. *Oncotarget* **2016**, *7*, 17442-17454.

128. Cheung, A.; Bax, H. J.; Josephs, D. H.; Ilieva, K. M.; Pellizzari, G.; Opzoomer, J.; Bloomfield, J.; Fittall, M.; Grigoriadis, A.; Figini, M.; Canevari, S.; Spicer, J. F.; Tutt, A. N.; Karagiannis, S. N. Targeting folate receptor  $\alpha$  for cancer treatment. *Oncotarget* **2016**, *7*, 52553-52574.

129. Senol, S.; Ceyran, A. B.; Aydin, A.; Zemheri, E.; Ozkanli, S.; Kösemetin, D.; Sehitoglu, I.; Akalin, I. Folate receptor  $\alpha$  expression and significance in endometrioid endometrium carcinoma and endometrial hyperplasia. *Int. J. Clin. Exp. Pathol.* **2015**, *8*, 5633-5641.

130. Kurahara, H.; Takao, S.; Kuwahata, T.; Nagai, T.; Ding, Q.; Maeda, K.; Shinchi, H.; Mataka, Y.; Maemura, K.; Matsuyama, T.; Natsugoe, S. Clinical significance of folate receptor beta-expressing tumor-associated macrophages in pancreatic cancer. *Ann Surg Oncol* **2012**, *19*, 2264-2271.

131. Shen, J.; Putt, K. S.; Visscher, D. W.; Murphy, L.; Cohen, C.; Singhal, S.; Sandusky, G.; Feng, Y.; Dimitrov, D. S.; Low, P. S. Assessment of folate receptor- $\beta$  expression in human neoplastic tissues. *Oncotarget* **2015**, *6*, 14700-14709.

132. Mathias, C. J.; Lewis, M. R.; Reichert, D. E.; Laforest, R.; Sharp, T. L.; Lewis, J. S.; Yang, Z. F.; Waters, D. J.; Snyder, P. W.; Low, P. S.; Welch, M. J.; Green, M. A. Preparation of  $^{66}\text{Ga}$ - and  $^{68}\text{Ga}$ -labeled Ga(III)-deferoxamine-folate as potential folate-receptor-targeted PET radiopharmaceuticals. *Nucl. Med. Biol.* **2003**, *30*, 725-731.

133. Turk, M. J.; Breur, G. J.; Widmer, W. R.; Paulos, C. M.; Xu, L. C.; Grote, L. A.; Low, P. S. Folate-targeted imaging of activated macrophages in rats with adjuvant-induced arthritis. *Arthritis Rheumatol.* **2002**, *46*, 1947-1955.

134. Trippett, T. M.; Garcia, S.; Manova, K.; Mody, R.; Cohen-Gould, L.; Flintoff, W.; Bertino, J. R. Localization of a human reduced folate carrier protein in the mitochondrial as well as the cell membrane of leukemia cells. *Cancer Res.* **2001**, *61*, 1941-1947.

135. Lee, R. J.; Wang, S.; Low, P. S. Measurement of endosome pH following folate receptor-mediated endocytosis. *Biochimica et Biophysica Acta* **1996**, *1312*, 237-242.

136. Yang, J.; Chen, H.; Vlahov, I. R.; Cheng, J.-X.; Low, P. S. Evaluation of disulfide reduction during receptor-mediated endocytosis by using FRET imaging. *Proceedings of the National Academy of Sciences of the United States of America* **2006**, *103*, 13872-13877.

137. Yang, J.; Chen, H.; Vlahov, I. R.; Cheng, J.; Low, P. S. Characterization of the pH of folate receptor-containing Endosomes and the Rate of Hydrolysis of internalized acid-labile folate-drug conjugates. *J. Pharmacol. Exp. Ther.* **2007**, *321*, 462-468.

138. Leamon, C. P.; Pastan, I.; Low, P. S. Cytotoxicity of folate-Pseudomonas exotoxin conjugates toward tumor cells. Contribution of translocation domain. *J. Biol. Chem.* **1993**, *268*, 24847-24854.

139. Leamon, C. P.; Low, P. S. Delivery of macromolecules into living cells: a method that exploits folate receptor endocytosis. *Proc. Natl. Acad. Sci.* **1991**, *88*, 5572-5576.
140. Leamon, C. P.; Low, P. S. Membrane folate-binding proteins are responsible for folate-protein conjugate endocytosis into cultured cells. *Biochem. J.* **1993**, *291*, 855-860.
141. Bandara, N. A.; Hansen, M. J.; Low, P. S. Effect of receptor occupancy on folate receptor internalization. *Mol. Pharm.* **2014**, *11*, 1007-1013.
142. Vlahov, I. R.; Leamon, C. P. Engineering Folate-Drug Conjugates to Target Cancer: From Chemistry to Clinic. *Bioconjugate Chem.* **2012**, *23*, 1357.
143. Leamon, C. P.; Reddy, J. A.; Vlahov, I. R.; Dorton, R.; Bloomfield, A.; Vetzal, M.; Klein, P. J.; Westrick, E.; Xu, L.; Wang, Y. Enhancing the therapeutic range of a targeted small-molecule tubulysin conjugate for folate receptor-based cancer therapy. *Cancer Chemother. Pharmacol.* **2017**, *79*, 1151-1160.
144. Paulos, C. M.; Reddy, J. A.; Leamon, C. P.; Turk, M. J.; Low, P. S. Ligand binding and kinetics of folate receptor recycling in vivo: impact on receptor-mediated drug delivery. *Mol. Pharmacol.* **2004**, *66*, 1406-1414.
145. Yang, J.; Chen, H.; Vlahov, I. R.; Cheng, J.-X.; Low, P. S. Evaluation of disulfide reduction during receptor-mediated endocytosis by using FRET imaging. *Proc. Natl. Acad. Sci. USA* **2006**, *103*, 13872-13877.
146. Jones, L. R.; Goun, E. A.; Shinde, R.; Rothbard, J. B.; Contag, C. H.; Wender, P. A. Releasable luciferin-transporter conjugates: Tools for the real-time analysis of cellular uptake and release. *J. Am. Chem. Soc.* **2006**, *128*, 6526-6527.
147. Henne, W. A.; Doorneweerd, D. D.; Hilgenbrink, A. R.; Kularatne, S. A.; Low, P. S. Synthesis and activity of a folate peptide camptothecin prodrug. *Bioorg. Med. Chem. Lett.* **2006**, *16*, 5350-5355.
148. Siwowska, K.; Schmid, R. M.; Cohrs, S.; Schibli, R.; Müller, C. Folate receptor-positive gynecological cancer cells: In vitro and in vivo characterization. *Pharmaceuticals (Basel)* **2017**, *10*, 72-88.
149. Ab, O.; Whiteman, K. R.; Bartle, L. M.; Sun, X.; Singh, R.; Tavares, D.; LaBelle, A.; Payne, G.; Lutz, R. J.; Pinkas, J.; Goldmacher, V. S.; Chittenden, T.; Lambert, J. M. IMG853, a folate receptor-alpha (FRalpha)-targeting antibody-drug conjugate, exhibits potent targeted antitumor activity against FRalpha-expressing tumors. *Mol. Cancer Ther.* **2015**, *14*, 1605-16013.
150. Leamon, C. P.; Reddy, J. A. Folate-targeted chemotherapy. *Adv. Drug Del. Rev.* **2004**, *56*, 1127-1141.
151. Lee, J. W.; Lu, J. Y.; Low, P. S.; Fuchs, P. L. Synthesis and evaluation of taxol-folic acid conjugates as targeted antineoplastics. *Bioorg. Med. Chem.* **2002**, *10*, 2397-2414.
152. Kobayashi, S.; Tsuchiya, K.; Harada, T.; Nishide, M.; Kurokawa, T.; Nakagawa, T.; Shimada, N.; Kobayashi, K. Pironetin, a novel plant growth regulator produced by *Streptomyces* sp. NK 10958. I. Taxonomy, production, isolation and preliminary characterization. *Journal of Antibiotics* **1994**, *47*, 697-702.
153. Leamon, C. P.; Vlahov, I. R.; Reddy, J. A.; Vetzal, M.; Santhapuram, H. K. R.; You, F.; Bloomfield, A.; Dorton, R.; Nelson, M.; Kleindl, P.; Vaughn, J. F.; Westrick, E. Folate-vinca alkaloid conjugates for cancer therapy: A structure-activity relationship. *Bioconjugate Chem.* **2014**, *25*, 560-568.

154. Canney, P. A.; Moore, M.; Wilkinson, P. M.; James, R. D. Ovarian-cancer antigen CA125 - A prospective clinical-assessment of its role as a tumor-marker. *Br. J. Cancer* **1984**, *50*, 765-769.
155. Serrano-Olvera, A.; Duenas-Gonzalez, A.; Gallardo-Rincon, D.; Candelaria, M.; De la Garza-Salazar, J. Prognostic, predictive and therapeutic implications of HER2 in invasive epithelial ovarian cancer. *Cancer Treat. Rev.* **2006**, *32*, 180-190.
156. Chen, Y.; Clark, S.; Wong, T.; Chen, Y.; Chen, Y.; Dennis, M. S.; Luis, E.; Zhong, F.; Bheddah, S.; Koeppen, H.; Gogineni, A.; Polakis, P.; Mallet, W. Armed antibodies targeting the mucin repeats of the ovarian cancer antigen, MUC16, are highly efficacious in animal tumor models. *Cancer Res.* **2007**, *67*, 4924-4932.
157. Liu, J. F.; Moore, K. N.; Birrer, M. J.; Berlin, S.; Matulonis, U. A.; Infante, J. R.; Wolpin, B.; Poon, K. A.; Firestein, R.; Kahn, J. X. R.; Wang, Y.; Wood, K.; Darbonne, W. C.; Lackner, M. R.; Kelley, S. K.; Lu, X.; Choic, Y. J.; Maslayar, D.; Humke, E. W.; Burris, H. A. Phase I study of safety and pharmacokinetics of the anti-MUC16 antibody–drug conjugate DMUC5754A in patients with platinum-resistant ovarian cancer or unresectable pancreatic cancer *Ann. Oncol.* **2016**, *27*, 2124-2130.
158. Kurokawa, T.; Kobayashi, K.; Tsuchi, K.; Hayaoka, T.; Shida, A.; Masui, A.; Nakagawa, T. Antibiotic NK10958 manufacture with *Streptomyces* as agrochemical. JP05025189A, 1993.
159. Delaunay, D.; Toupet, L.; Le Corre, M. Reactivity of beta-amino alcohols with carbon disulfide. Study on the synthesis of 2-oxazolidinethiones and 2-thiazolidinethiones. *J. Am. Chem. Soc.* **1995**, *60*, 6604-6607.
160. McKennon, M. J.; Meyers, A. I.; Drauz, K.; Schwarm, M. A convenient reduction of amino acids and their derivatives. *J. Org. Chem.* **1993**, *58*, 3568-3571.
161. Touchard, F. P. Phosphonate modification for a highly (Z)-selective synthesis of unsaturated esters by Horner–Wadsworth–Emmons olefination. *Eur. J. Org. Chem.* **2005**, 1790-1794.